

**ROBUST LAGRANGIAN NUMERICAL SCHEMES
IN COMPUTING EFFECTIVE DIFFUSIVITIES FOR
CHAOTIC AND RANDOM FLOWS**

by

Wang Zhongjian

B.Sc. *Tsinghua*

A thesis submitted in partial fulfillment of the requirements for
the Degree of Doctor of Philosophy
at The University of Hong Kong.

March, 2020

Temporary Binding for Examination Purposes

Abstract of thesis entitled

**ROBUST LAGRANGIAN NUMERICAL SCHEMES
IN COMPUTING EFFECTIVE DIFFUSIVITIES FOR
CHAOTIC AND RANDOM FLOWS**

Submitted by

Wang Zhongjian

for the degree of Doctor of Philosophy
at The University of Hong Kong
in March, 2020

Effective diffusivities of passive scalars diffusion in incompressible velocity fields have theoretical and practical importance. In this thesis, efforts have been made to develop a Lagrangian approach to calculate effective diffusivities and to analyze the error and physic phenomenons based on numerical results.

Our approach is to integrate the stochastic differential equations of the particles by proposed discrete schemes via Monte Carlo methods. To compute the effective diffusivities, we take the variance of the sampled positions divided by computational time. The computational time should be longer than the mixing time of dynamics, so the discrete schemes should preserve the inherent structures of the dynamics.

Via backward error analysis techniques, we proved the proposed schemes converge asymptotically with respect to the time step. Later on, we developed a new proof to show the convergence is uniform in computational time. The key ingredient of the proof is to propose discrete type cell problems, which are analogs to cell problems in traditional parabolic homogenization theory. And we concluded the schemes should preserve the invariant measure on torus space introduced by the periodicity of velocity fields. We generalized the proof to time-dependent cases and random cases.

Numerical examples were presented to verify the convergence in each case. We calculated the effective diffusivities of chaotic and random flows, including the Taylor Green field in two dimensions, the Arnold-Beltrami-Childress flow and Kolmogorov flow in three dimensions and also their generalizations to time-dependent and random cases. We investigated the convection-enhanced diffusion phenomenon in the large Péclet number regime. Our results showed that the diffusion enhancement has a strong correlation to mixing time and Lyapunov exponent.

**ROBUST LAGRANGIAN NUMERICAL SCHEMES
IN COMPUTING EFFECTIVE DIFFUSIVITIES FOR
CHAOTIC AND RANDOM FLOWS**

by

Wang Zhongjian

B.Sc. *Tsinghua*

A thesis submitted in partial fulfillment of the requirements for
the Degree of Doctor of Philosophy
at The University of Hong Kong.

March, 2020

Declaration

I declare that this thesis represents my own work, except where due acknowledgement is made, and that it has not been previously included in a thesis, dissertation or report submitted to this University or to any other institution for a degree, diploma or other qualifications.

WANG Zhongjian

Wang Zhongjian

Acknowledgments

I would like to express my sincere gratitude to my supervisor Dr. Zhiwen Zhang for his inspiring guidance, constant encouragement and help throughout the period of my Ph.D. study and in the preparation of this thesis. I would like to thank my collaborators Prof. Jack Xin and Mr. Junlong Lyu for discussion in research aspect of this thesis. I would like to thank Prof. Wak-Ki Ching for his help as my co-supervisor. I would like to thank Prof. Guangyue Han, Prof. Wenan Zang and Prof. Zhen Zhang (SUSTech) for their precious time to read my thesis and serve on the committee. I would also like to thank Prof. Thomas Y.Z. Hou, Prof. Stephen S.T. Yau, Prof. Xue Luo, Mr. Sijing Li for collaboration in other research projects.

I would like to thank various grants that support my research activities. I am grateful to the University of Hong Kong and Research Grant Council for the Hong Kong Ph.D. Fellowship, Pilot Scheme on International Experience, Doris Chen Postgraduate Travel Grant and other grants of my supervisor that support my oversea research activities. I highly appreciate the generous support from exterior groups, including twice SIAM student travel awards from Society for Industrial and Applied Mathematics, a trip to attend ICCM 2019 by Yau Mathematical Sciences Center, seminars in APAM at the Columbia University and in Cermics Lab at the Ecole des Ponts ParisTech (ENPC).

I fell grateful to my colleagues and friends, for their continued encouragement, support and help. Runbin offered me great help in coding and career plan as a peer. I am lucky to have Botong, Haoyu, Yizhen and Mengmou to chat with on our lives. 2C Football Club filled every of my Sunday afternoons with vigor and fun. I am happy to live and serve in the Lapchee College for four years.

The utmost gratitude is for my family. Their company and support are the main reasons I have survived this strenuous Ph.D. journey.

Contents

1	Introduction	1
1.1	Overview	1
1.2	Summary of the thesis	5
2	Preliminaries	6
2.1	Passive tracer model	6
2.1.1	Stochastic differential equation	7
2.1.2	Numerical approximation to SDE	8
2.2	Homogenization theory	9
2.2.1	Probabilistic approach	9
2.2.2	Effective diffusivities	12
3	Symplectic Schemes and Asymptotic Error Analysis	15
3.1	New stochastic integrators	15
3.2	Convergence analysis	17
3.2.1	Weak Taylor expansion	18
3.2.2	First order modified equation	20

3.2.3	Error analysis for computing the effective diffusivity . . .	26
3.3	Numerical results	30
3.3.1	Chaotic cellular flow with oscillating vortices	31
3.3.2	Investigating residual diffusivity	33
3.3.3	Investigating stochastic flows	34
3.3.4	Behavior of the long-time integration	37
4	Sharp and Uniform in Time Error Analysis in Time-Independent Flows	41
4.1	Symplectic stochastic integrators	41
4.1.1	Derivation of numerical integrators	41
4.1.2	The backward Kolmogorov equation and related results .	43
4.2	Convergence analysis	45
4.2.1	Convergence to an invariant measure	45
4.2.2	A discrete-type cell problem	48
4.2.3	Convergence estimate of the discrete-type cell problem .	50
4.2.4	Convergence estimate for the effective diffusivity	52
4.2.5	Generalizations to high-dimensional cases	55
4.3	Numerical results	57
4.3.1	Verification of the convergence rate	57
4.3.2	Investigation of the convection-enhanced diffusion phe- nomenon	59

5	Sharp and Uniform in Time Error Analysis in Time-Dependent Flows	65
5.1	Stochastic structure-preserving schemes	66
5.1.1	Derivation of numerical schemes	66
5.1.2	The backward Kolmogorov equation and related results .	67
5.2	Convergence analysis	69
5.2.1	Convergence to an invariant measure	69
5.2.2	A discrete-type cell problem	72
5.2.3	Convergence estimate of the discrete-type cell problem .	75
5.2.4	Convergence analysis for the effective diffusivity	76
5.2.5	Generalizations to high-dimensional cases	81
5.3	Numerical results	83
5.3.1	Verification of the convergence rate	83
5.3.2	Investigation of the convection-enhanced diffusion phenomenon	85
6	Sharp and Uniform in Time Error Analysis in Random Flows	92
6.1	Preliminaries	92
6.1.1	Some formulations and results for diffusion in random flows	92
6.1.2	The continuous-type corrector problem and effective diffusivity	95
6.2	Stochastic structure-preserving schemes and related properties .	97

6.2.1	Derivation of numerical schemes	97
6.2.2	Some properties of the numerical schemes	100
6.2.3	A discrete-type corrector problem	105
6.3	Convergence analysis	107
6.3.1	Convergence of the discrete-type corrector problem to the continuous one	107
6.3.2	Convergence of the numerical method in computing ef- fective diffusivity	109
6.4	Numerical results	114
6.4.1	Numerical methods for generating random flows	115
6.4.2	Verification of the convergence analysis	116
6.4.3	Verification of the exponential decay property.	118
6.4.4	Investigation of the convection-enhanced diffusion phe- nomenon	120
7	Concluding Discussions	123
7.1	Future direction	125
	Appendix: Notations and Abbreviations	127
	Bibliography	129

Chapter 1

Introduction

1.1 Overview

Diffusion enhancement in fluid advection is a fundamental problem to characterize and quantify the large-scale effective diffusion in fluid flows containing complex and turbulent streamlines, which is of great theoretical and practical importance, see [5, 16, 18] and references therein. Its applications can be found in many physical and engineering sciences, including atmosphere/ocean science, chemical engineering, and combustion. In this thesis, we shall study a passive tracer model, which describes particle motion with zero inertia:

$$\dot{X}(t) = v(t, X) + \sigma W_t, \quad X \in \mathbb{R}^d, \quad (1.1)$$

where X is the particle position, $\sigma \geq 0$ is the molecular diffusion coefficient, and $W_t \in \mathbb{R}^d$ is a white noise. The velocity $v(x, t)$ satisfies either the Euler or the Navier-Stokes equation. We will also investigate when $v(t, x)$ is modeled by a random field which mimics energy spectra of the velocity fields. We set $v(t, x) = \nabla^\perp \phi(t, x)$ and the streamline function ϕ satisfies $\phi_t = A\phi + \sqrt{Q}\zeta(t, x)$, which is a random field generated by appropriately choosing operators A and Q and $\zeta(x, t)$ is a space-time white noise independent of W_t .

For spatial-temporal periodic velocity fields and random velocity fields with short-range correlations, the homogenization theory [4, 24, 29, 43] confirms

that the long-time large-scale behavior of the particles is governed by a Brownian motion. More precisely, let $D^E \in \mathbb{R}^{d \times d}$ denote the effective diffusivity matrix and $X^\epsilon(t) \equiv \epsilon X(t/\epsilon^2)$. Then, $X^\epsilon(t)$ converges in distribution to a Brownian motion $\tilde{W}(t)$ with covariance matrix D^E , i.e., $X^\epsilon(t) \xrightarrow{d} \sqrt{2D^E} \tilde{W}(t)$. The D^E can be expressed in terms of particle ensemble average (Lagrangian framework) or cell problems (Eulerian framework). The dependence of D^E on the velocity field of the problem is highly nontrivial. Moreover, the scaling of D^E when the molecular diffusion vanishes attracts great attention.

The residual diffusivity refers to the non-zero effective diffusivity in the limit of zero molecular diffusion as a result of a fully chaotic mixing of the streamlines. It is expected that the corresponding long-time large-scale behavior will follow a different law and sensitively depend on the velocity fields. In [36], the authors solved computed the cell problem of the advection-diffusion type and observed the residual diffusion phenomenon. This approach allows adaptive basis learning for parameterized flows.

For time-independent Taylor-Green velocity field, the authors of [44] proposed a stochastic splitting method and calculated the effective diffusivity in the limit of vanishing molecular diffusion. It is theoretically shown and numerically observed that the effective diffusion is greater in scale than molecular diffusion (σ) but still vanishing as σ vanishes.

Due to the energy estimate of cell problems in homogenization theory, it is well known that the scaling of enhancement is not greater than $\frac{1}{\sigma^2}$. In [5], the maximum enhancement was studied. It is found by numerical experiments that in ABC flows, the scaling is likely $\frac{1}{\sigma^2}$. There is no further result as their approach is costly for small σ .

For random velocity fields with long-range correlations, various forms of anomalous diffusion, such as super-diffusion and sub-diffusion, can be obtained for some exactly solvable models (see [37] for a review). In [8] the authors proved the existence of the effective diffusivity for a two-dimensional time-dependent incompressible Gaussian velocity field. In [35], the authors proved

the homogenization of convection-diffusion in a time-dependent, ergodic, incompressible random flow. In [17, 19], the authors proved some necessary conditions under which the long-time behavior for convection-diffusion in a turbulent flow is diffusive. Those results show that the dependence of the effective diffusivity upon the molecular diffusion σ and the velocity field v in the random flow is complicated and how to describe this dependence is very difficult in general.

This motivates us to study numerically the dependence of D^E on complicated incompressible velocity fields. We will also investigate the scaling of enhancement in vanishing diffusion regime for several different velocity fields. However, the solutions of the advection-diffusion equation develop sharp gradients as molecular diffusion approaches zero and demand a large amount of computational costs in standard Fourier basis. To overcome this difficulty, we shall adopt the Lagrangian framework and compute an ensemble of particles governed by Eq.(1.1) directly.

Though there are several prior works on structure-preserving schemes for ODEs and SDEs, the novelty of this thesis is the rigorous theory in the numerical error analysis in computing the effective diffusivity and investigation of nonlinear/random phenomena, such as the different scale of effective diffusion in different flows.

The error is analyzed first asymptotically and then uniformly in computational time.

We first get inspired by the symplectic integrators in the Hamiltonian system. In [27], broad topics in dynamics of Hamiltonian system and its numerical approximation are reviewed. As the dynamics of deterministic Hamiltonian system preserves its Hamiltonian, we naturally hope the numerical scheme can preserve the Hamiltonian in discrete time. Generally speaking, such structure preserving schemes are called symplectic integrators. In two dimension, a separable Hamiltonian implies each component of the velocity field is independent of the corresponding component of x . Such v is divergence free and

if the Hamiltonian is periodic in space, then mean of v along each direction is zero. Base on these, we adopt a composite scheme[41] whose first step is the symplectic Euler scheme and second is Euler Maruyama scheme following the Brownian dynamics.

Backward Error Analysis (BEA) [46] is a great tool for estimating error of symplectic integrators. Weak backward error analysis in [11] is the generalization of BEA theory to SDEs. We will apply weak BEA to our symplectic operators and prove the error of effective diffusivities converges asymptotically. Specifically, we can remove the exponentially error growth in the first order term (with respect to time step) of Lyapunov estimate of error of Euler scheme (i.e. first term right hand side of Eq.(2.10)).

To improve the error analysis, we will explore the cancellation in discrete schemes. We view the integrator as a discrete flow operation given by a convolution kernel. We re-define the Poisson equation (cell problem) in discrete manner, named discrete cell problem. It is also the discretization of Green-Kubo formula in asymptotic analysis [45]. The discrete cell problem reflects the cancellation in homogenization theory. Base on this characteristic, we prove the convergence is uniform in computational time.

The last step in error analysis is to revisit the proof and explore the possibilities of generalization. We claim that the key structure to preserve thought such systems is the invariant measure and mean zero advection. So we combine the volume preserving schemes and Euler method for Brownian dynamics to integrate time-dependent and random flows in higher dimension. We also extend our proof to such cases.

In numerical study part, our study compute the effective diffusivities of chaotic and random flows in 2D and 3D, including Taylor-Green, Arnold-Beltrami-Childress (ABC), Kolmogorov and random flows generated by corresponding spectral measures. We verify the convergence rate for each case, i.e., time-independent, time-dependent, random. The convergence in our analysis is shown to be optimal in order and uniform in computational time.

Further more, we study diffusion enhancement phenomena in vanishing monocular diffusivity regime. Our results reveal the correlation between the scale of effective diffusivities and several chaotic quantities including, Lyapunov exponent, mixing time. Overall speaking, when the flow is more chaotic, the scale varies from maximal to sub-maximal, residual then vanishing; the mixing time becomes shorting and the Lyapunov exponent increases.

1.2 Summary of the thesis

This thesis is divided into four parts.

The first part of the thesis plays an introductory role. In Chapter 1, we overview the significance and existed study of effective diffusivities. In Chapter 2, we review the tools we may use in our analysis including numerical integrators to stochastic differential equations, probabilistic approach in homogenization theory and the an ergodic theorem in the probabilistic approach.

As the second part, Chapter 3, we view the our scheme as a modified symplectic integrator then analyze the error via backward error analysis. Vanishing and residual diffusion phenomena are studied in chaotic and random 2D flows.

The third part consists of Chapter 4, Chapter 5, Chapter 6. We introduce the novel uniform in time error analysis technique in time-independent, time-dependent, random flows correspondingly. Diffusion enhancement in 3D are divided into three types, residual, sub-maximal and maximal. The specific velocity fields includes ABC, Kolmogorov and random ones generated from energy spectra.

In the last part, Chapter 7, we give conclusion remarks and future direction. Additionally, lists of notations and abbreviations adopted in this thesis are given in the Appendix.

Chapter 2

Preliminaries

2.1 Passive tracer model

In this section, we will first introduce the passive tracer model described by a stochastic differential equation. The definition of stochastic differential equation (SDE) and its numerical approximation will be discussed in the subsequent subsections.

A flow tracer uses any property of fluid to track the flow. The property may include magnitude, direction and circulation patterns. A passive tracer indicates it has no influence on the flow. In context of my thesis, we will consider the concentration of some specific kinds of particles. Then in the passive tracer model, we assume the motion of these particles does not alter the velocity field they follow. To replicate the diffusion phenomenon, we assume the motions of particles are independent from each other and any one of them can be described by the following stochastic differential equation,

$$\dot{X}(t) = v(X) + \Sigma(X)W_t, \quad X \in \mathbb{R}^d, \quad (2.1)$$

where $X(t)$ is the position of the particle at time t . $v(X)$ is the Eulerian velocity field at position X , continuously differentiable. It defines the convection of the dynamics. $\Sigma > 0$ is the molecular diffusion coefficient matrix. W_t is a Gaussian white noise with zero mean and correlation function $\langle W_t^i W_{t'}^j \rangle = \delta_{ij} \delta(t - t')$.

In most cases, the covariance matrix of the random parts of the dynamics, i.e. $\Sigma\Sigma^T$ is positive definite, it corresponds to non-degenerate elliptic operator as its generator. In context of this thesis, we assume $\Sigma(X) = \sigma I_d$, where $\sigma > 0$ is a constant and I_d is identity matrix in \mathbb{R}^d . Colored noise cases will be studied in my future work.

2.1.1 Stochastic differential equation

In this subsection, we introduce a more general setting of SDE than in Eq.(2.1). It is adopted in [32] and detailed properties can also be found in [30, 42]. A general SDE is considered in the symbolic differential form,

$$dX_t = a(X_t)dt + b(X_t)dW_t, \quad (2.2)$$

or more accurately as an integral equation,

$$X_t = X_0 + \int_0^t a(X_s)ds + \int_0^t b(X_s)dW_s. \quad (2.3)$$

The second integral is an Ito integral along the Brownian motion W_t . W_t is a Brownian motion on the given probability space $\{\Omega, \mathcal{F}_t, P\}$. Ω is the set of all possibilities, $\{\mathcal{F}_t, t \geq 0\}$ is an increasing family of σ -algebras such that W_t is \mathcal{F}_t -measurable for each $t \geq 0$, P is the probability measure on Ω . In \mathbb{R}^d , W_t denotes a vector whose components are $W_{1,t}, W_{2,t}, \dots, W_{d,t}$. We call X_t is a strong solution if X_t satisfies Eq.(2.3), is \mathcal{F}_t -measurable and square-integrable over Ω .

To make sure the existence of the strong solution, we suppose a and b are *Lipschitz continuous* and *linear growth*. The Lipschitz constants are L_1 and L_2 . And the linear growth constants are G_1 and G_2 . i.e. $\forall x, y \in \mathbb{R}^d$

$$\begin{cases} \|a(x) - a(y)\| \leq L_1 \|x - y\| \\ \|b(x) - b(y)\| \leq L_2 \|x - y\| \\ \|a(x)\|^2 \leq G_1(1 + \|x\|^2) \\ \|b(x)\|^2 \leq G_2(1 + \|x\|^2) \end{cases} \quad (2.4)$$

Theorem 2.1 (Existence of Strong Solution, Theorem 5.2.9 of [30]). *In the SDE Eq.(2.3), a and b satisfy Eq.(2.4). Then on $(\Omega, \mathcal{F}_t, P)$, let X_0 be a random vector, independent of the Brownian motion W_t , and*

$$E\|X_0\|^2 < \infty \quad (2.5)$$

Then there exists a continuous, adapted process X_t which is an unique strong solution of Eq.(2.3).

2.1.2 Numerical approximation to SDE

When approximating the SDE in a specific filtration generated by the Brownian motion talked before, we cannot calculate infinitely many points of one path of the Brownian motion by computer. So, we first suppose $T > 0$ and only concern about the error in $[0, T]$. We suppose $0 = t_0 < t_1 < t_2 < \dots < t_n = T$ be a frozen partition of $[0, T]$, and we only calculate $\{W_{t_k}\}_{k=0}^n$ for the approximation. *Foot step* δ is defined by

$$\delta = \max_{k=1 \dots n} |t_k - t_{k-1}|. \quad (2.6)$$

Throughout the thesis, we adopt uniform mesh, i.e., $t_n = n\Delta t$. Then $\delta = \Delta t$.

Euler-Maruyama (EM) scheme is broadly used in integrating Eq.(2.3). Here we study the error of this conventional method and comparing it with our schemes which is proposed later.

Definition 2.1. *In Euler's Scheme, we use a generator to give a standard Brownian motion path W_t . We first approximate in discrete time.*

$$Z_{n+1} = Z_n + a(Z_n)(t_{n+1} - t_n) + b(Z_n)(W_{t_{n+1}} - W_{t_n}) \quad (2.7)$$

with

$$n_s = \max\{n : t_n \leq s\} \quad (2.8)$$

Then we give an adapted interpolation.

$$Y_s = Z_{n_s} + a(Y_{n_s})(s - t_{n_s}) + b(Y_{n_s})(W_s - W_{t_{n_s}}) \quad (2.9)$$

Analysis of general numerical integrators of SDEs can be found in [32]. For the Euler-Maruyama Scheme, in [53], the dependence on Lipschitz and growth factor in error estimate is explicitly shown in the following theorem.

Theorem 2.2 (Error Estimation for EM scheme,[53]). *X_t and Y_t are defined in Eq.(2.3) and Eq.(2.1). a, b satisfies Eq.(2.4). Given T , suppose $X_0 = Y_0$ a.s. then*

$$\sup_{s \leq T} E \|X_s - Y_s\|^2 \leq \Delta t \frac{c_2}{c_1} e^{c_1 T} + \delta^2 c_2 \quad (2.10)$$

in which, $c_1 = 1 + (4 + 2\Delta t)L_1^2 + 4L_2^2$, $c_2 = ((2 + \Delta t)L_1^2 + 2L_2^2)c(T)$ and $c(T) = (1 + e^{(1+G_1^2+2G_2^2)T}(1 + EX_0^2))(G_2^2 + 2TG_1^2)$.

Base on this, for different computational time T we expect the error grows exponentially fast against T .

2.2 Homogenization theory

In this subsection, we will introduce effective diffusivity for time-independent flows in homogenization theory. The velocity $v(X)$ in Eq.(1.1) is assume to be time-independent. In Chapter 3,5 and 6, we will generalize the study to other cases , including time-dependent flows and random flows. We will consider the classic homogenization from probabilistic viewpoint. It is well discussed in Chapter 3 of [4] and we outlined a simplified version here for sake of completeness.

2.2.1 Probabilistic approach

To study the large scale diffusion of Eq.(2.1), we re-scale $X(t)$ by,

$$Y^\epsilon = \epsilon X(t/\epsilon^2). \quad (2.11)$$

Then, we assume equation of y^ϵ in form of,

$$dY^\epsilon = \frac{1}{\epsilon} v\left(\frac{Y^\epsilon}{\epsilon}\right) + \sigma dw(s). \quad (2.12)$$

But comparing with Eq.(2.1) we know, w is a Gaussian white noise with zero mean and correlation function $\langle w_i(t)w_j(t') \rangle = \delta_{ij}\delta(t - t')$. $w(t)$ is same with W_t in distribution. Denoting distribution of $Y^\epsilon(t)$ starting from x as μ_{xt}^ϵ .

To assuring the existence of effective process, we assume v periodic in $\mathcal{O}(1)$ scale in space and mean zero in space. Without loss of generality, the period of $v(x)$ is assumed to be 1 in each dimension of the physical space. We denote the periodic space by $Y = \mathbb{T}^d$.

One natural way to study the expectation of the paths for the SDE given by the Eq.(2.1) is to consider its associated backward Kolmogorov equation. Specifically, given a sufficiently smooth function $\phi(x)$ in \mathbb{R}^d , let $u(x, t) = \mathbb{E}(\phi(X_t)|X_0 = x)$ and $X_t = (x_1(t), \dots, x_d(t))^T$ is the solution to Eq.(2.1), then $u(x, t)$ satisfies the backward Kolmogorov equation as

$$u_t = \mathcal{L}u, \quad u(x, 0) = \phi(x). \quad (2.13)$$

In Eq.(2.13), the generator \mathcal{L} is defined as

$$\mathcal{L}u = v \cdot \nabla u + D_0 \Delta u, \quad (2.14)$$

where $D_0 = \sigma^2/2$ is the diffusion coefficient. Denote by \mathcal{L}^* its formal adjoint,

$$\mathcal{L}^*u = -\nabla \cdot (vu) + D_0 \Delta u, \quad (2.15)$$

Let $\rho(x, t)$ denote the density function of the particle $X(t)$ of Eq.(2.1). Then, $\rho(x, t)$ satisfies the Fokker-Planck equation $\rho_t = \mathcal{L}^*\rho$ with the initial density $\rho(x, 0) = \rho_0(x)$, where $\rho_0(x)$ is the density of the particle $X(0)$.

Proposition 2.1 (Fredholm alternative for the evolution operator). *The homogeneous equations,*

$$\mathcal{L}z = 0, \quad z \text{ periodic in } Y, \quad (2.16)$$

$$\mathcal{L}^*\mu = 0, \quad \mu \text{ periodic in } Y, \quad (2.17)$$

exist one and only one solution (up to a multiplicative constant). Let ϕ, ψ satisfies,

$$\int_Y \phi \mu = 0 \quad (2.18)$$

$$\int_Y \psi = 0, \quad (2.19)$$

then there exists one and only one solution of the inhomogeneous equations,

$$\mathcal{L}\xi = \phi, \quad \int_Y \xi = 0, \quad (2.20)$$

$$\mathcal{L}^*\pi = \phi, \quad \int_Y \pi = 1. \quad (2.21)$$

We further assume $v(x)$ is incompressible (i.e. $\nabla_x \cdot v(x) = 0$). As we know \mathcal{L}^* is the evolution operator for the Fokker-Planck equation on the density function of X , μ in Eq.(2.18) (up to a constant) is the invariant measure of X on torus space Y . A incompressible v implies μ is the Lebesgue (uniform, Haar) measure.

Now we can claim for the main result in our probabilistic approach,

Proposition 2.2 (Theorem 10.8 in Chapter 3 of [4]). *By previous assumption on regularity, mean, incompressibility of v , let χ to be solution of cell problem,*

$$-\mathcal{L}v := -D_0\Delta\chi - v(y) \cdot \nabla\chi = v(y), \quad y \in \mathbb{T}^d. \quad (2.22)$$

Let D^E be the effective diffusivity matrix,

$$D^E = D_0I - \int_Y v \otimes \chi \quad (2.23)$$

Let $y(t)$ be the Gaussian process whose correlation matrix is given by $2D^E$ and its distribution starting from x be μ_{xt} .

Then, when $\epsilon \rightarrow 0$,

$$\forall x, t, \quad \mu_{xt}^\epsilon \rightarrow \mu_{xt}, \quad \text{weakly.} \quad (2.24)$$

An ergodic theorem in the proof Before continuing to study of effective diffusivities, we would like to review an ergodic theorem, which is the key in the proof of Proposition 2.2. We shall also see later that it plays fundamental role in our proof. The theorem is stated in very general setting to accommodate both continuous case and our discrete case.

Let (S, Σ) be a probability space, on which a family $P(x, E)$, $x \in S$, $E \in \Sigma$, of probability measure is defined. We assume $x \rightarrow P(x, E)$ is measurable, $\forall E \in$

Σ . This corresponds to a linear bounded operator on $\mathcal{B}(S)$. This operator, denoted by P , is defined by,

$$P\phi(x) = \int_S P(x, dz)\phi(z), \quad \forall \phi \in \mathcal{B}(S). \quad (2.25)$$

Clearly $\|P\| \leq 1$. One of the main objectives of ergodic theory is to study the limit of the operator sequence P^n as $n \rightarrow +\infty$. The result can be summarized into the following proposition, which plays a fundamental role in our convergence analysis.

Proposition 2.3 (Theorem 3.1 in Chapter 3 of [4]). *We assume that,*

1. S is a compact metric space, and Σ is the Borel σ -algebra;
2. there exists a probability measure μ on (S, Σ) such that

$$P(x, E) = \int_E p(x, y)\mu(dy);$$

3. $p(x, y) : S \times S \rightarrow \mathbb{R}^+$ is continuous;
4. there exists a ball U_0 such that $\mu(U_0) > 0$ and a positive number $\delta > 0$ (depending on U_0) such that $p(x, y) \geq \delta$, $x \in S$, $\forall y \in U_0$.

Then, there exists one and only one invariant probability measure (π) on (S, Σ) and one has,

$$\sup_{x \in S} \left| P^n \phi(x) - \int \phi \pi(dx) \right| \leq C \|\phi\| e^{-\rho n}, \quad \forall \phi \in \mathcal{B}(S), \quad (2.26)$$

where $\rho = \log \frac{1}{1-\delta\mu(U_0)} > 0$ and $C = \frac{2}{1-\delta\mu(U_0)} > 0$ are independent of ϕ .

2.2.2 Effective diffusivities

In this subsection, we will discuss more on effective diffusivity including its Eulerian and Lagrangian approach, and scale in vanishing D_0 regime.

By multiplying χ to Eq.(2.22) and integrating in \mathbb{T}^d with consideration of periodicity of χ and v , we will get another equivalent formula for the effective

diffusivity,

$$D^E = D_0 I + D_0 \int_Y \nabla \chi \otimes \nabla \chi. \quad (2.27)$$

The correction to D_0 is nonnegative definite in Eq.(2.27). We can see that $e^T D^E e \geq D_0$ for all unit column vectors $e \in \mathbb{R}^d$, which is called convection-enhanced diffusion. By using energy estimate of Eq.(2.22), one can find an upper bound for the effective diffusivity, i.e., for all nonzero unit column vector $e \in \mathbb{R}^d$, we have

$$e^T D^E e \preceq \frac{1}{D_0}, \quad \text{as } D_0 \rightarrow 0. \quad (2.28)$$

More details of the derivation can be found in [5, 16, 40]. We are interested in studying the scale of convection-enhanced diffusion phenomenon for chaotic and random flows in this thesis. We will see in Taylor Green field, $D^E \sim \sqrt{D_0}$ as Fig.3.2. The residual diffusivity phenomenon means D^E will converge to a constant. We will see it happens when the flow strong mixing like, time-dependent flows and random flows in Fig.3.5 and Fig.5.6. When the flow is less chaotic, stronger diffusion enhancement happens. See Fig.4.2 for the result of the ABC flow obtained using our method. It probably attains the upper bound given by Eq.(2.28), which is called convection-enhanced diffusion with maximal enhancement [40].

In practice, the cell problem (2.22) can be solved using numerical methods, such as spectral methods. In [36], a small set of adaptive basis functions were constructed from fully resolved spectral solutions to reduce the computation cost. However, when D_0 becomes extremely small, the solutions of Eq.(2.22) develop sharp gradients and demand a large number of Fourier modes to resolve, which makes the Eulerian framework computationally expensive and unstable.

Alternatively, one can use the Lagrangian framework to compute the effective diffusivity matrix, which is defined by,

$$D_{ij}^E = \lim_{t \rightarrow \infty} \frac{\langle (x_i(t) - x_i(0))(x_j(t) - x_j(0)) \rangle}{2t}, \quad 1 \leq i, j \leq d, \quad (2.29)$$

where $X(t) = (x_1(t), \dots, x_d(t))^T$ is the position of a particle tracer at time t and the average $\langle \cdot \rangle$ is taken over an ensemble of test particles. The equivalence to Eq.(2.23) is due to the weak convergence given in Prop.2.2.

If the above limit exists, that means the transport of the particle is a standard diffusion process, at least on a long-time scale. If the passive tracer model has a deterministic divergence-free and periodic velocity field, this is the typical situation, i.e., the spreading of the particle $\langle (x_i(t) - x_i(0))(x_j(t) - x_j(0)) \rangle$ grows linearly with respect to the time t . For example when the velocity field is given by the Taylor-Green velocity field [16, 44], the long-time and large-scale behavior of the passive tracer model is a diffusion process. However, there are also cases showing that the spreading of particles does not grow linearly with time but has a power law t^γ , where $\gamma > 1$ and $\gamma < 1$ correspond to super-diffusive and sub-diffusive behaviors, respectively [2, 5, 37].

We shall consider the Lagrangian approach in this thesis. The Lagrangian framework has the advantages that it is easy to implement and does not directly suffer from a small molecular diffusion coefficient σ during the computation. However, we should point out that the major difficulty in solving Eq.(2.1) comes from the fact that the computational time should be long enough to approach the diffusion time scale. The diffusion time (a.k.a, mixing time, dissipation time) may be as long as $\mathcal{O}(\frac{1}{D_0})$. By reviewing the Lyapunov type error estimate in Proposition 2.2, we know the EM or other general schemes may fail. To address this challenge, we shall develop robust numerical integrators, which are structure-preserving and accurate for long-time integration.

Chapter 3

Symplectic Schemes and Asymptotic Error Analysis

3.1 New stochastic integrators

In this section, we construct the new stochastic integrators for the passive tracer model, which is based on the operator splitting methods [38, 51]. We consider the following *two-dimensional* model problems to illustrate the main idea and emphasize that our method can be used to solve high-dimensional problems without any difficulty,

$$\begin{cases} dx_1 = v_1(t, x_1, x_2)dt + \sigma_1 dW_{1,t}, & x_1(0) = x_{10}, \\ dx_2 = v_2(t, x_1, x_2)dt + \sigma_2 dW_{2,t}, & x_2(0) = x_{20}. \end{cases} \quad (3.1)$$

Furthermore, we assume that there exists a Hamiltonian function $H(t, x_1, x_2)$ such that

$$v_1(t, x_1, x_2) = -\frac{\partial H(t, x_1, x_2)}{\partial x_2}, \quad v_2(t, x_1, x_2) = \frac{\partial H(t, x_1, x_2)}{\partial x_1}. \quad (3.2)$$

In this chapter, we assume that the Hamiltonian $H(t, x_1, x_2)$ is sufficiently smooth and that first order derivatives of $v_i(t, x_1, x_2)$, $i = 1, 2$ are bounded. These conditions are necessary to guarantee the existence and uniqueness of solutions of Eq.(3.1), see [42]. Moreover, the boundedness of some higher order

derivatives of $v_i(t, x_1, x_2)$ is required when we prove the convergence analysis in Section 3.2.

We first rewrite the particle tracer model Eq.(3.1) into an abstract form $\dot{X} = \mathcal{L}X$, where $X = (x_1, x_2)^T$. We then split the operator \mathcal{L} into two operators \mathcal{L}_i , $i = 1, 2$, where

$$\mathcal{L}_1 : \quad dx_1 = v_1(t, x_1, x_2)dt, \quad dx_2 = v_2(t, x_1, x_2)dt, \quad (3.3)$$

$$\mathcal{L}_2 : \quad dx_1 = \sigma_1 dW_{1,t}, \quad dx_2 = \sigma_2 dW_{2,t}, \quad (3.4)$$

corresponding to the deterministic part and the stochastic part, respectively. Finally, we apply composition methods to approximate the integrator $\varphi(\tau) = \exp(\tau(\mathcal{L}_1 + \mathcal{L}_2))$ generated from Eq.(3.1). Though the operator splitting methods have been successfully applied to various problems, there is limited work on solving SDEs and SPDEs. We refer to [6, 41] for recent works on Hamiltonian systems with additive noise.

We approximate the integrator $\varphi(\tau)$ by the Lie-Trotter splitting method and get

$$\varphi(\tau) = \exp(\tau(\mathcal{L}_1 + \mathcal{L}_2)) \approx \exp(\tau\mathcal{L}_1)\exp(\tau\mathcal{L}_2). \quad (3.5)$$

Now we discuss how to discretize the numerical integrator Eq.(3.5). From time $t = t_k$ to time $t = t_{k+1}$, where $t_{k+1} = t_k + \tau$, $t_0 = 0$, assuming the solution $(x_1^k, x_2^k)^T \equiv (x_1(t_k), x_2(t_k))^T$ is given, one can solve the subproblems corresponding to \mathcal{L}_1 and \mathcal{L}_2 in a small time step τ to obtain $(x_1^{k+1}, x_2^{k+1})^T$. In our numerical method, we discretize the operator \mathcal{L}_1 by numerical schemes that preserve symplectic structure and the operator \mathcal{L}_2 by the Milstein scheme [42], so we obtain the new stochastic integrators for Eq.(3.1) as follows,

$$\begin{cases} x_1^* = x_1^k + \tau v_1(t_k + \beta\tau, \alpha x_1^k + (1 - \alpha)x_1^k, (1 - \alpha)x_2^k + \alpha x_2^k), \\ x_2^* = x_2^k + \tau v_2(t_k + \beta\tau, \alpha x_1^k + (1 - \alpha)x_1^k, (1 - \alpha)x_2^k + \alpha x_2^k), \end{cases} \quad (3.6)$$

where the parameters $\alpha, \beta \in [0, 1]$ and

$$\begin{cases} x_1^{k+1} = x_1^* + \sigma_1 \Delta_k W_{1,\tau}, \\ x_2^{k+1} = x_2^* + \sigma_2 \Delta_k W_{2,\tau}, \end{cases} \quad (3.7)$$

with $\Delta_k W_{i,\tau} = W_{i,t_k+\tau} - W_{i,t_k}$, $i = 1, 2$. In practice, each $\Delta_k W_i(\tau)$ is an independent random variable of the form $\sqrt{\tau}\mathcal{N}(0, 1)$.

The symplectic-preserving schemes Eq.(3.6) are implicit in general. Compared with explicit schemes, however, they allow us to choose a relatively large time step to compute. In practice, we find that few steps of Newton iterations are enough to maintain accurate results. Therefore, the computational cost is controllable. To design adaptive time-stepping method for Eq.(3.1) is an interesting issue, which will be studied in our future work.

In general, the second-order Strang splitting [51] is more frequently adopted in application, for which the integrator $\varphi(\tau)$ is approximated by

$$\varphi(\tau) = \exp(\tau(\mathcal{L}_1 + \mathcal{L}_2)) \approx \exp\left(\frac{\tau}{2}\mathcal{L}_2\right)\exp(\tau\mathcal{L}_1)\exp\left(\frac{\tau}{2}\mathcal{L}_2\right). \quad (3.8)$$

In fact, the only difference between the Strang splitting method and the Lie-Trotter splitting method is that the first and last steps are half of the normal step τ . Thus a more accurate method can be implemented in a very simple way. We skip the details in implementing the Strang splitting scheme here as it is straightforward.

We remark that our new stochastic integrators provide an efficient way to investigate the residual diffusivity. Because we do not need to solve the advection-diffusion equation Eq.(2.22), which becomes extremely challenging when D_0 is small. Most importantly, symplectic-preserving schemes provide a robust and accurate numerical integrator for long-time integrations. We shall theoretically and numerically study its performance over existing numerical integrators, such as Euler schemes, in the subsequent sections.

3.2 Convergence analysis

In this section, we shall provide some convergence results. We prove that a linear growth of the global error can be obtained if we apply our numerical methods to solve a Hamiltonian system with a separable Hamiltonian. In

addition, we shall estimate the numerical error of our method in computing the effective diffusivity. Our analysis is based on the BEA technique [46], which is a powerful tool for the study of the long-time behaviors of numerical integrators.

3.2.1 Weak Taylor expansion

In our derivation, we use (p, q) to denote the position of the particle interchangeably with (x_1, x_2) . Thus, the Hamiltonian system defined by Eq.(3.1) is rewritten as

$$\begin{cases} dp = -H_q dt + \sigma dW_{1,t}, \\ dq = H_p dt + \sigma dW_{2,t}, \end{cases} \quad (3.9)$$

where $H \equiv H(t, p, q)$ is the Hamiltonian, $\sigma_1 = \sigma_2 = \sigma$ is a positive constant, and $dW_{i,t}$, $i = 1, 2$ are two independent Brownian motion processes. We assume the Hamiltonian system has a separable form [27]

$$H(t, p, q) = F(t, p) + G(t, q) \quad (3.10)$$

with $g \equiv H_q = g(t, q)$ and $f \equiv H_p = f(t, q)$.

Remark 3.1. *The separable Hamiltonian is quite a natural assumption and has many applications in physical and engineering sciences. For instance, $H(p, q) = \frac{1}{2}p^T p + U(q)$, where the first term is the kinetic energy and the second one is the potential energy.*

One natural way to study the expectations of the paths for the SDE given by Eq.(3.9) is to consider its associated backward Kolmogorov equation [47]. Specifically, we associate the SDE with a partial differential operator \mathcal{L}_0 , which is called the generator of the SDE, also known as the flow operator. For the Hamiltonian system Eq.(3.9), the corresponding backward Kolmogorov equation associated is given by

$$\begin{cases} \frac{\partial}{\partial t} \phi = \mathcal{L}_0 \phi, \\ \phi(x, 0) = \phi_0(x), \end{cases} \quad (3.11)$$

where the operator \mathcal{L}_0 is given by

$$\mathcal{L}_0 = -g\partial_p + f\partial_q + \frac{1}{2}\sigma^2\partial_p^2 + \frac{1}{2}\sigma^2\partial_q^2. \quad (3.12)$$

The probabilistic interpretation of Eq.(3.11) is that given initial data $\phi_0(x)$, the solution of Eq.(3.11), $\phi(x, t)$, satisfies $\phi(x, t) = E(\phi_0(X_t)|X_0 = x)$, where $X_t = (p(t), q(t))$ is the solution to Eq.(3.9). We integrate Eq.(3.11) from $t = 0$ to $t = \Delta t$ and obtain

$$\phi(x, \Delta t) = \phi(x, 0) + \mathcal{L}_0 \int_0^{\Delta t} \phi(x, s) ds. \quad (3.13)$$

Under certain regularity assumptions on the solution $\phi(x, t)$, we have the Taylor expansion

$$\phi(x, s) = \phi(x, 0) + s\frac{\partial}{\partial s}\phi(x, 0) + \cdots + \frac{s^N}{N!}\frac{\partial^N}{\partial s^N}\phi(x, 0) + R_N(x, s), \quad (3.14)$$

where $R_N(x, s)$ is the remainder term in the Taylor expansion. We substitute the Taylor expansion Eq.(3.14) into Eq.(3.13) and get

$$\phi(x, \Delta t) = \phi(x, 0) + \Delta t\mathcal{L}_0\phi(x, 0) + \sum_{k=1}^N \frac{\Delta t^{k+1}}{(k+1)!}\mathcal{L}_0\frac{\partial^k}{\partial s^k}\phi(x, 0) + O(\Delta t^{N+2}). \quad (3.15)$$

Recall that $\phi(x, 0) = \phi_0(x)$ and $\frac{\partial^k}{\partial s^k}\phi(x, 0) = \mathcal{L}_0^k\phi_0(x)$, we finally obtain

$$\phi(x, \Delta t) = \phi_0(x) + \sum_{k=0}^N \frac{\Delta t^{k+1}}{(k+1)!}\mathcal{L}_0^{k+1}\phi_0(x) + O(\Delta t^{N+2}). \quad (3.16)$$

The operator \mathcal{L}_0^{k+1} can be computed systematically. For instance, \mathcal{L}_0 has 4 terms, then \mathcal{L}_0^2 should have at most $4^2 = 16$ terms. We find that the first order modified equation has already indicated the advantage of the structure preserving scheme and shall show this in next subsections.

Remark 3.2. Eq.(3.16) provides the general framework for us to analyse the truncation error by numerical methods. Namely, the numerical flow $\phi^{num}(x, \Delta t) = E[\phi_0(X_{\Delta t}^{num, k})|X_0 = x]$ generated by some k -th order weak method should satisfy Eq.(3.16) up to terms of order $O(\Delta t^k)$.

3.2.2 First order modified equation

In this section, we shall analyze the numerical errors obtained by our symplectic splitting scheme and Euler Maruyama scheme [32], respectively. We find that the solution obtained by the symplectic splitting scheme follows an asymptotic Hamiltonian while the solution obtained by the Euler Maruyama scheme does not. With our new method, we can achieve a linear growth (instead of an exponential growth) of the global error when we compute effective diffusivity.

After numerical discretization, we find the following expansion using a first order weak method at $t = \Delta t$,

$$\phi^{num}(x, \Delta t) = \phi_0(x) + \Delta t \mathcal{L}_0 \phi_0(x) + \Delta t^2 \mathcal{A}_1 \phi_0(x) + O(\Delta t^3), \quad (3.17)$$

where \mathcal{A}_1 is a partial differential operator acting on $\phi_0(x)$ that depends on the choice of the numerical method used to solve Eq.(3.9). If we choose a convergent method to discretize the operator \mathcal{L}_0 in Eq.(3.17) and Eq.(3.15), then the local truncation error is $O(\Delta t^2)$ and the numerical scheme is of weak order one. We refer to [32] for the definition and discussion of the weak convergence and strong convergence.

In detail, let $X^{num}(\Delta t) = (p(\Delta t), q(\Delta t))$ denote the numerical solution obtained by one specific choice of the numerical method in solving Eq.(3.9). For instance, if we choose the symplectic splitting method stated in Eq.(3.7), we get

$$\begin{cases} p(\Delta t) = p_0 - \Delta t g(\frac{\Delta t}{2}, q_0) + \sigma \Delta W_1, \\ q(\Delta t) = q_0 + \Delta t f(\frac{\Delta t}{2}, p_0 - \Delta t g(\frac{\Delta t}{2}, q_0)) + \sigma \Delta W_2. \end{cases} \quad (3.18)$$

Now $\Delta W_1, \Delta W_2$ are two independent random variables of the form $\sqrt{\Delta t} \mathcal{N}(0, 1)$. To get \mathcal{A}_1 , we only need to expand $E(\phi_0(p(\Delta t), q(\Delta t)))$ around point $\phi_0(p_0, q_0)$ along the time variable Δt . Since we are dealing with a separable Hamiltonian H , the operator splitting scheme helps us obtain a straight-forward adaptive interpolation of Eq.(3.18) for $t \in [0, \Delta t]$, saying X_t^{num} . We then have the

form[56],

$$\phi^{num}(x, t) = E[\phi_0(X_t^{num}) | X_0 = (p_0, q_0)] \quad (3.19)$$

$$= \phi_0(x) + \Delta t \mathcal{L}_0 \phi_0(x) + \Delta t^2 \mathcal{A}_1 \phi_0(x) + O(\Delta t^3) \quad (3.20)$$

In the BEA [46], we aim to find the generator \mathcal{L}^{num} of this process and the associated backward Kolmogorov equation,

$$\begin{cases} \frac{\partial}{\partial t} \phi^{num} = \mathcal{L}^{num} \phi^{num} \\ \phi^{num}(x, 0) = \phi_0(x). \end{cases} \quad (3.21)$$

We now denote the generator of this modified equation in an asymptotic form in terms of Δt ,

$$\mathcal{L}^{num} \equiv \mathcal{L}_0 + \Delta t \mathcal{L}_1 + \Delta t^2 \mathcal{L}_2 + \dots \quad (3.22)$$

Recall that the operator \mathcal{L}_0 is defined in Eq.(3.12) and the definition of operators \mathcal{L}_i , $i \geq 1$ depends on the choice of the numerical method in solving Eq.(3.9), i.e. sub (3.22) into (3.16) then compare with (3.20), we get

$$\mathcal{L}_1 = \mathcal{A}_1 - \frac{1}{2} \mathcal{L}_0^2. \quad (3.23)$$

Now let us denote the truncated generator by,

$$\mathcal{L}^{\Delta t, k} := \mathcal{L}_0 + \Delta t \mathcal{L}_1 + \dots + \Delta t^k \mathcal{L}_k. \quad (3.24)$$

and denote the corresponding modified flow (if it exists),

$$\begin{cases} \frac{\partial}{\partial t} \phi^{\Delta t} = \mathcal{L}^{\Delta t, k} \phi^{\Delta t} \\ \phi^{\Delta t}(x, 0) = \phi_0(x). \end{cases} \quad (3.25)$$

Inspired by the weak convergence proof in [32], we shall focus on estimating the upper bound of the uniform numerical error for the perturbed flows.

Lemma 3.1. *Let ϕ^{num} and $\phi^{\Delta t}$ be defined in (3.21) and (3.25), respectively. We assume that $\phi_0 \in C^\infty$ and its Ito-Taylor expansion coefficients in the hierarchy set $\Gamma_{k+1} \cup B(\Gamma_{k+1})$ are Lipschitz and have at most linear growth. If the solution to the first order modified flow, $\phi^{\Delta t}$ converges to ϕ as $\Delta t \rightarrow 0$, then we have the following error estimate*

$$\|\phi^{num}(x, t) - \phi^{\Delta t}(x, t)\| \leq C(T) \Delta t^{k+1} \quad (3.26)$$

Proof. Eq.(3.17) shows that the operator $L^{\Delta t}$ approximates the operator $L^{\Delta t,k}$ locally in the time interval $[0, \Delta t]$ with the truncation error $O(\Delta t^{k+2})$. This implies that $X_t^{\Delta t}$ is a $k + 1$ -th order weak approximation to the SDE related to $X_t^{\Delta t,k}$ locally, i.e.

$$\phi_0(X_{\Delta t}^{num}) - \phi_0(X_{\Delta t}^{\Delta t,k}) = \phi_0(X_0^{num}) - \phi_0(X_0^{\Delta t,k}) + \sum_{\alpha \in B(\Gamma_{k+1})} I_\alpha[\phi_{0,\alpha}(X_{(\cdot)}^{\Delta t,k})]_{0,\Delta t} \quad (3.27)$$

Here we refer to the Chapter 5.5 in [32] for more detailed definition of multi-index stochastic Ito integration notation I_α . Proposition 5.11.1 in [32] gives an estimate for the I_α ,

$$|E \sum_{\alpha \in B(\Gamma_{k+1})} I_\alpha[\phi_{0,\alpha}(X_{(\cdot)}^{\Delta t,k})]_{0,\Delta t}| \leq C(L^{\Delta t,k})\Delta t^{k+2} \quad (3.28)$$

Since the operator $L^{\Delta t,k}$ approximates L_0 , $\lim_{\Delta t \rightarrow 0} C(L^{\Delta t,k}) = C(L)$. Combining with Lipschitz and linear growth condition, the final weak convergence order should be $C(T)O(\Delta t^{k+1})$ when Δt is small enough. \square

Remark 3.3. *Figure 3.1 shows the general procedure of our convergence analysis. Our goal is to develop efficient numerical method so that we can reduce the error in calculating effective diffusivity $|D^{E,num} - D^E|$, which is the dashed line on the left. Terms (namely $D^{E,\Delta t}$, $X_t^{\Delta t,k}$ (or $X_t^{\Delta t}$), $\mathcal{L}^{\Delta t,k} : \phi^{\Delta t}$) are introduced from the BEA and play intermediate roles between the numerical solutions (shown in the upper row) and the analytic ones (shown in the bottom row). This framework clearly reveals the main sources of error (i.e. $|D^{E,\Delta t} - D^E|$).*

The foregoing derivation shows that modified flows allow us to approximate the interpolation of numerical solution with a higher-order accuracy. Hence the modified flows dominate the error in numerical result. Now we intend to study the behavior of the modified flows.

Theorem 3.1. *For the stochastic differential equation system Eq.(3.9) with a time independent and separable Hamiltonian $H(p, q)$ Eq.(3.10), the numerical solution obtained using the symplectic splitting scheme follows an asymptotic Hamiltonian $H^{\Delta t}(p, q)$, or equivalently, the first order modified equation (density function) of the solution is divergence-free. The invariant measure on*

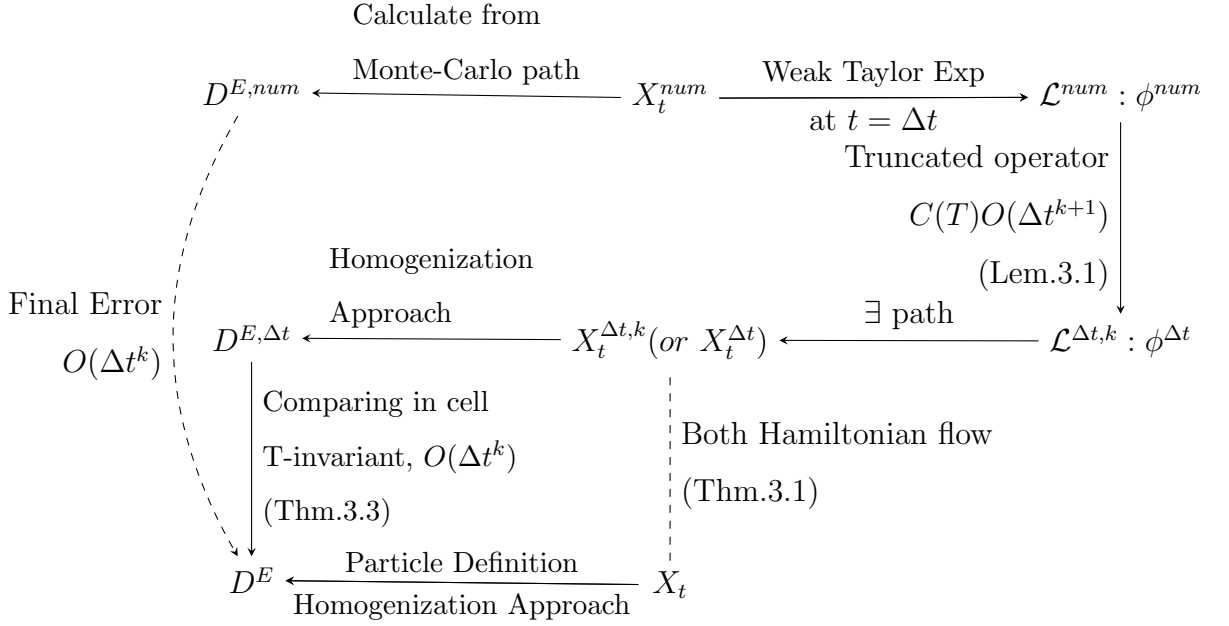


Figure 3.1: Illustration of backward error analysis for k -th order weak scheme

torus (defined by $\mathbb{R}^d/\mathbb{Z}^d$, when period is 1) remains trivial. While the numerical solution obtained using the Euler Maruyama scheme does not have these properties.

Proof. We shall compare the generators of modified equations obtained by using the symplectic splitting scheme and Euler Maruyama scheme, respectively. More specifically, we compare the operator \mathcal{L}_1 in Eq.(3.22) obtained from different methods. In the symplectic splitting scheme, we compute the weak Taylor expansion at time $t = \Delta t$ and get,

$$\mathcal{L}_1\phi = (\mathcal{A}_1 - \frac{1}{2}\mathcal{L}_0^2)\phi = (\frac{1}{2}fg' + \frac{\sigma^2}{4}g'')\phi_p + (-\frac{1}{2}f'g - \frac{\sigma^2}{4}f'')\phi_q + (-\frac{\sigma^2}{2}f' + \frac{\sigma^2}{2}g')\phi_{pq} \quad (3.29)$$

Hence, the modified flow of $X^{\Delta t, k}$ can be written as

$$\begin{cases} dp = (-g + (\frac{1}{2}fg' + \frac{\sigma^2}{4}g'')\Delta t)dt + \sigma dW_{1,t} + \Delta t \frac{\sigma}{2}g'dW_{2,t} \\ dq = (f - (\frac{1}{2}f'g + \frac{\sigma^2}{4}f'')\Delta t)dt + \sigma dW_{2,t} - \Delta t \frac{\sigma}{2}f'dW_{1,t} \end{cases} \quad (3.30)$$

Similarly, in the Euler Maruyama scheme, we get that

$$\mathcal{L}_1\phi = (\mathcal{A}_1 - \frac{1}{2}\mathcal{L}_0^2)\phi = (\frac{1}{2}fg' + \frac{\sigma^2}{4}g'')\phi_p + (\frac{1}{2}f'g - \frac{\sigma^2}{4}f'')\phi_q + (-\frac{\sigma^2}{2}f' + \frac{\sigma^2}{2}g')\phi_{pq} \quad (3.31)$$

And the associated modified flow can be written as

$$\begin{cases} dp = (-g + (\frac{1}{2}fg' + \frac{\sigma^2}{4}g'')\Delta t)dt + \sigma dW_{1,t} + \Delta t \frac{\sigma}{2}g'dW_{2,t} \\ dq = (f - (-\frac{1}{2}f'g + \frac{\sigma^2}{4}f'')\Delta t)dt + \sigma dW_{2,t} - \Delta t \frac{\sigma}{2}f'dW_{1,t} \end{cases} \quad (3.32)$$

Compare the results from Eq.(3.30) and Eq.(3.32), we can easily find that Eq.(3.30) follows an asymptotic Hamiltonian,

$$H^{\Delta t} \equiv H - \Delta t \left(\frac{1}{2}fg + \frac{\sigma^2}{4}(f' + g') \right), \quad (3.33)$$

while the flow Eq.(3.32) obtained from the Euler Maruyama scheme does not have this structure. Furthermore, we introduce notations v_1 and d_1 to denote extra terms in the modified flow Eq.(3.30), which are defined as

$$v_1 = \begin{pmatrix} \frac{1}{2}fg' + \frac{\sigma^2}{4}g'' \\ -\frac{1}{2}f'g - \frac{\sigma^2}{4}f' \end{pmatrix}, \quad \text{and} \quad d_1 = \begin{pmatrix} 0 & \frac{1}{2}g' \\ -\frac{1}{2}f' & 0 \end{pmatrix} \quad (3.34)$$

Since our numerical method solves a stochastic differential equations determined by a modified flow Eq.(3.30), the density function of particles $u(x, t)$ obtained from our method satisfy a modified Fokker-Planck equation given by

$$u_t = -(v + \Delta tv_1)\nabla u + D_0\nabla\nabla : (I + \Delta tD_1)u, \quad (3.35)$$

where $D_1 = ((I_d + \Delta td_1)(I_d + \Delta td_1)^T - T_d)/\Delta t = \begin{pmatrix} \frac{\Delta t}{4}(g')^2 & \frac{1}{2}(g' - f') \\ \frac{1}{2}(g' - f') & \frac{\Delta t}{4}(f')^2 \end{pmatrix}$ and we have used the condition $\nabla \cdot v_1 = 0$ to get $\nabla((v + \Delta tv_1)u) = (v + \Delta tv_1)\nabla u$. The inner product between matrices is denoted by $A : B = \text{tr}(A^T B) = \sum_{i,j} a_{ij}b_{ij}$. It follows that $\Delta = \nabla\nabla : I$ and $\nabla\nabla : D_1$ are defined accordingly. Then we can check that Eq.(3.35) admits trivial invariant measure $u_0(x, t) \equiv 1$. \square

We can repeat a similar calculation and generalize the result in Theorem 3.1 to a general time dependant and separable Hamiltonian. Therefore, we obtain the result as follows,

Corollary 3.1. *For the stochastic differential equation system Eq.(3.9) with a time dependent and separable Hamiltonian H Eq.(3.10), the numerical solution obtained using the symplectic splitting scheme follows an asymptotic Hamiltonian $H^{\Delta t}$, or equivalently, the first order modified equation (density function)*

of the solution is divergence-free. The invariant measure on torus (defined by $\mathbb{R}^d/\mathbb{Z}^d$, when period is 1) remains trivial.. While the numerical solution obtained using the Euler Maruyama scheme does not have these properties.

Proof. We repeat the same computation as we did in Theorem 3.1. In the symplectic splitting scheme, we find that the corresponding modified flow can be written as

$$\begin{cases} dp = \left(-g + \left(\frac{1}{2}fg' + \frac{\sigma^2}{4}g'' + \frac{1}{2}g_t\right)\Delta t \right)dt + \sigma dW_{1,t} + \Delta t \frac{\sigma}{2}g'dW_{2,t} \\ dq = \left(f - \left(\frac{1}{2}f'g + \frac{\sigma^2}{4}f'' + \frac{1}{2}f_t\right)\Delta t \right)dt + \sigma dW_{2,t} - \Delta t \frac{\sigma}{2}f'dW_{1,t} \end{cases} \quad (3.36)$$

The rest part is similar with Theorem 3.1. \square

Before we end this subsection, we use an example to demonstrate our main idea. We consider the flow driven by the Taylor-Green velocity field,

$$\begin{cases} dp = -\cos(q)\sin(p)dt + \sigma dW_{1,t}, \\ dq = \sin(q)\cos(p)dt + \sigma dW_{2,t}. \end{cases} \quad (3.37)$$

By introducing two variables $P = p + q$ and $Q = p - q$, we know the dynamic system Eq.(3.37) possesses a separable Hamiltonian, $H = -\cos P - \cos Q$ and the system can be expressed by

$$\begin{cases} dP = -\sin Q + \sqrt{2}\sigma d\eta_1, \\ dQ = \sin P + \sqrt{2}\sigma d\eta_2, \end{cases} \quad (3.38)$$

where η_1 and η_2 are two independent Brownian motions that are linear combinations of $W_{1,t}$ and $W_{2,t}$. Substituting into Eq.(3.33) and Eq.(3.30), we get,

$$H^{\Delta t} = H - \Delta t \left(\frac{1}{2} \sin P \sin Q + \frac{\sigma^2}{2} (\cos P + \cos Q) \right), \quad (3.39)$$

and

$$\begin{cases} dP = -\frac{\partial H^{\Delta t}}{\partial Q} dt + \sqrt{2}\sigma d\eta_1 + \Delta t \frac{\sigma}{\sqrt{2}} \cos Q d\eta_2, \\ dQ = \frac{\partial H^{\Delta t}}{\partial P} dt + \sqrt{2}\sigma d\eta_2 + \Delta t \frac{\sigma}{\sqrt{2}} \cos P d\eta_1. \end{cases} \quad (3.40)$$

Up to now, the new integrator Eq.(3.1) is shown to preserve structure of original Hamiltonian system Eq.(3.9) asymptotically at $O(\Delta t)$. In next subsection, we study effective diffusivity as a behavior of the structure.

3.2.3 Error analysis for computing the effective diffusivity

Recalling Eq.(2.29), only distribution of the process is needed, so Eulerian framework is sufficient to get an error estimate. For sake of comparison, we re-write the effective diffusivity formula Eq.(2.23) for Eq.(3.1) as,

$$D^E = D_0 \langle (I_d + \nabla w)(I_d + \nabla w)^T \rangle_p. \quad (3.41)$$

where $D_0 = \sigma^2/2$, which is globally used in context, $\langle \cdot \rangle_p$ denotes the spatial average (integration in \mathbb{T}^d), and cell problem w satisfies,

$$w_t + (v \cdot \nabla w) + D_0 \Delta w = -v. \quad (3.42)$$

, with the velocity field $v = (-g, f)^T$. To study effective diffusivity in Eq.(3.35), we turn to the Section 3.10 of [3], where an exact formula for D^E in a non-constant diffusion case is provided. Let $w^{\Delta t} \equiv w^{\Delta t}(t, x)$ denote the periodic solution of the cell problem that is corresponding to the modified Fokker-Planck equation Eq.(3.35), i.e., $w^{\Delta t}$ satisfies the following equation

$$w_t^{\Delta t} = -(v + \Delta t v_1) \cdot \nabla w^{\Delta t} - D_0 \nabla \nabla : (I + \Delta t D_1) w^{\Delta t} - (v + \Delta t v_1). \quad (3.43)$$

We introduce the operators $\mathcal{P}_0 w^{\Delta t} \equiv -v \nabla w^{\Delta t} - \frac{\sigma^2}{2} \Delta w^{\Delta t}$ and $\mathcal{P}_1 w^{\Delta t} \equiv -v_1 \nabla w^{\Delta t} - \frac{\sigma^2}{2} \nabla \nabla : D_1 w^{\Delta t}$ to simplify Eq.(3.43) as

$$w_t^{\Delta t} = (\mathcal{P}_0 + \Delta t \mathcal{P}_1) w^{\Delta t} - (v + \Delta t v_1). \quad (3.44)$$

Now by Theorem 3.1 and Corollary 3.1, Eq.(3.30) admits trivial invariant measure, so formula for the effective diffusivity tensor turns into,

$$D^{E, \Delta t} = D_0 \left\langle (I_d + \nabla w^{\Delta t})(I_d + \Delta t D_1)(I_d + \nabla w^{\Delta t})^T \right\rangle_p. \quad (3.45)$$

The modified cell problem (3.43) and the corresponding effective diffusivity tensor Eq.(3.45) enable us to analyse the error in our new method.

Lemma 3.2. *Eq.(3.43) has a unique solution if the condition $\int_{U_T} w^{\Delta t} dx dt = 0$ holds, where $U_T = [0, T] \times U$ is the space-time domain for the periodic function w .*

Proof. We first notice that when $\Delta t \ll D_0$, the operator $(\mathcal{P}_0 + \Delta t \mathcal{P}_1)$ is uniformly elliptic. The space average of the source term $-(v + \Delta t v_1)$ vanishes. By the Fredholm alternative, Eq.(3.44) has nontrivial solutions if $-(v + \Delta t v_1) \not\equiv 0$. Then, using the maximum principle, we get the conclusion that the solution $w^{\Delta t}$ to Eq.(3.43) is unique if the condition $\int_{U_T} w^{\Delta t} dx dt = 0$ is satisfied. \square

Now we derive regularity estimate in this Poincaré map problem (3.43).

Theorem 3.2. *Suppose $w = w(t, x)$ is a space-time periodic solution over the domain $U_T = [0, T] \times U$, which satisfies*

$$w_t + (v \cdot \nabla w) + D : \nabla \nabla w = S, \quad (t, x) \in U_T = [0, T] \times U, \quad (3.46)$$

where $\nabla \cdot v = 0$, D is symmetric and its eigen values are between $[D_-, D_+]$, $\forall (x, t)$, $S = S(t, x)$ is the source term, which vanishes in average at any time t . Then, we have the regularity estimate for w as $|\nabla w|_{L_2(U_T)} \leq C|S|_{L_2(U_T)}$ where the constant C depends only on the length of the physical domain U and the parameter D .

Proof. We multiply the equation Eq.(3.46) by w^T and integrate in U

$$\int_U (w^T w_t + w^T v \nabla w + w^T D : \nabla \nabla w) dx = \int_U w^T S dx \quad (3.47)$$

We shall notice that,

$$\begin{aligned} \int_U w^T w_t dx &= \frac{d}{dt} \int_U |w|^2 dx, \\ \int_U w^T v \nabla w dx &= - \int_U w^T v \nabla w dx = 0, \\ \int_U -w^T D : \nabla \nabla w dx &= \int_U \nabla w^T D \nabla w dx, \end{aligned}$$

where we have used the condition $\nabla \cdot v = 0$. Then, we integrate Eq.(3.47) over the time period $[0, T]$ and the periodic condition of w implies

$$\int_{U^T} \nabla w^T D \nabla w dx = \int_{U^T} w^T S dx dt \quad (3.48)$$

Let $\bar{w}(t)$ denote the space average of w at time t . Since S vanishes in space average at any time t , we have

$$\int_{U^T} \bar{w}^T S dx dt = 0. \quad (3.49)$$

In addition, we get the equality

$$\left(\int_{U^T} \nabla w^T D \nabla w dx \right)^2 = \left(\int_{U^T} (w^T - \bar{w}^T) S dx dt \right)^2 \quad (3.50)$$

Applying Poincare inequality on the right hand side and Cauchy-Schwartz on the left, we obtain the estimate

$$\int_{U^T} \nabla w^T D \nabla w dx \geq D_- \int_{U^T} |\nabla w|^2 dx dt \geq \int_{[0,T]} C_U \int_U |w - \bar{w}|^2 dx dt = \int_{U^T} |w - \bar{w}|^2 dx dt \quad (3.51)$$

$$\left(\int_{U^T} (w^T - \bar{w}^T) S dx dt \right)^2 \leq \int_{U^T} |S|^2 dx dt \int_{U^T} |w - \bar{w}|^2 dx dt \quad (3.52)$$

Combining the inequalities Eq.(3.51) and Eq.(3.52), we finally get the regularity estimate in L_2 norm.

$$|\nabla w|_{L_2(U^T)} \leq \frac{C(U)}{D_-} |S|_{L_2(U^T)}. \quad (3.53)$$

□

Given the regularity estimate of $w^{\Delta t}$ in (3.43), we can easily get estimate for the error between solutions to Eq.(3.42) and Eq.(3.43). We summarize the main result into the following theorem.

Theorem 3.3. *Let $w(x, t)$ and $w^{\Delta t}(x, t)$ be the solution to the Eq.(3.42) and Eq.(3.43), respectively. We have the estimate $|\nabla w - \nabla w^{\Delta t}|_{L_2(U_T)} \leq C_U \frac{\Delta t}{D_0} |S_e|_{L_2(U_T)}$, where $S_e = \mathcal{P}_1 w^{\Delta t} - v_1$ is the source term.*

Proof. Let $e \equiv e(x, t) = w(x, t) - w^{\Delta t}(x, t)$ denote the error. One can easily find that e is a space-time periodic function over $U_T = [0, T] \times U$ and satisfies the following equation

$$e_t + (v \cdot \nabla e) + D_0 \Delta e = (\Delta t) S_e, \quad (3.54)$$

where the source term S_e is defined above. So we directly apply the regularity estimate for the parabolic-type equation obtained in Thm.3.2 and obtain,

$$|\nabla e|_{L_2(U^T)} \leq C(U) \frac{\Delta t}{D_0} |\mathcal{P}_1 w^{\Delta t} - v_1|_{L_2(U^T)} \quad (3.55)$$

Again when $\Delta t \ll D_0$, the operator $\frac{\partial}{\partial t} + (\mathcal{P}_0 + \Delta t \mathcal{P}_1)$ is uniformly parabolic and the diffusion coefficients $D = D_0 + \Delta t D_1$ is positive and uniformly bounded

below (i.e. $D_- \rightarrow D_0$) for any Δt small enough. By regularity estimate of parabolic equation (a concrete estimate may comes from [15]), we can get $w^{\Delta t}$, $\nabla w^{\Delta t}$ and $\nabla \nabla : w^{\Delta t}$ are uniformly bounded in $L_2(U_T)$ for any Δt small enough, hence,

$$|\mathcal{P}_1 w^{\Delta t} - v_1|_{L_2(U_T)} = |(-v_1 \nabla - D_0 \nabla \nabla : D_1) w^{\Delta t} - v_1|_{L_2(U_T)} \leq C, \quad (3.56)$$

where the constant C is independent of Δt . \square

Finally, based on the error estimate for the solutions to the cell problems (3.42) and (3.43), we are able to get the error analysis for the effective diffusivity.

Remark 3.4. From Eq.(3.55), we shall state, a proper setting in calculating effective diffusivity should be

$$\Delta t \sim D_0 = \frac{\sigma^2}{2}. \quad (3.57)$$

Corollary 3.2. Let D^E and $D^{E,\Delta t}$ denote the effective diffusivity tensor computed by Eq.(3.41) and Eq.(3.45). Then, the error of the effective diffusivity tensor can be bounded by

$$|D^{E,\Delta t} - D^E| \leq C \Delta t, \quad (3.58)$$

where the constant C does not depend on time T .

Proof. Recalling Eq.(3.45), $D^{E,\Delta t} = D_0 \left\langle (I_d + \nabla w^{\Delta t})(I_d + \Delta t D_1)(I_d + \nabla w^{\Delta t})^T \right\rangle_p$

where $D_1 = \begin{pmatrix} \frac{\Delta t}{4}(g')^2 & \frac{1}{2}(g' - f') \\ \frac{1}{2}(g' - f') & \frac{\Delta t}{4}(f')^2 \end{pmatrix}$. We shall see the fact that $\langle \frac{1}{2}(g' - f') \rangle_p = 0$, $\langle \nabla w^{\Delta t} \rangle_p = 0$. Hence,

$$D^{E,\Delta t} - D^E = D_0 (\langle \nabla w^{\Delta t} \nabla w^{\Delta t, T} - \nabla w \nabla w^T \rangle_p + O(\Delta t^2)) \quad (3.59)$$

$$= D_0 ((\nabla w^{\Delta t} - \nabla w) \nabla w^T + \nabla w (\nabla w^{\Delta t} - \nabla w)^T \quad (3.60)$$

$$+ (\nabla w^{\Delta t} - \nabla w)(\nabla w^{\Delta t} - \nabla w)^T + O(\Delta t^2)). \quad (3.61)$$

Then considering Thm.3.2, and we can find that the order of the error in Eq.(3.58) is $O(\Delta t)$. \square

Theorem 3.4. *Solution of Eq.(3.9) is denoted as X_t and adaptive interpolated process of Eq.(3.6) as X_t^{num} . To calculate effective diffusivity of X_t^{num} which both start at x , we define $\tilde{D}^{E,num}(x, t) = E[\frac{(X_t^{num}-X_0)\otimes(X_t^{num}-X_0)}{2t}|X_0 = x]$ for $0 < t \leq T$.*

$$\sup_x |\tilde{D}^{E,num}(x, t) - D^E| \leq C\Delta t + C(T)\Delta t^2 \quad (3.62)$$

Proof. Let $\tilde{D}^{E,\Delta t}(x, t) = E[\frac{(X_t^{\Delta t}-X_0^{\Delta t})\otimes(X_t^{\Delta t}-X_0^{\Delta t})}{2t}|X_0^{\Delta t} = x]$. For any $\epsilon > 0$. We assume $\phi_0(x) = \sqrt{\epsilon + (x - X_0)^T(x - X_0)}$ in Lem.3.1, we see that $|\sqrt{\tilde{D}^{E,num}(x, t)} - \sqrt{\tilde{D}^{E,\Delta t}(x, t)}| \leq C(T)\Delta t^2$. By homogenization theory (like [3], [43]), we shall see $\lim_{t \rightarrow \infty} |\tilde{D}^{E,\Delta t}(x, t) - D^{E,\Delta t}| = 0$. Finally, Col.3.2 states $|D^{E,\Delta t} - D^E| \leq C\Delta t^2$. Eq.(3.62) is the result of triangle inequality. \square

Remark 3.5. *We shall see that in calculating effective diffusivity, we approximate D^E by $\tilde{D}^{E,num}$ in which taking expectation corresponds to simulation ignoring error of Monte-Carlo.*

Remark 3.6. *If a long-time behavior of a flow (i.e. effective diffusivity) can be approximated by a truncated flow of the numerical method, the error in approximating such behavior may be dominant by the truncated flow which can be studied analytically. In case of Thm.3.4, general error analysis (like in [32]) will state $|\tilde{D}^{E,num}(x, t) - D^E| \leq C(T)\Delta t$ where $C(T)$ grows exponentially as $T \rightarrow \infty$.*

3.3 Numerical results

In this section, we shall apply our methods to investigate the behaviors of several time-dependent chaotic and stochastic flows. We are interested in understanding the mechanisms of the diffusion enhancement, the existence of residual diffusivity, highlighting the influence of Lagrangian chaos on flow transport, and long-time performance of different numerical methods.

3.3.1 Chaotic cellular flow with oscillating vortices

For the first example, we consider the passive tracer model in which the velocity field is given by a chaotic cellular flow with oscillating vortices. Specifically, the flow is generated by a Hamiltonian defined as $H(t, p, q) = -\frac{1}{k} \cos(kp + B \sin(\omega t)) \sin(kq)$. The motion of a particle moving in this chaotic cellular flow is described by the SDE,

$$\begin{cases} dp = \sin(kp + B \sin(\omega t)) \cos(kq) dt + \sigma dW_{1,t}, \\ dq = -\cos(kp + B \sin(\omega t)) \sin(kq) dt + \sigma dW_{2,t}, \end{cases} \quad (3.63)$$

with initial data (p_0, q_0) . The behavior of Eq.(3.63) with $\sigma = 0$ was intensively studied in [9], which is a two-dimensional incompressible flow representing a lattice of oscillating vortices or roll cells. Moreover, when $B = 0$ the flow in Eq.(3.63) turns into the classic Taylor-Green velocity field. In this setting real fluid elements follow trajectories that are level curves of its Hamiltonian. When $B \neq 0$, the trajectories of the passive tracers differ from the streamlines, due to the oscillating vortex in the flow.

When $\sigma > 0$ the dynamics of the Eq.(3.63) will exhibit more structures, which is an interesting model problem to test the performance of our method. We point out that when $B \neq 0$ and $\sigma > 0$, the long-time large-scale behavior of the particle model of Eq.(3.63) has been studied by many researchers, for example in [16, 44]. It shows that the asymptotic behaviors of effective diffusivity $D^E \sim \sigma I_2$ (,or equivalently $D^E \sim \sqrt{2D_0} I_2$), which means that for this type of flow there does not exist residual diffusivity.

In our numerical experiments, we choose $k = 2\pi$, $\omega = \pi$, $(p_0, q_0) = (0, 0)$ in the SDE Eq.(3.63). The time step is $\Delta t = 10^{-2}$ and the final computational time is $T = 10^4$. We consider different B to study the behaviours of effective diffusivity in vanishing viscosity (i.e. $\sigma \rightarrow 0$). We compare the numerical obtained using the symplectic splitting scheme and Euler-Maruyama scheme. In our comparison, we use the same Monte Carlo samples to discretize the Brownian motions $dW_{1,t}$ and $dW_{2,t}$. The sample number is $N_{mc} = 5000$.

In Figure 3.2, we show the numerical results of effective diffusivity D_{11}^E obtained using different methods and parameters. Left part of the figure shows the results for Taylor-Green velocity field ($B = 0$). One can see that the Euler-Maruyama scheme fails to achieve the theoretical analysis for D^E , i.e., $D^E \sim \sigma I_2$, while the result obtained using our symplectic splitting scheme agrees with the theory well. Right part of the figure shows the results for $B = 2.72$. One again finds that the behaviors of the Euler-Maruyama scheme and our scheme are different.

To further compare the performance of the Euler-Maruyama scheme and our method, we repeat the same experiment with $k = 2\pi$, $\omega = \pi$, $(p_0, q_0) = (0, 0)$ and $\sigma = 10^{-2}$ in Eq.(3.63), but try different time step Δt with $B = 0$ and $B = 2.72$ correspondingly. In Figure 3.3, we find that symplectic scheme can achieve very accurate results even using a relatively larger time step, while the Euler-Maruyama scheme cannot give the right answer even using a very smallest time step. As a result of our analysis 3.2 and Eq.(3.63), we can say that the numerical result for D_{11}^E has converged to the analytical result. Therefore, we conjecture that the time dependent cellular flow we studied in Eq.(3.63) with $B = 2.72$, we still have $D^E \sim \sigma I_2$. More theoretic analysis of this flow will be reported in our future work.

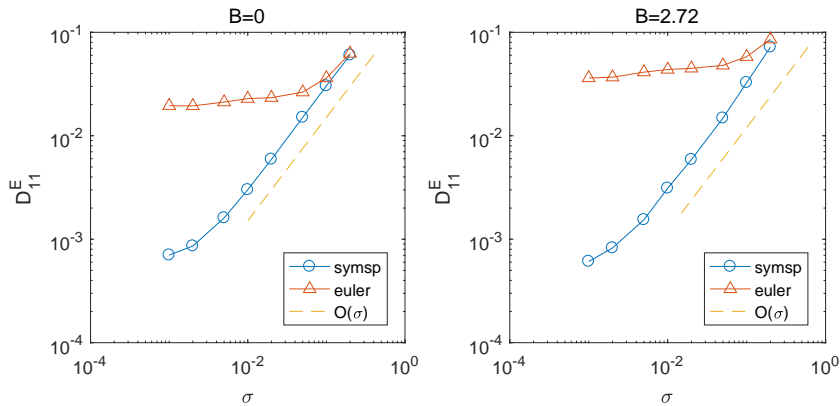
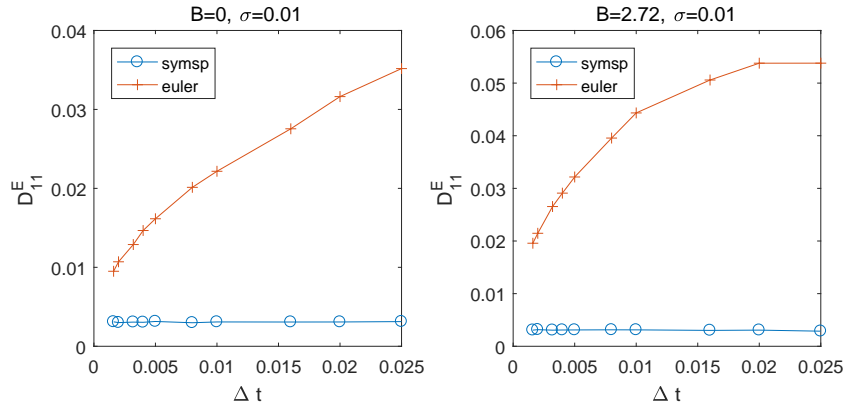


Figure 3.2: Numerical result for D_{11}^E , along with different σ

Remark 3.7. We also tested a time-dependent Taylor-Green velocity field, which is generated by the Hamiltonian defined as

$$H(t, p, q) = \frac{1}{k} (1 + B \sin(\omega t)) \cos(kp) \sin(kq). \quad (3.64)$$

Figure 3.3: Numerical result for D_{11}^E , along with different Δt

This field can be used to model particle motion in the ocean and in the atmosphere since it contains both vortices (convection cells) and linear uprising/sinking regions. Our numerical results indicate that the asymptotic behaviours of effective diffusivity $D^E \sim \sigma I_2$. Namely, there does not exist residual diffusivity for this time-dependent Taylor-Green velocity field.

3.3.2 Investigating residual diffusivity

We now turn to another chaotic cellular flow which is generated from a Hamiltonian defined as $H(t, p, q) = (\sin(p) - \sin(q)) + \theta \cos(t) (\cos(q) - \cos(p))$. Then the particle path satisfies the following SDE,

$$\begin{cases} dp = (\cos(q) + \theta \cos(t) \sin(q)) dt + \sigma dW_{1,t}, \\ dq = (\cos(p) + \theta \cos(t) \sin(p)) dt + \sigma dW_{2,t}. \end{cases} \quad (3.65)$$

The flow in Eq.(3.65) is fully chaotic (well-mixed at $\theta = 1$). The first term of the velocity field $(\cos(q), \cos(p))$ is a steady cellular flow, but the second term of the velocity field $\theta \cos(t) (\sin(q), \sin(p))$ is a time periodic perturbation that introduces an increasing amount of disorder in the flow trajectories as θ increases.

The flow in Eq.(3.65) has served as a model of chaotic advection for Rayleigh-Bénard experiment [25]. This type of flow has been investigated numerically in [36] by solving the cell problem Eq.(3.42). It was found that $D_{11}^E = \mathcal{O}(1)$

as $D_0 \downarrow 0$, which implies the existence of the residual diffusivity. However, the solutions of the advection-diffusion equation Eq.(3.42) develop sharp gradients as $D_0 \downarrow 0$ and demand a large amount of computational costs. We shall show that our numerical method gives comparable results with far less computational costs.

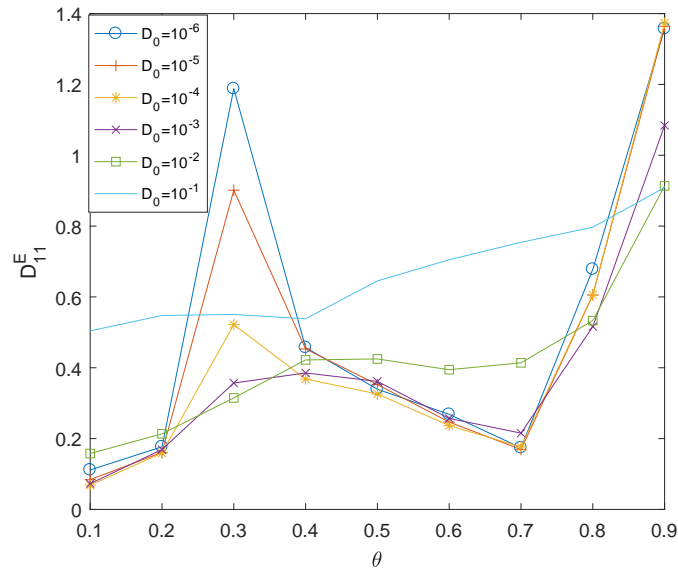
In our numerical experiments, we choose time step $\Delta t = 5 \times 10^{-2}$ and final time $T = 5 \times 10^3$ in our symplectic scheme as smaller values of Δt and larger values of T do not alter the results significantly. We use $N_{mc} = 5000$ independent Monte Carlo sample paths to discretize the Brownian motions $dW1$ and $dW2$.

In Tab.3.1, we show the numerical results of D_{11}^E for different D_0 and θ . We also show the results in Fig.3.4. We observed a *nonmonotone* dependence of D_{11}^E vs. θ in the small D_0 regime, though the overall trend is that D_{11}^E increases with the amount of chaos in the flows. Our numerical results again imply the existence of residual diffusivity for this type of chaotic flow. As suggested in our previous numerical investigation, the Euler-Maruyama scheme needs a much finer time step to compute the residual diffusivity and the numerical results can be polluted by the diffusion of the scheme. Therefore, we do not test the Euler-Maruyama scheme in this experiment.

3.3.3 Investigating stochastic flows

We are also interested in investigating the existence of the residual diffusivity for stochastic flows. The homogenization of time-dependent random flows had been studied in literatures. Under certain integrability condition, it is proved that the effective diffusivity exists for the long-time large scale behavior of the solutions [18, 35]. However, there are few numerical experiments to investigate effective diffusivity quantitatively. We shall use our symplectic splitting scheme to compute the effective diffusivity for stochastic flows. More theoretical study will be reported in Chapter 6.

θ	$D_0 = 10^{-6}$	$D_0 = 10^{-5}$	$D_0 = 10^{-4}$	$D_0 = 10^{-3}$	$D_0 = 10^{-2}$	$D_0 = 10^{-1}$
0.1	0.11155	0.08405	0.06883	0.07276	0.15795	0.50409
0.2	0.17678	0.16109	0.15918	0.16901	0.21342	0.54775
0.3	1.18786	0.90120	0.52176	0.35692	0.31484	0.55054
0.4	0.45719	0.45312	0.36819	0.38533	0.42212	0.53841
0.5	0.33937	0.35246	0.32603	0.36147	0.42486	0.64521
0.6	0.26844	0.24674	0.23670	0.25699	0.39448	0.70488
0.7	0.17402	0.16913	0.17664	0.21547	0.41394	0.75420
0.8	0.67800	0.60529	0.60658	0.51621	0.53321	0.79679
0.9	1.35703	1.36383	1.37339	1.08412	0.91342	0.90877

Table 3.1: Numerical results of D_{11}^E by the symplectic splitting scheme.Figure 3.4: The y results. D_{11}^E vs. θ for the fully chaotic flow defined in Eq.(3.65).

The stochastic flow is constructed from the fully chaotic flow in Eq.(3.65), where the time periodic function $\cos(t)$ is replaced by an Ornstein-Uhlenbeck (OU) process η_t [52]. The OU process satisfies,

$$d\eta_t = \theta_{ou}(\mu_{ou} - \eta_t)dt + \sigma_{ou}dW_t. \quad (3.66)$$

where $\theta_{ou} > 0$, μ_{ou} , and $\sigma_{ou} > 0$ are parameters and dW_t denotes a Wiener process. Specifically, θ_{ou} controls the speed of reversion, μ_{ou} is the long term mean level, and σ_{ou} is the volatility or diffusion strength. In our numerical experiments, we choose $\mu_{ou} = 0$, $\theta_{ou} = 1$, and $\sigma_{ou} = 1$, so that the OU process has zero mean and the stationary variance is $\frac{\sigma_{ou}^2}{2\theta_{ou}} = \frac{1}{2}$. We choose the parameters in the OU process in such a way that its qualitative behavior is the same as $\cos(t)$. The particle path satisfies the following SDE,

$$\begin{cases} dp = (\cos(q) + \theta \eta_t \sin(q))dt + \sigma dW_t^1 \\ dq = (\cos(p) + \theta \eta_t \sin(p))dt + \sigma dW_t^2. \end{cases} \quad (3.67)$$

where the Brownian motions dW_t^1 and dW_t^2 are independent from the one used in the definition of the OU process Eq.(3.66).

Since OU process has ergodic property, we choose a small amount of sample paths, say $n_{ou} = 40$, and final computational time $T = 5 \times 10^3$ to compute the effective diffusivity. In Tab.3.2, we show the numerical results of D_{11}^E for different D_0 and θ , where each D_{11}^E is the average values obtained from the n_{ou} paths. In Fig.3.5, we show the results corresponding to Tab.3.2. We observed a nonmonotone dependence of D_{11}^E vs θ in time periodic cellular. Our numerical results again imply the existence of residual diffusivity for this type of stochastic flow. We observe however that the non-monotonic dependence in θ disappears. Namely, the residual diffusivity is an increasing function of θ . Such phenomenon is due to the absence of resonance in stochastic flows. Furthermore, we show the ergodicity results of the effective diffusivity in Fig.3.6. In this test, we choose the parameters $\theta = 0.1$, $D_0 = 10^{-2}$ and compute the effective diffusivity along 2000 OU path. We show the histogram of $D^E(\omega_{OU})$ at $T = 100$, $T = 200$, $T = 500$, $T = 5000$, and $T = 20000$ respectively. This figure illustrates two facts: firstly, as the computational time become long enough the

histogram appears to converge to a limiting distribution. The limiting distribution has much smaller variance and is centered closer to 0.156084. Secondly, in the Tab.3.1 we show the residual diffusivity obtained from the fully chaotic (well-mixed) flow. When the parameters $\theta = 0.1$, $D_0 = 10^{-2}$, the corresponding residual diffusivity is $D_{11}^E = 0.157947$. Thus, the chaotic and stochastic flows may share some similar mechanism in long time behavior. More theoretic and numerical investigations will be studied in our future work.

θ	$D_0 = 10^{-6}$	$D_0 = 10^{-5}$	$D_0 = 10^{-4}$	$D_0 = 10^{-3}$	$D_0 = 10^{-2}$	$D_0 = 10^{-1}$
0.1	0.03644	0.03782	0.04265	0.06441	0.15608	0.48565
0.2	0.07070	0.07410	0.07553	0.09442	0.17228	0.49187
0.3	0.10624	0.10499	0.11215	0.12387	0.19542	0.49633
0.4	0.13734	0.14170	0.14579	0.15488	0.22119	0.51338
0.5	0.17133	0.17371	0.17636	0.18787	0.25286	0.52213
0.6	0.19719	0.20051	0.20510	0.22081	0.27269	0.53947
0.7	0.23278	0.23147	0.24067	0.24835	0.31460	0.56399
0.8	0.25992	0.25548	0.26805	0.28024	0.33211	0.58981
0.9	0.28671	0.29156	0.29021	0.29478	0.36550	0.60534

Table 3.2: Numerical results of D_{11}^E by the symplectic splitting scheme. The flow is defined by OU process.

3.3.4 Behavior of the long-time integration

Theorem 3.1 proves that the symplectic splitting scheme preserves the asymptotic Hamiltonian structure that enables us to compute the stable long-time behaviour of the effective diffusivity of chaotic and stochastic flows. We now keep using the flow Eq.(3.65) and compute a much longer time solution with final time $T = 5 \times 10^5$.

In Figure 3.7, we plot the effective diffusivity D_{11}^E as a function of time obtained using different methods and parameters. The top two lines correspond to the Euler-Maruyama method for $\sigma = 10^{-5}$ and $\sigma = 10^{-6}$, while the bottom

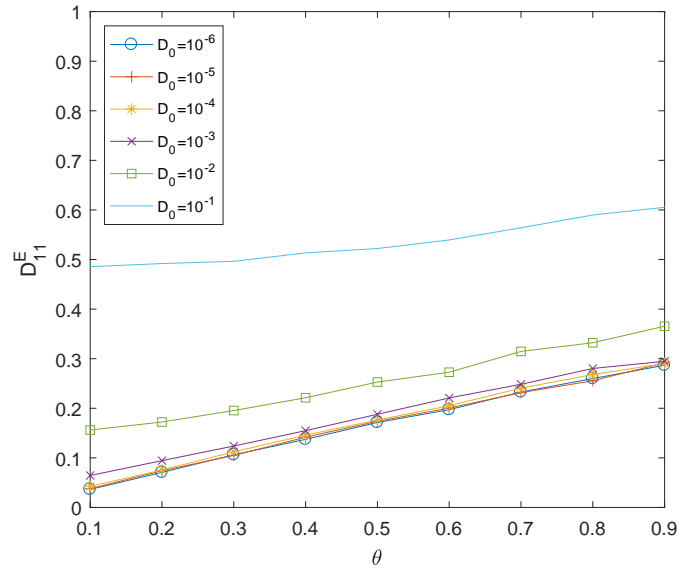


Figure 3.5: The residual diffusivity results. D_{11}^E vs. θ for the Stochastic flow driven by an OU process defined in Eq.(3.67).

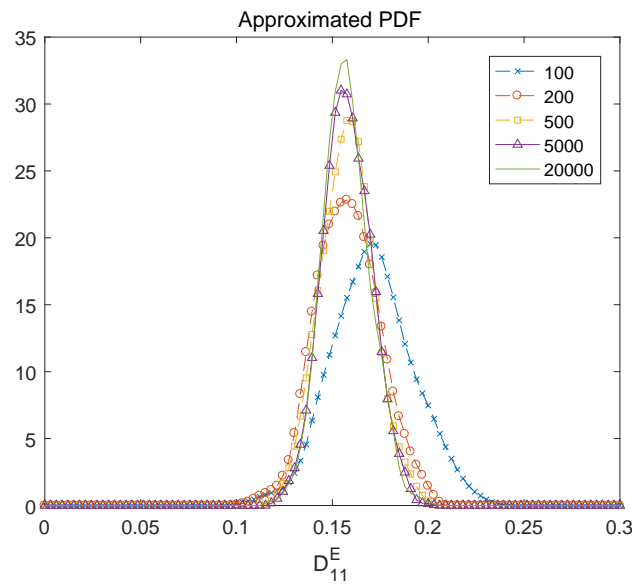


Figure 3.6: Histogram of the residual diffusivity results. D_{11}^E for the Stochastic flow driven by an OU process defined in Eq.(3.67) that are computed at different final times.

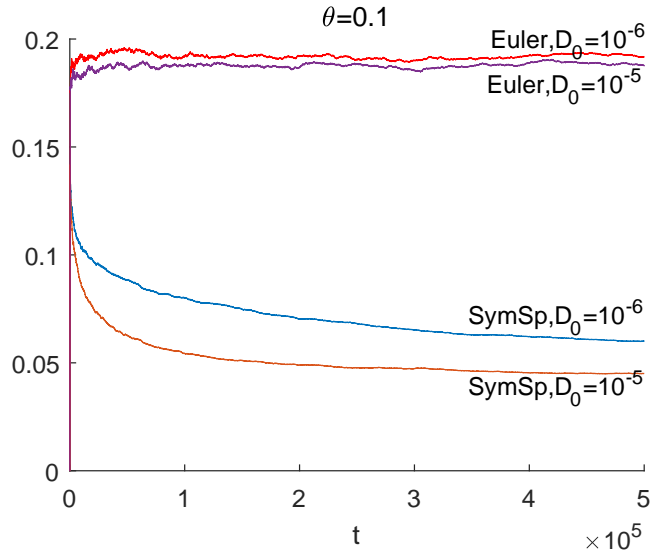


Figure 3.7: Behavior of $\frac{\langle (x_1(t) - x_1(0))^2 \rangle}{2t}$ as a function of time for two different methods.

two lines correspond to the symplectic splitting method. It is clear that results obtained from symplectic splitting method converge to a more stable value. A probable explanation is that modified flow of Euler method is not divergence-free while the solution obtained using the symplectic splitting scheme follows an asymptotic Hamiltonian. This is proved in our Theorem 3.1.

Another evidence comes from Figure 3.8, where we plot the phase plane for two different numerical methods. The realization of the noise is the same and we integrated up to time $T = 10^3$ with time step $\Delta t = 10^{-2}$. We choose the parameters $\theta = 0.1$ and $D_0 = 10^{-5}$. From these results, we find that the paths oscillate near a line with slope 1. It is clear that the behavior of the particle is drastically different. In the case of Euler-Maruyama method the particle appears to be much more diffusive than in the case of the symplectic splitting scheme.

In Figure 3.9, we show how the modified equation approximate the original problem, where we consider the chaotic cellular flow (3.65). More specifically, we plot the effective diffusivity $2(D_{11}^E + D_{22}^E)$ as of function of time obtained using different methods and we choose the parameter $\theta = 0.1$ and $D_0 = 10^{-5}$. From our numerical results, we find that the effective diffusivity obtained using

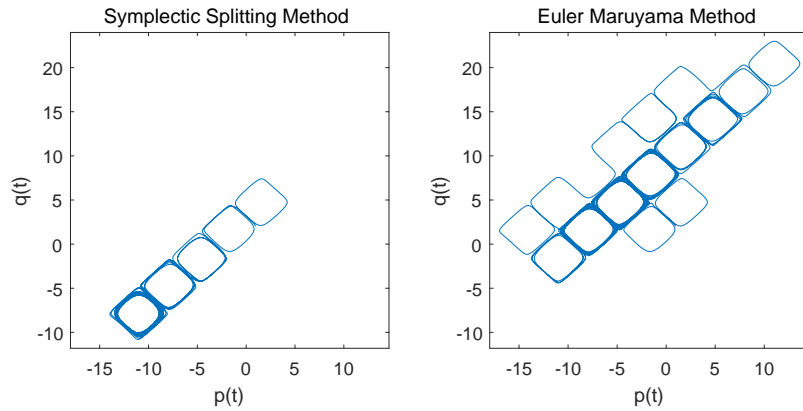
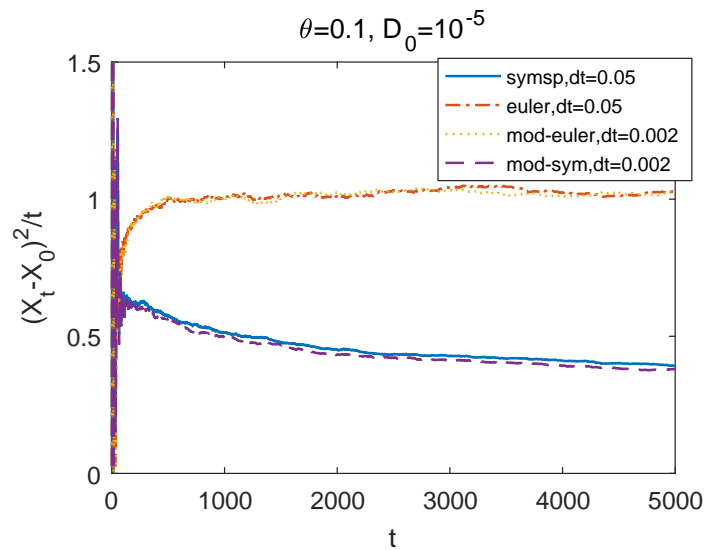


Figure 3.8: Phase plane for the two different methods.

our method with time step $dt = 0.05$ agrees very well that one obtained from solving the modified equation using the Euler-Maruyama method with time step $dt = 0.002$. Namely, we approximately achieve a 25X speedup over the Euler-Maruyama method. The Euler method with $dt = 0.05$ also generates results that agrees with its corresponding modified equation with finer time step. But the effective diffusivity converges to the wrong result.

Figure 3.9: Behavior of $\frac{\langle (x_1(t) - x_1(0))^2 \rangle + \langle (x_2(t) - x_2(0))^2 \rangle}{t}$ for two different methods.

Chapter 4

Sharp and Uniform in Time Error Analysis in Time-Independent Flows

4.1 Symplectic stochastic integrators

In this section, we will first revisit the scheme proposed in Chapter 3 and consider it in probabilistic viewpoint. To demonstrate the main idea, we first construct a symplectic stochastic integrator for a two-dimensional passive tracer model with a separable Hamiltonian. Then we will generalize our integrator to multi-dimension cases in Section 4.2.5.

4.1.1 Derivation of numerical integrators

Let $X = (p, q)$ denote the position of the particle, then the passive tracer model can be written as

$$\begin{cases} dp = -f(q)dt + \sigma W_{1,t}, & p(0) = p_0, \\ dq = g(p)dt + \sigma W_{2,t}, & q(0) = q_0, \end{cases} \quad (4.1)$$

where $W_{i,t}$ are independent Brownian motions and we have assumed that there exists a separable Hamiltonian function $H(p, q) = F(q) + G(p)$ such that $f(q) = H_q(p, q)$, $g(p) = H_p(p, q)$, and $H(p, q)$ is a periodic function on \mathbb{R}^2 with period 1.

In Chapter 3, we proposed a structure-preserving scheme based on a Lie-Trotter splitting idea to solve the SDE (4.1). Specifically, we split the Eq.(4.1) into a deterministic subproblem,

$$\begin{cases} dp = -f(q)dt, \\ dq = g(p)dt, \end{cases} \quad (4.2)$$

that is solved using a symplectic-preserving scheme (the symplectic Euler scheme for deterministic equations) and a stochastic subproblem,

$$\begin{cases} dp = \sigma W_{1,t}, \\ dq = \sigma W_{2,t}, \end{cases} \quad (4.3)$$

that is solved using the Euler-Maruyama scheme [42]. Eventually, the one step integrator of Eq.(4.1) is given by,

$$\begin{cases} p_{n+1} = p_n - f(q_n)\Delta t + \sigma\sqrt{\Delta t}N_n^p, \\ q_{n+1} = q_n + g(p_n - f(q_n)\Delta t)\Delta t + \sigma\sqrt{\Delta t}N_n^q, \end{cases} \quad (4.4)$$

where $N_n^p, N_n^q \sim \mathcal{N}(0, 1)$ are i.i.d. normal random variables in direction of p and q at step n . We denote the stochastic process generated by (4.4) as $X_n = (p_n, q_n)$, which is the numerical approximation to the exact solution $X(n\Delta t)$ to the SDE (4.1).

When the Hamiltonian system contains additive temporal noise, the noise itself is considered to be symplectic path-wisely [41]. We state that the scheme (4.4) is stochastic symplectic-preserving since it preserves symplecticity as a composition of symplectic transforms and it converges as time-step turns to zero. Though there are several prior works on developing symplectic-preserving scheme for solving ODEs and PDEs (see [1, 27, 28] and references therein), the novelty of our work is the rigorous theory and sharp estimate on the numerical error in computing the effective diffusivity.

Remark 4.1. *In general, the second-order Strang splitting [51] is more frequently adopted to solve ODEs and PDEs. The only difference between the Strang splitting method and the Lie-Trotter splitting method is that the first and last steps are modified by half of the time-step Δt . For the SDEs, however, the dominant source of error comes from the random subproblem (4.3). Thus, it is not necessary to implement the Strang splitting scheme.*

4.1.2 The backward Kolmogorov equation and related results

For the convenience of the reader, we first give a brief review of the theoretical results for the scheme (4.4) obtained in Chapter 3 and references therein. We first define the backward Kolmogorov equation associated with the Eq.(4.1) as

$$u_t = \mathcal{L}u, \quad u(x, 0) = u_0(x), \quad (4.5)$$

where the generator \mathcal{L} (associated with the Markov process in Eq. (4.1)) is given by

$$\mathcal{L} = -f\partial_q + g\partial_p + \frac{1}{2}\sigma^2\partial_p^2 + \frac{1}{2}\sigma^2\partial_q^2. \quad (4.6)$$

Recall that the solution $u(x, t)$ to the Eq.(4.5) satisfies $u(x, t) = \mathbb{E}(\phi(X_t)|X_0 = x)$, where $X_t = (p(t), q(t))^T$ is the solution to Eq.(4.1) and ϕ is a smooth function in \mathbb{R}^2 .

Similarly, we can study the flow generated by the symplectic splitting scheme (4.4). Recalling the splitting method during the derivation of the scheme in Section 4.1.1, we define $\mathcal{L}_1 = -f\partial_p$, $\mathcal{L}_2 = g\partial_q$ and $\mathcal{L}_3 = \frac{\sigma^2}{2}(\partial_{pp} + \partial_{qq})$. Starting from $u(\cdot, 0)$, we compute

$$\begin{cases} \partial_t u^1 &= \mathcal{L}_1 u^1, & u^1(\cdot, 0) &= u(\cdot, 0), \\ \partial_t u^2 &= \mathcal{L}_2 u^2, & u^2(\cdot, 0) &= u^1(\cdot, \Delta t), \\ \partial_t u^3 &= \mathcal{L}_3 u^3, & u^3(\cdot, 0) &= u^2(\cdot, \Delta t). \end{cases} \quad (4.7)$$

Then $u^3(\cdot, \Delta t)$ will be the flow at time $t = \Delta t$ generated by our scheme and it approximates the solution $u(\cdot, \Delta t)$ to the Eq.(4.5). It is also worth mentioning that, $u^2(\cdot, \Delta t)$ is the exact flow generated by deterministic symplectic Euler scheme in solving Eq.(4.2). Later on, we repeat this process to compute the flow equations of our scheme at other time steps, which approximate $u(\cdot, n\Delta t), n = 2, 3, \dots$

To analyze the error between the flow operator in Eq.(4.5) and the composited operator in Eq.(4.7), we shall resort to the Baker-Campbell-Hausdorff (BCH) formula, which is widely used in non-commutative algebra [26]. For example, in the matrix theory,

$$\exp(At)\exp(Bt) = \exp\left(t(A+B) + t^2\frac{[A, B]}{2} + \frac{t^3}{12}\left([A, [A, B]] + [B, [B, A]]\right) + \dots\right), \quad (4.8)$$

where t is a scalar, A and B are two square matrices with the same size, $[,]$ is the Lie-Bracket, and the remaining terms on the right hand side are all nested Lie-brackets.

In our analysis, we replace the matrices in Eq.(4.8) by PDE operators and the BCH formula yields some insights into the particular structure of splitting errors. Let $I_{\Delta t}$ denote the composited flow operator associated with Eq.(4.7), i.e.,

$$I_{\Delta t}u(\cdot, 0) := \exp(\Delta t\mathcal{L}_3)\exp(\Delta t\mathcal{L}_2)\exp(\Delta t\mathcal{L}_1)u(\cdot, 0). \quad (4.9)$$

Recall that the exact solution to the Eq.(4.5) at time $t = \Delta t$ can be represented as

$$u(\cdot, \Delta t) = \exp(\Delta t\mathcal{L})u(\cdot, 0) = \exp(\Delta t(\mathcal{L}_1 + \mathcal{L}_2 + \mathcal{L}_3))u(\cdot, 0). \quad (4.10)$$

Therefore, we can apply the BCH formula to analyze the error between the original flow and the approximated flow. Moreover, we find that computing the k -th order modified equation associated with Eq.(4.1) in BEA is equivalent to computing the terms of BCH formula up to order $(\Delta t)^k$ in the Eq.(4.9). To show that the solution generated by Eq.(4.4) follows a perturbed Hamiltonian system (with divergence free velocity and additive noise) at any order p , we only need to consider the $(p + 1)$ -nested Lie bracket consists of

$\{-f\partial_q, g\partial_p, \partial_{pp} + \partial_{qq}\}$ and we can easily see that they will not generate non-divergence free field.

In Chapter 3, we proved that for the SDE (4.1) with a time-dependent and separable Hamiltonian $H(p, q, t) = F(p, t) + G(q, t)$, the numerical solution obtained using the symplectic-preserving scheme (4.4) follows an asymptotic Hamiltonian $H^{\Delta t}(p, q, t)$, which is a first-order approximation to $H(p, q, t)$. Equivalently, the velocity field in the first-order modified backward Kolmogorov equation is divergence-free and the invariant measure on the torus (defined by $\mathbb{R}^d/\mathbb{Z}^d$, when period is 1) remains uniform, which is also known as the Haar measure. However, the numerical solution obtained using the Euler-Maruyama scheme does not have these properties.

Moreover, given any explicit splitting scheme for deterministic systems, by adding additive noise we shall have a similar form of flow propagation. And we shall see in later proof that, such operator formulation is very effective in analyzing the order of convergence and volume-preserving property.

4.2 Convergence analysis

We shall prove the convergence rate of our symplectic stochastic integrators in computing effective diffusivity based on a probabilistic approach, which allows us to get rid of the exponential growth factor in our error estimate.

4.2.1 Convergence to an invariant measure

The numerical method to compute effective diffusivity of a passive tracer model is closely related to study the limit of a sequence generated by the stochastic integrators. Therefore, we can apply the results from ergodic theory to study the convergence of the solution. The following result is fundamental for the proof of our convergence analysis.

Proposition 4.1. *On the torus space $\tilde{Y} = \mathbb{R}^d/\mathbb{Z}^d$, let $I_{\Delta t}^*$ denote the transform*

of the density function during Δt using the numerical scheme (4.4). Let $I_{\Delta t}$ denote the adjoint operator (i.e., the flow operator) of $I_{\Delta t}^*$ in the space of $\mathcal{B}(\tilde{Y})$, which is the set of bounded measurable functions on \tilde{Y} . Then $I_{\Delta t}$ is a compact operator from $\mathcal{B}(\tilde{Y})$ to itself. And there exists one and only one invariant probability measure on (\tilde{Y}, Σ) , denoted as π , satisfying,

$$\sup_{x \in \tilde{Y}} \left| (I_{\Delta t}^n \phi)(x) - \int \phi(x') \pi(dx') \right| \leq K \|\phi\|_{L^\infty} e^{-\rho n}, \quad \forall \phi \in \mathcal{B}(\tilde{Y}), \quad (4.11)$$

where $\rho > 0$, $K > 0$ are independent of $\phi(\cdot)$.

Proof. We shall verify that the transition kernel associated with the numerical scheme (4.4) satisfies the assumptions of Prop.2.3. First in the \mathbb{R}^n space, the integration process associated with the numerical scheme can be expressed as a Markov process with the transition kernel,

$$\begin{aligned} K_{\Delta t}((p, q), (P, Q)) = \\ \frac{1}{2\pi\sigma^2\Delta t} \exp \left(- \frac{\left(P - p + f(q)\Delta t \right)^2 + \left(Q - q - g(p - f(q)\Delta t)\Delta t \right)^2}{2\sigma^2\Delta t} \right), \end{aligned} \quad (4.12)$$

where (p, q) is the current solution and (P, Q) is the solution obtained by applying the scheme on (p, q) with time step Δt .

Then using the periodicity of $f(x)$ and $g(x)$, we extend Eq.(4.12) directly to the torus space \tilde{Y} as

$$\begin{aligned} \tilde{K}_{\Delta t}((p, q), (P, Q)) = \sum_{i, j \in \mathbb{Z}} \frac{1}{2\pi\sigma^2\Delta t} \cdot \\ \exp \left(- \frac{\left(P + i - p + f(q)\Delta t \right)^2 + \left(Q + j - q - g(p - f(q)\Delta t)\Delta t \right)^2}{2\sigma^2\Delta t} \right). \end{aligned} \quad (4.13)$$

One can see that if $0 < \Delta t \ll 1$, then \tilde{K} is smooth and is essentially bounded above zero, i.e., $\text{essn } \tilde{K} > 0$, $\forall ((p, q), (P, Q)) \in \tilde{Y} \times \tilde{Y}$. Thus, the operator $I_{\Delta t}$ is compact since it is an integral operator with a smooth kernel. Then applying the Theorem 3.3.1 in [4], we prove the assertion of the Proposition 4.1. \square

Now, we state a corollary that is a simple conclusion of exponential decay property proved in Proposition 4.1, which will be useful in the proof of main results.

Corollary 4.1. *Given that the assumptions in Proposition 4.1 are satisfied and $\phi \in \mathcal{B}(\tilde{Y})$, we have*

$$\lim_{n \rightarrow \infty} \frac{1}{n} \sum_{i=1}^n E\phi(X_i) = \int_{\tilde{Y}} \phi \pi(dx). \quad (4.14)$$

Before we close this subsection, we prove a convergence result for the inverse of operator sequences, which will be useful in our analysis.

Proposition 4.2. *Let X, Y denote two Banach spaces. Assume T_n, T are bounded linear operators from X to Y , satisfying $\lim_{n \rightarrow \infty} \|T_n - T\|_{\mathcal{B}(X, Y)} = 0$, and $T^{-1} \in \mathcal{B}(Y, X)$. Given $f \in Y$, if $T_n^{-1}f$, $n = 1, 2, \dots$ uniquely exist, then we have a convergence estimate as follows,*

$$\lim_{n \rightarrow \infty} \|(T_n^{-1} - T^{-1})f\| = 0 \quad (4.15)$$

Proof. After some simple calculations, we get

$$\begin{aligned} T_n^{-1} - T^{-1} &= T^{-1}(T - T_n)T_n^{-1} \\ &= T^{-1}(T - T_n)T^{-1} + T^{-1}(T - T_n)(T_n^{-1} - T^{-1}). \end{aligned} \quad (4.16)$$

Now applying $T_n^{-1} - T^{-1}$ on f , we get

$$\begin{aligned} \|(T_n^{-1} - T^{-1})f\| &\leq \|T^{-1}\|^2 \cdot \|T - T_n\| \cdot \|f\| \\ &\quad + \|T^{-1}\| \cdot \|T - T_n\| \cdot \|(T_n^{-1} - T^{-1})f\| \end{aligned} \quad (4.17)$$

Since $\lim_{n \rightarrow \infty} \|T_n - T\| = 0$, we assume for $n \geq N_0$, $\|T_n - T\| \cdot \|T^{-1}\| < \frac{1}{2}$, then,

$$\|(T_n^{-1} - T^{-1})f\| \leq 2\|T^{-1}\|^2 \cdot \|T - T_n\| \cdot \|f\|, \quad \forall n \geq N_0, \quad (4.18)$$

Eq.(4.15) follows if we take the limit as $n \rightarrow \infty$ on both sides. \square

Remark 4.2. *The proof is quite standard. It can also be viewed as a modification of Theorem 1.16 in Section IV of [31].*

4.2.2 A discrete-type cell problem

In the Eulerian framework, the periodic solution of the cell problem (2.22) and the corresponding formula for the effective diffusivity (2.23) play a key role in studying the behaviors of the chaotic and stochastic flows. In the Lagrangian framework, we shall define a discrete analogue of the cell problem that enables us to compute the effective diffusivity. We revisit the scheme Eq.(4.4),

$$\begin{cases} p_n = p_{n-1} - f(q_{n-1})\Delta t + \sigma N_{n-1}^p \\ q_n = q_{n-1} + g(p_{n-1} - f(q_{n-1})\Delta t)\Delta t + \sigma N_{n-1}^q, \end{cases} \quad (4.19)$$

where $N_{n-1}^p, N_{n-1}^q \sim \sqrt{\Delta t}\mathcal{N}(0, 1)$ are i.i.d. normal random variables.

We will show that the solutions p_n and q_n obtained by the scheme (4.19) have bounded expectations if the initial values are bounded. Taking expectation of the first equation of Eq.(4.19) on both sides, we obtain

$$Ep_n = Ep_{n-1} - \Delta t Ef(q_{n-1}) = Ep_0 - \Delta t \sum_{k=0}^{n-1} Ef(q_k). \quad (4.20)$$

Applying the Proposition 4.1 and using the fact that f is a periodic function with zero mean, we know that,

$$\sup_{(p_0, q_0) \in \tilde{Y}} |Ef(q_k)| \leq e^{-\rho k} \|f\|_\infty \quad (4.21)$$

By applying triangle inequalities in Eq.(4.20) and using the result in Eq.(4.21), we arrive at,

$$Ep_n \leq |Ep_0| + C_1 \|f\|_\infty, \quad (4.22)$$

where C_1 does not depend on n . Using the same approach, we know that Eq_n is also bounded. Now, we are in the position to define the discrete-type cell problem. We first define

$$\hat{f}(x) = -\Delta t \sum_{n=0}^{\infty} E[f(X_n)|X_0 = x], \quad x \in \tilde{Y}, \quad (4.23)$$

where the summability is guaranteed by Eq.(4.21). Then, we shall show that $\hat{f}(x)$ satisfies the following properties.

Lemma 4.1. *According to our assumption on the Hamiltonian, which is separable and periodic along each dimension, we know that f is a periodic function with zero mean on \tilde{Y} , i.e., $\int_{\tilde{Y}} f = 0$. Therefore, $\hat{f}(x)$ is the unique solution in $\mathcal{B}_0(\tilde{Y})$ such that,*

$$\hat{f}(X_0) + \Delta t f(X_0) = E[\hat{f}(X_1)|X_0]. \quad (4.24)$$

Moreover, $\hat{f}(x)$ is smooth.

Proof. Throughout the proof, we shall use the fact that if x, y are random processes and y is measurable under a filtration \mathcal{F} , then with appropriate integrability assumption, we have

$$E[xy] = E\left[E[xy|\mathcal{F}]\right] = E\left[E[x|\mathcal{F}]y\right]. \quad (4.25)$$

Some simple calculations will give that

$$\begin{aligned} \hat{f}(X_0) + \Delta t f(X_0) &= \Delta t E\left[\sum_{m=0}^{\infty} -f(X_m)|X_0\right] + \Delta t f(X_0) = -\Delta t E\left[\sum_{m=1}^{\infty} f(X_m)|X_0\right] \\ &= -\Delta t E\left[E\left[\sum_{m=1}^{\infty} f(X_m)|X_1\right]|X_0\right] = E[\hat{f}(X_1)|X_0]. \end{aligned} \quad (4.26)$$

Recall the definition of the operator (4.9), Eq.(4.26) implies that

$$(I_{\Delta t} - I_d)\hat{f} = I_{\Delta t}\hat{f} - \hat{f} = \Delta t f, \quad (4.27)$$

where I_d is the identity operator. Moreover, since f is smooth and the mapping of the operator $I_{\Delta t}$ on bounded functions will generate smooth functions, so \hat{f} is smooth.

According to Proposition 4.1, the invariant (measure) of $I_{\Delta t}^*$ is unique, i.e. $\dim \mathcal{N}(I_{\Delta t}^* - I_d) = 1$. By the Fredholm alternative and the fact that $I_{\Delta t}$ is a compact operator, we arrive at the conclusion that the solution \hat{f} to Eq.(4.27) is unique in $\mathcal{B}(\tilde{Y})$ up to a constant and it smoothly depends on f , given the assumption that $\int_{\tilde{Y}} f = 0$. \square

When the flow is time-independent, we obtain

$$E[\hat{f}(X_{n+1})|X_n] - \hat{f}(X_n) = \Delta t f(X_n), \quad a.s. \quad \forall n \in \mathbb{N}. \quad (4.28)$$

Remark 4.3. For the second component of the solution, i.e., q_n , we can define the discrete cell problem in the same manner. Specifically, we define

$$\hat{g}(x) = \Delta t \sum_{n=0}^{\infty} E[g(X'_n) | X_0 = x], \quad x \in \tilde{Y}, \quad (4.29)$$

where $X'_n = X_n - \Delta t f(X_n)$. There is no substantial difficulties in carrying out the analysis for $\hat{g}(x)$. Because under the assumption that the drift terms f and g in Eq.(4.1) are smooth enough, the leading order term of $g(X'_n)$ is $g(\tilde{X}_n)$, where \tilde{X}_n belongs to the torus space \tilde{Y} and other terms are small perturbations.

The Proposition 4.1 and the Lemma 4.1 are very general results. We only need the result that \hat{f} is unique in an Hölder space $\mathbb{C}_0^{p,\alpha}(\tilde{Y}) \subsetneq \mathcal{B}(\tilde{Y})$. To be precise, given a smooth drift function f , \hat{f} shall be in $\mathbb{C}_0^{p,\alpha}(\tilde{Y})$, where $p \geq 6, 0 < \alpha < 1$ and the subscript index 0 indicates that it is a subspace with zero-mean functions. To prove that $I_{\Delta t}$ is a compact operator from $\mathbb{C}_0^{p,\alpha}(\tilde{Y})$ to itself is quite standard. We can apply the Arzelà-Ascoli theorem to verify the relative compactness of the operator $I_{\Delta t}$ by studying its mapped results on a bounded set. Both equicontinuity and point-wise boundedness come as the result that $I_{\Delta t}$ is an integral operator with a smooth kernel. However, we do not want to complicate the presentation by pursuing this avenue.

4.2.3 Convergence estimate of the discrete-type cell problem

After defining the discrete-type cell problem (e.g., Eq.(4.27)) and proving the existence and uniqueness of the solution \hat{f} , we shall prove that \hat{f} converges to the solution of a continuous cell problem in certain subspace, e.g., $\mathbb{C}_0^{6,\alpha}(\tilde{Y})$. We remark that in the remaining part of the proof, we shall choose the space $\mathbb{C}_0^{6,\alpha}(\tilde{Y})$ to carry out our analysis. However there is no requirement that we have to choose this space. In fact, any space that has certain regularity (belongs to the domain of the operator \mathcal{L}) will work. To start with, we define the following continuous cell problem

$$\mathcal{L}\chi_1 = f, \quad (4.30)$$

where the operator \mathcal{L} is defined in Eq.(4.6). Given f is a smooth function defined on \tilde{Y} with zero mean, the Eq.(4.30) admits a unique solution χ_1 in $\mathbb{C}_0^{6,\alpha}(\tilde{Y})$. This is a standard result of elliptic PDEs in Hölder space (see, e.g., the Theorem 6.5.3 in [34]). Moreover, \mathcal{L} is a bijection between two Banach spaces $\mathbb{C}_0^{6,\alpha}(\tilde{Y})$ and $\mathbb{C}_0^{4,\alpha}(\tilde{Y})$, and its inverse is bounded. Integrating Eq.(4.30) along time gives,

$$\exp(\Delta t \mathcal{L})\chi_1 - \chi_1 = f\Delta t + O(\Delta t^2) := \Delta t \bar{f}, \quad (4.31)$$

where $\bar{f} = f + O(\Delta t)$. Combining Eqs.(4.27) and (4.31), we obtain

$$\exp(\Delta t \mathcal{L})\chi_1 - I_{\Delta t} \hat{f} - (\chi_1 - \hat{f}) = \Delta t(\bar{f} - f) \quad (4.32)$$

Eq.(4.32) shows the connection between χ_1 and \hat{f} . After some simple calculations, we get

$$\mathcal{L}(\chi_1 - \hat{f}) = (\mathcal{L} - \tilde{L}_1)(\chi_1 - \hat{f}) + \tilde{L}_2 \hat{f} + (\bar{f} - f), \quad (4.33)$$

where

$$\tilde{L}_1 := \frac{\exp(\Delta t \mathcal{L}) - I_d}{\Delta t}, \quad \text{and} \quad \tilde{L}_2 := \frac{I_{\Delta t} - \exp(\Delta t \mathcal{L})}{\Delta t}. \quad (4.34)$$

One can easily verify that in the space of bounded linear operators from $\mathbb{C}_0^{6,\alpha}(\tilde{Y})$ to $\mathbb{C}_0^{4,\alpha}(\tilde{Y})$, there is a strong convergence in the operator norm,

$$\tilde{L}_1 - \mathcal{L} = O(\Delta t) \quad \text{as } \Delta t \rightarrow 0. \quad (4.35)$$

Then for the operator \tilde{L}_2 , by using the BCH formula (4.8) we can obtain,

$$\begin{aligned} \tilde{L}_2 &\rightarrow \frac{\exp\left(\frac{\Delta t^2}{2}([L_3, L_2] + [L_2, L_1] + [L_3, L_1]) + O(\Delta t^3)\right) - I_d}{\Delta t} \cdot \exp(\Delta t \mathcal{L}) \\ &\rightarrow \frac{\Delta t}{2}([L_3, L_2] + [L_2, L_1] + [L_3, L_1]) + O(\Delta t^2). \end{aligned} \quad (4.36)$$

Denoting $\tilde{L}_3 := \tilde{L}_1 + \tilde{L}_2 \equiv \frac{I_{\Delta t} - I_d}{\Delta t}$, we have $\tilde{L}_3 \rightarrow \mathcal{L}$ in $\mathcal{B}(\mathbb{C}_0^{6,\alpha}(\tilde{Y}), \mathbb{C}_0^{4,\alpha}(\tilde{Y}))$.

Then applying the Proposition 4.2, we get,

$$\lim_{\Delta t \rightarrow 0} \hat{f} = \lim_{\Delta t \rightarrow 0} \tilde{L}_3^{-1} f = \mathcal{L}^{-1} f = \chi_1. \quad (4.37)$$

In addition, combining the results of the Eqns.(4.31), (4.35), (4.36) and (4.37) for the right hand side of Eq.(4.33), we know that when Δt small enough

(does not depend on the total computational time T , but may depend on the estimate of f , g and σ), the following convergence estimate holds

$$\chi_1 - \hat{f} = O(\Delta t). \quad (4.38)$$

Based on the conclusions discussed above, we obtain the convergence estimate of the discrete-type cell problem. We summarize our result into a lemma as follows.

Lemma 4.2. *When $\Delta t \rightarrow 0$, the solution \hat{f} to the discrete-type cell problem converges to the solution χ_1 to the cell problem in $\mathbb{C}_0^{p,\alpha}$, at the rate of $O(\Delta t)$, where $p \geq 6$ and $0 < \alpha < 1$.*

4.2.4 Convergence estimate for the effective diffusivity

We shall show the main estimates in this section. We first prove that the second-order moment of the solution obtained by using our numerical scheme has an (at most) linear growth rate. Secondly, we provide the convergence rate of our method in computing the effective diffusivity.

Theorem 4.1. *Let $X_n^{\Delta t} = (p_n, q_n)$ denote the solution of the passive tracer model (4.1) obtained by using our numerical scheme with time-step Δt . If the Hamiltonian $H(p, q)$ is separable, periodic and smooth enough (in order to guarantee the existence and uniqueness of the solution to the SDE (4.1)), then we can prove that the second-order moment of the solution $X_n^{\Delta t}$ (a discrete Markov process) is at most linear growth, i.e.,*

$$\max_n \left\{ \mathbb{E} \frac{\|X_n^{\Delta t}\|^2}{n} \right\} \text{ is bounded.} \quad (4.39)$$

Proof. We first estimate the second-order moment of the first component of $X_n^{\Delta t} = (p_n, q_n)$, since the other one can be estimated in the same manner. Simple calculations show that

$$\begin{aligned} E[p_n^2 | (p_{n-1}, q_{n-1})] &= E(p_{n-1} - f(q_{n-1})\Delta t + \sigma N_{i-1}^p)^2 \\ &= E p_{n-1}^2 + \Delta t (\sigma^2 - 2E[p_{n-1}f(q_{n-1})]) + \Delta t^2 E f^2(q_{n-1}). \end{aligned} \quad (4.40)$$

We should point out that the term $E[p_{n-1}f(q_{n-1})]$ corresponds to the convection enhanced level of the diffusivity. Our goal is to prove that the term $E[p_{n-1}f(q_{n-1})]$ is bounded over n , though it may depend on f , g and σ . We now directly compute the contribution of the term $E[p_{n-1}f(q_{n-1})]$ to the effective diffusivity with the help of Eq.(4.28),

$$\Delta t \sum_{i=0}^{n-1} E[p_i f(q_i)] = \sum_{i=0}^{n-1} E[p_i (E[\hat{f}(X_{i+1})|X_i] - \hat{f}(X_i))]. \quad (4.41)$$

Let \mathcal{F}_i denote the filtration generated by the solution process until X_i . Notice that $p_i \in \mathcal{F}_i$, for the Eq.(4.41), we have

$$\begin{aligned} RHS &= \sum_{i=0}^{n-1} E[p_i (\hat{f}(X_{i+1}) - \hat{f}(X_i))] \\ &= \sum_{i=1}^n E[\hat{f}(X_i)(p_{i-1} - p_i)] - \hat{f}(X_0)p_0 + E[\hat{f}(X_n)p_n] \\ &= \sum_{i=1}^n E[\hat{f}(X_i)(f(p_{i-1})\Delta t - \sigma N_{i-1}^p)] - \hat{f}(X_0)p_0 + E[\hat{f}(X_n)p_n]. \end{aligned} \quad (4.42)$$

Hence,

$$\begin{aligned} \frac{1}{n} E[p_n^2|(p_0, q_0)] &= \frac{1}{n} p_0^2 + \Delta t \sigma^2 - 2\Delta t \frac{1}{n} \sum_{i=0}^{n-1} E[p_i f(q_i)] + (\Delta t)^2 \frac{1}{n} \sum_{i=0}^{n-1} E f^2(q_i) \\ &= \frac{1}{n} p_0^2 + \Delta t \sigma^2 + (\Delta t)^2 \frac{1}{n} \sum_{i=0}^{n-1} E f^2(q_i) - \frac{2}{n} \sum_{i=1}^n E[\hat{f}(X_i)(f(q_{i-1})\Delta t - \sigma N_{i-1}^p)] \\ &\quad - \frac{2}{n} (\hat{f}(X_0)p_0 - E[\hat{f}(X_n)p_n]). \end{aligned} \quad (4.43)$$

Recall the fact that $X_n = (p_n, q_n)$ converges to the uniform measure in distribution. So given any continuous periodic function f^* , the Corollary 4.1 implies

$$\lim_{n \rightarrow \infty} E f^*(X_n) = \int_{\tilde{Y}} f^*(x) dx. \quad (4.44)$$

Furthermore, we have the estimate

$$\limsup_{n \rightarrow \infty} \frac{1}{n} \sum_{i=0}^n f^*(X_n) < \infty. \quad (4.45)$$

Applying the Cauchy-Schwartz inequality for the term $\frac{2}{n} \sum_{i=1}^n E[\hat{f}(X_i)(f(q_{i-1})\Delta t - \sigma N_{i-1}^p)]$ in Eq.(4.43) and replacing f^* by f^2 and \hat{f}^2 in Eq.(4.45), we can prove that $\frac{1}{n} E[p_n^2|(p_0, q_0)]$ is bounded. Repeat the same trick, we know that $\frac{1}{n} E[q_n^2|(p_0, q_0)]$ is also bounded. Thus, the assertion in Eq.(4.39) is proved. \square

In our numerical scheme (4.4), we first fix the time-step Δt and use it to compute the effective diffusivity until the result converges to a constant, which may depend on Δt . Next, we shall prove that the limit of the constant converges to the exact effective diffusivity of the original passive tracer model as Δt approaches zero. Namely, we shall prove that our numerical scheme is robust in computing the effective diffusivity.

Theorem 4.2. *Let p_n , $n = 0, 1, \dots$ be the numerical solution of the first component of the scheme (4.4) and Δt denote the time-step. We have the convergence estimate of the effective diffusivity as*

$$\lim_{n \rightarrow \infty} \frac{E p_n^2}{n \Delta t} = \sigma^2 - 2 \int_{\mathbb{T}^2} \chi_1 f + O(\Delta t), \quad (4.46)$$

where the constant in $O(\Delta t)$ does not depend on the computational time T .

Proof. We divide both sides of the Eq.(4.43) by Δt and obtain

$$\begin{aligned} \frac{1}{n \Delta t} E[p_n^2 | (p_0, q_0)] &= \frac{1}{n \Delta t} p_0^2 + \sigma^2 + \frac{\Delta t}{n} \sum_{i=0}^{n-1} E f^2(q_i) \\ &\quad - \frac{2}{n \Delta t} \sum_{i=1}^n E[\hat{f}(X_i)(f(q_{i-1})\Delta t - \sigma N_{i-1}^p)] \\ &\quad - \frac{2}{n \Delta t} (\hat{f}(X_0)p_0 - E[\hat{f}(X_n)p_n]) \end{aligned} \quad (4.47)$$

First, we notice that for a fixed Δt , the terms $\frac{1}{n \Delta t} p_0^2$ and $\frac{2}{n \Delta t} \hat{f}(X_0)p_0$ converge to zero as $n \rightarrow \infty$, where we have used the fact $\hat{f}(X_0)$ is bounded. Then, for a fixed Δt , we have

$$\lim_{n \rightarrow \infty} \frac{2}{n \Delta t} |E[\hat{f}(X_n)p_n]| \leq \lim_{n \rightarrow \infty} \frac{2}{\sqrt{n} \Delta t} \|\hat{f}\|_{\infty} E\left|\frac{p_n}{\sqrt{n}}\right| \leq \lim_{n \rightarrow \infty} \frac{1}{\sqrt{n} \Delta t} \|\hat{f}\|_{\infty} E\left[\frac{p_n^2}{n} + 1\right] = 0, \quad (4.48)$$

where the term $E[\frac{p_n^2}{n}]$ is bounded due to the Theorem 4.1 and $\|\hat{f}\|_{\infty} \rightarrow \|\chi_1\|_{\infty} < \infty$ due to the Lemma 4.2. Therefore, we only need to focus on the estimate of terms in the second line of Eq.(4.47), which correspond to the convection-enhanced diffusion effect. Notice that $\hat{f} \in \mathbb{C}^{6,\alpha}$, we compute the Ito-Taylor series approximation of $\hat{f}(X_i)$,

$$\begin{aligned} \hat{f}(X_i) &= \hat{f}(X_{i-1}) + \hat{f}_p(X_{i-1})(-f(q_{i-1})\Delta t + \sigma N_{i-1}^p) + \hat{f}_q(X_{i-1})(g(p_{i-1})\Delta t + \sigma N_{i-1}^q) \\ &\quad + \frac{1}{2}(\hat{f}_{pp}(X_{i-1}) + \hat{f}_{qq}(X_{i-1}))\sigma^2 \Delta t + O(\Delta t^2). \end{aligned} \quad (4.49)$$

Since $\hat{f} \rightarrow \chi_1$ in $\mathbb{C}_0^{6,\alpha}$, the truncated term $O(\Delta t^2)$ in Eq.(4.49) is uniformly bounded when Δt is small enough. Substituting the Taylor expansion of $\hat{f}(X_i)$ into the target term of our estimate, we get

$$\begin{aligned} E[\hat{f}(X_i)(f(q_{i-1})\Delta t - \sigma N_{i-1}^p)] &= E\left[\left(f(q_{i-1})\Delta t - \sigma N_{i-1}^p\right) \right. \\ &\quad \left. \left(\hat{f}(X_{i-1}) + \hat{f}_p(X_{i-1})(-f(q_{i-1})\Delta t + \sigma N_{i-1}^p) \right. \right. \\ &\quad \left. \left. + \hat{f}_q(X_{i-1})(g(p_{i-1})\Delta t + \sigma N_{i-1}^q) + \frac{1}{2}(\hat{f}_{pp}(X_{i-1}) + \hat{f}_{qq}(X_{i-1}))\sigma^2\Delta t + O(\Delta t^2)\right)\right]. \end{aligned} \quad (4.50)$$

Combining the terms with the same order of Δt , we obtain

$$E[\hat{f}(X_i)(f(q_{i-1})\Delta t - \sigma N_{i-1}^p)] = \Delta t E[\hat{f}(X_{i-1})f(q_{i-1}) - \sigma^2 \hat{f}_p(X_{i-1})] + O(\Delta t^2), \quad (4.51)$$

where we have used the facts that (1) X_{i-1} is independent with N_{i-1}^p and N_{i-1}^q so the expectations of the corresponding terms vanish; (2) N_{i-1}^p and N_{i-1}^q are independent so $E(N_{i-1}^p N_{i-1}^q) = 0$; and (3) $E(N_{i-1}^p)^2 = \Delta t$. Finally, by using the Corollary 4.1 and noticing the invariant measure is the uniform measure, we obtain from Eq.(4.47) that

$$\lim_{n \rightarrow \infty} \frac{1}{n\Delta t} E[p_n^2 | (p_0, q_0)] = \sigma^2 - 2 \int (\hat{f}f - \sigma^2 \hat{f}_p) + O(\Delta t). \quad (4.52)$$

Thus, our statement in the Eq.(4.46) is proved using the facts that \hat{f} converges to χ_1 (see Lemma 4.2) and $\int \hat{f}_p = 0$. \square

Remark 4.4. *If we divide two on both sides of the Eq.(4.46), we can find that our result recovers the definition of the effective diffusivity D_{11}^E defined in the Eq.(2.23).*

4.2.5 Generalizations to high-dimensional cases

To show the essential idea of our probabilistic approach, we have carried out our convergence analysis based on a two-dimensional model problem (4.1). In fact, the extension of our approach to higher-dimensional problems is straightforward. Now we consider a high-dimensional problem as follow,

$$dX_t = v(X_t)dt + \Sigma W_t, \quad (4.53)$$

where $X = (X^1, X^2, \dots, X^d)^T \in \mathbb{R}^d$ is the position of a particle, $v = (v^1, v^2, \dots, v^d)^T \in \mathbb{R}^d$ is the Eulerian velocity field at position X , Σ is a $d \times d$ constant non-singular matrix, and W_t is a d -dimension Brownian motion vector. In particular, we assume the v^i does not depend on X^i , $i = 1, \dots, d$. Thus, the incompressible condition for $v(X)$ (i.e. $\nabla_X \cdot v(X) = 0$) is easily guaranteed.

For a deterministic and divergence-free dynamic system, Feng et. al. proposed a volume-preserving method [20], which splits an n -dimensional problem into $n - 1$ subproblems with each of them being volume-preserving. We shall modify Feng's method (first order case) by including the randomness as the last subproblem to take into account the additive noise, i.e.,

$$\begin{cases} X^{1*} = X_0^1 + \Delta t v^1(X_0^1, X_0^2, X_0^3, \dots, X_0^{d-1}, X_0^d), \\ X^{2*} = X_0^2 + \Delta t v^2(X^{1*}, X_0^2, X_0^3, \dots, X_0^{d-1}, X_0^d), \\ \dots, \\ X^{d*} = X_0^d + \Delta t v^d(X^{1*}, X^{2*}, X^{3*}, \dots, X^{(d-1)*}, X_0^d), \\ X_1 = X^* + \Sigma(W_1 - W_0), \end{cases} \quad (4.54)$$

where $W_1 - W_0$ is represented by a d -dimensional independent random vector with each component of the form $\sqrt{\Delta t} \xi_i$, $\xi_i \sim \mathcal{N}(0, 1)$.

The techniques of the convergence analysis for two-dimensional problem can be applied to high-dimensional problems without much difficulty. For the high-dimensional problem (4.53), the smoothness and strict positivity of the transition kernel in the discrete process can be guaranteed if one assumes that the covariance matrix Σ is non-singular and the scheme (4.54) is explicit. According to our assumption for the velocity field, the scheme (4.54) is volume-preserving. Thus, the solution to the first-order modified equation is divergence-free and the invariant measure on the torus (defined by $\mathbb{R}^d/\mathbb{Z}^d$, when period is 1) remains uniform. Finally, the convergence of the cell problem can be studied by using the BCH formula (4.8) with $d + 1$ PDE operators. Recall that in the Eq.(4.9) we have three PDE operators when we study the two-dimensional problem. Therefore, our numerical methods are robust in computing effective diffusivity for high-dimensional problems, which will be

demonstrated through the three-dimensional chaotic flow problems in the Section 4.3.

4.3 Numerical results

The aim of this section is two-fold. First, we shall design challenging numerical examples to verify the convergence analysis proposed in Theorem 4.2, especially the Theorem 4.2. Secondly, we shall investigate the existence of residual diffusivity for several chaotic velocity fields. Without loss of generality, we compute the quantity $\frac{E[p(T)^2]}{2T}$, which is used to approximate D_{11}^E in the effective diffusivity matrix (2.23).

4.3.1 Verification of the convergence rate

We first consider a passive tracer model, where the velocity field is given by a chaotic cellular flow with oscillating vortices. Specifically, the flow is generated by a Hamiltonian defined as

$$H(p, q) = \frac{1}{2\pi} \exp(\sin(2\pi p)) - \frac{1}{4\pi} \exp(\cos(4\pi q + 1)). \quad (4.55)$$

The motion of a particle moving in this chaotic cellular flow is described by the SDE,

$$\begin{cases} dp = \sin(4\pi q + 1) \exp(\cos(4\pi q + 1)) dt + \sigma W_1, \\ dq = \cos(2\pi p) \exp(\sin(2\pi p)) dt + \sigma W_2, \end{cases} \quad (4.56)$$

where $\sigma = \sqrt{2 \times 0.01}$, W_i are independent Brownian motions, and the initial data (p_0, q_0) follows uniform distributions in $[-0.5, 0.5]^2$.

In our numerical experiments, we use Monte Carlo samples to discretize the Brownian motions W_1 and W_2 . The sample number is denoted by N_{mc} . We choose $\Delta t_{ref} = 0.001$ and $N_{mc} = 640,000$ to solve the SDE (4.56) and compute the reference solution, i.e., the ‘‘exact’’ effective diffusivity, where the final computational time is $T = 12000$ so that the calculated effective diffusivity

converges to a constant. It takes about 20 hours to compute the reference solution on a 64-core server (Gridpoint System at HKU). The reference solution for the effective diffusivity is $D_{11}^E = 0.12629$.

In Fig.4.1(a), we plot the convergence results of the effective diffusivity using our method (i.e., $\frac{E[p(T)^2]}{2T}$) with respect to different time-step Δt at $T = 6000$ and $T = 12000$. In addition, we show a fitted straight line with the slope 1.04, i.e., the convergence rate is about $(\Delta t)^{1.04}$. Meanwhile, by comparing two sets of data in the Fig.4.1(a), corresponding to the numerical effective diffusivity obtained at different computational times, we can see that error does not grow with respect to time, which justifies the statement in Theorem 4.2.

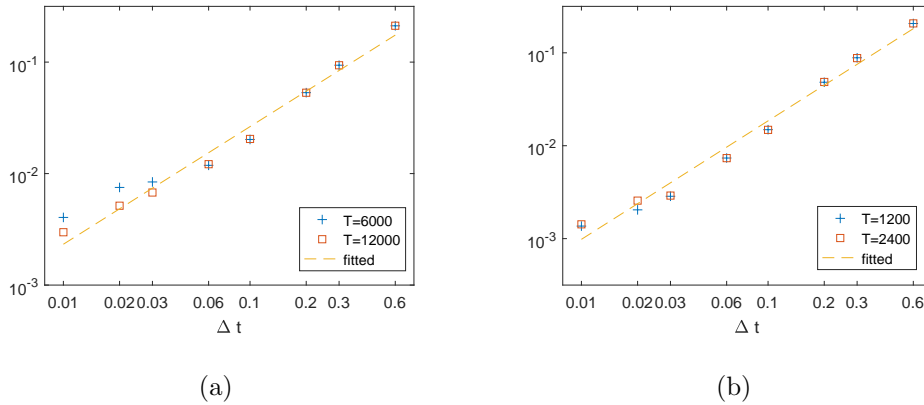


Figure 4.1: Error of D_{11}^E in different computational times and flows with different time-steps. Left: 2D chaotic cellular flow, fitted slope ≈ 1.04 ; right: 3D Kolmogorov-type flow, fitted slope ≈ 1.27 .

To further study the accuracy and robustness of our numerical method in solving high-dimensional problems, we consider a 3D Kolmogorov-type flow. Let $(p, q, r) \in \mathbb{R}^3$ denote the position of a particle in the 3D Cartesian coordinate system. The motion of a particle moving in the 3D Kolmogorov-type

flow is described by the following SDE,

$$\begin{cases} dp = \cos(4\pi r + 1) \exp(\sin(4\pi r + 1))dt + \sigma W_1, \\ dq = \cos(6\pi p + 2) \exp(\sin(6\pi p + 2))dt + \sigma W_2, \\ dr = \cos(2\pi q + 3) \exp(\sin(2\pi q + 3))dt + \sigma W_3, \end{cases} \quad (4.57)$$

where W_i are independent Brownian motions. This is inspired by the so-called Kolmogorov flow [23] (see Eq.(4.59)). The Kolmogorov flow is obtained from the Arnold-Beltrami-Childress (ABC) flow with $A = B = C = 1$ and with cosines taken out. Behaviors of the classic Kolmogorov flow will be discussed later.

In our numerical experiments, we choose $\Delta t_{ref} = 0.001$ and $N_{mc} = 6,400,000$ to solve the SDE (4.57) and compute the reference solution, i.e., the “exact” effective diffusivity. After some numerical tests, we find that the passive tracer model will enter a mixing stage if the computational time is set to be $T = 2400$. It takes about 56 hours to compute the reference solution on the server and the reference solution for the effective diffusivity is $D_{11}^E = 0.13106$.

In Fig. 4.1(b), we plot the convergence results of the effective diffusivity using our method with respect to different time-step Δt . In addition, we show a fitted straight line with the slope 1.27, i.e., the convergence rate is about $(\Delta t)^{1.27}$. This numerical result also agrees with our error analysis.

4.3.2 Investigation of the convection-enhanced diffusion phenomenon

We first consider the classical ABC flow with our symplectic stochastic integrators. The ABC flow is a three-dimensional incompressible velocity field which is an exact solution to the Euler’s equation. It is notable as a simple example of a fluid flow that can have chaotic trajectories. The particle is transported by the velocity field $V = (A \sin(r) + C \cos(q), B \sin(p) + A \cos(r), C \sin(q) + B \cos(p))$ and perturbed by an additive noise. The associ-

ated passive tracer model reads

$$\begin{cases} dp = (A \sin(r) + C \cos(q))dt + \sigma W_1, \\ dq = (B \sin(p) + A \cos(r))dt + \sigma W_2, \\ dr = (C \sin(q) + B \cos(p))dt + \sigma W_3, \end{cases} \quad (4.58)$$

where W_i are independent Brownian motions. In Fig.4.2, we show the relation between D_{11}^E and D_0 . Recall that the parameter $D_0 = \sigma^2/2$. By setting $A = B = C = 1$, we recover the same phenomenon as the Fig.2 in [5], for $D_0 \in [10^{-3}, 10^{-1}]$ and can extend to $D_0 \in [10^{-5}, 10^{-4}]$; see Fig.4.2. At the same time, we can see that the Euler method failed when D_0 is small, which is also confirmed in Section 3.3. The Fig.4.2 shows that the D_{11}^E of the ABC flow obtained by our symplectic method corresponds to upper-bound of Eq.(2.28), i.e. the maximal enhancement, $D_{11}^E \sim \mathcal{O}(1/D_0)$. This maximal enhancement phenomenon may be attributed to the ballistic orbits of the ABC flow, which was discussed in [39, 55].

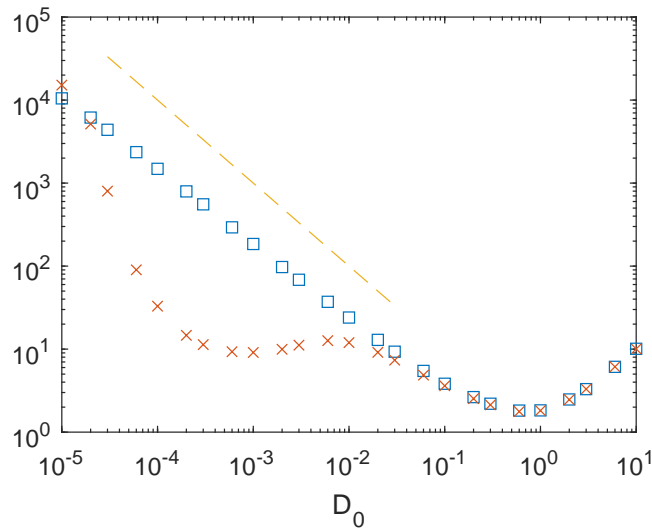


Figure 4.2: Convection-enhanced diffusion with maximal enhancement in ABC flow: \square for the symplectic scheme, \times for the Euler scheme, $--$ for reference line $y = \frac{1}{D_0}$.

From Fig.4.3(a) we can see that diffusing time, i.e., the time that $\frac{E[p(t)^2]}{2t}$ approaches a constant, increases as $\mathcal{O}(1/D_0)$ when $D_0 \rightarrow 0$ in the symplectic scheme. To the best of our knowledge, the $\mathcal{O}(1/D_0)$ scale of the diffusion

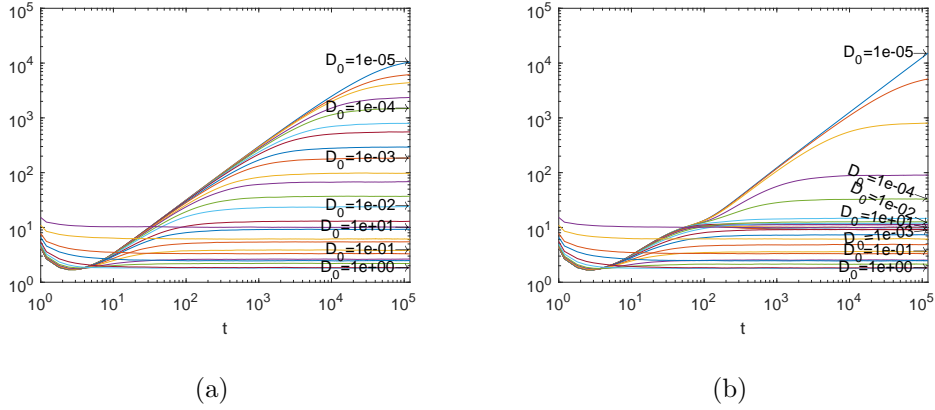


Figure 4.3: Calculated D_{11}^E in the ABC flow along time via two different schemes. Left: symplectic; right: Euler.

time of the ABC flow is not known before. Moreover, Fig.4.3(a) shows that our numerical scheme is very robust in computing the effective diffusivity for the ABC flow. However, the Euler scheme gives a wrong result in Fig.4.3(b) since the time $\frac{E[p(t)^2]}{2t}$ approaching a constant does not agree with the expected diffusion time $O(1/D_0)$. The statement that the Euler scheme will generate wrong results can also be found in the Fig.4.2.

We point out that the error estimate in Theorem 4.2 is just an upper bound. Fig.4.4 shows that when D_0 is 10^{-3} , the convergence rate is about $\mathcal{O}(\Delta t^{1.42})$. It is very expensive to study the passive tracer model for the ABC flow since the diffusing time is extremely long. In our numerical test for the Fig.4.4, we choose $N_{mc} = 120,000$, $\Delta t = 0.001$, and $T = 12,000$. In this setting, the error of the Monte Carlo simulation cannot be avoided, so there is a small oscillation around the fitted slope.

Finally, we investigate the convection-enhanced diffusion phenomenon for another chaotic flow, i.e., the Kolmogorov flow. The associated passive tracer model reads,

$$\begin{cases} dp = \sin(r)dt + \sigma W_1, \\ dq = \sin(p)dt + \sigma W_2, \\ dr = \sin(q)dt + \sigma W_3, \end{cases} \quad (4.59)$$

where W_i are independent Brownian motions. In Fig.4.5, we show the relation

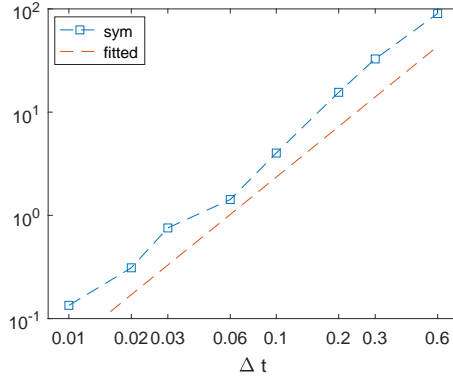


Figure 4.4: Error of D_{11}^E in the ABC flow, the dashed line with \square is for the symplectic scheme, and the slope of the fitted is ≈ 1.42 .

between D_{11}^E and D_0 , where $D_0 = \sigma^2/2$. For each D_0 , we use $N_{mc} = 120,000$ particles to solve the SDE (4.59) via the symplectic method and the Euler method with $\Delta t = 0.1$. The final computational time is $T = 12,000$ so that the particles are fully mixed for $D_0 \geq 10^{-6}$.

Under such setting, we find that the dependency of D_{11}^E on D_0 is quite different from the chaotic and stochastic flows that we have studied in Section 3.3 and from the foregoing ABC flow (maximal enhancement). The fitted slope within $D_0 \in [10^{-6}, 10^{-5}]$ is -0.13 , which indicates that $D_{11}^E \sim \mathcal{O}(1/D_0^{0.13})$. This can be called sub-maximal enhancement, which may be explained by the fact that the Kolmogorov flow is more chaotic than the ABC flow [23]. The chaotic trajectories in Kolmogorov flow enhance diffusion much less than channel like structures such as the ballistic orbits of ABC flows [39, 55]. More studies on the diffusion enhancement phenomenon of the ABC flow and the Kolmogorov flow, especially the time-dependent cases will be reported in our future work.

We also compare the performance of the symplectic scheme and Euler scheme in computing the effective diffusivity for the Kolmogorov flow. Specifically, we implement the symplectic scheme and Euler scheme with time step $\Delta t = 0.1$ and $\Delta t = 0.01$, respectively. In Fig.4.5, we find that (1) the symplectic scheme with $\Delta t = 0.1$ and $\Delta t = 0.01$ will give similar results in computing the effective diffusivity; (2) the symplectic scheme and the Euler scheme with $\Delta t = 0.01$ will give almost the same convergent results in computing the effec-

tive diffusivity, which provides evidence that our statement on the Kolmogorov flow (i.e., the sub-maximal enhancement phenomenon) is correct; (3) the Euler scheme with $\Delta t = 0.1$ gives wrong results but the symplectic scheme with $\Delta t = 0.1$ gives acceptable results, which provides evidence that the symplectic scheme is very robust in computing the effective diffusivity. In this example, the symplectic scheme approximately achieves a $10\times$ speedup over the Euler scheme.

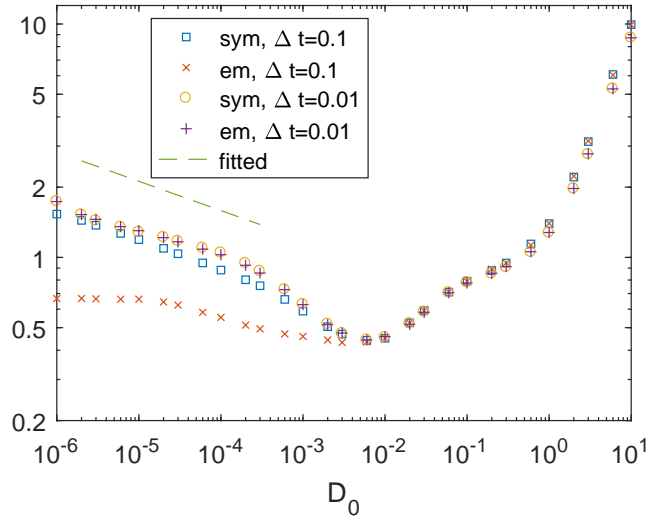


Figure 4.5: Convection-enhanced diffusion with sub-maximal enhancement in Kolmogorov flow. “sym” means the results for symplectic scheme and “em” means the results for Euler scheme. -- means the fitted line for small D_0 with slope ≈ -0.13 .

Fig.4.6(a) and Fig.4.6(b) show different behaviors of the numerical effective diffusivity $\frac{E[p(t)^2]}{2t}$ obtained using the symplectic scheme and the Euler scheme with respect to computational time. Specifically, Fig.4.6(a) shows $T = 12000$ is quite enough for $D_0 \geq 10^{-6}$. And in Fig.4.6(b), it seems that in Euler scheme, the diffusion time is much smaller. Our understanding is that the numerical diffusion in Euler scheme helps reach its own diffusion time earlier. In Fig.4.7, we also study the convergence rate of the symplectic scheme in computing the effective diffusivity for the Kolmogorov flow (4.59). We find that the convergence rate is $\mathcal{O}(\Delta t^{1.3})$ in this example.

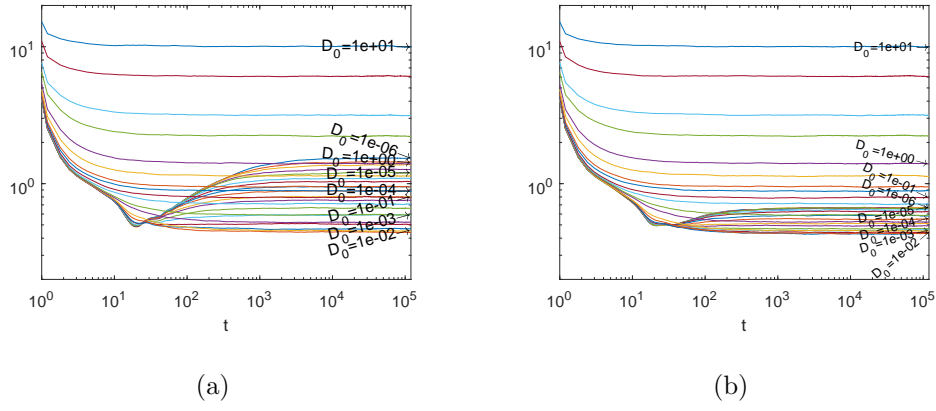


Figure 4.6: Calculated $D_{11}^E = \frac{E[p(t)^2]}{2t}$ in the Kolmogorov flow via two different schemes. Left: symplectic; right: Euler

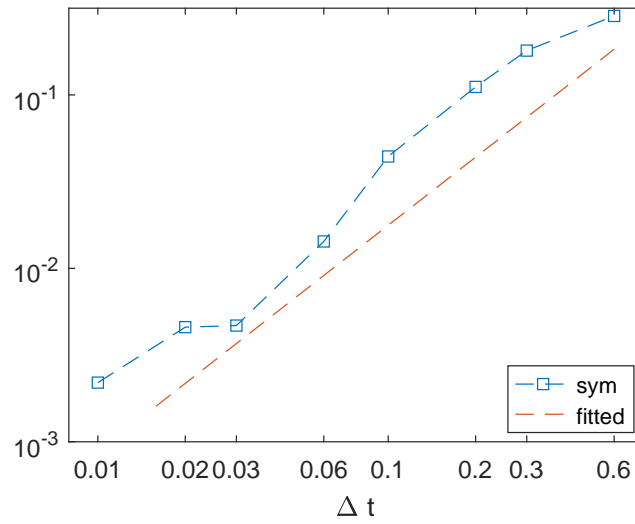


Figure 4.7: Error of D_{11}^E in the Kolmogorov flow. The slope of the fitted line is ≈ 1.3 .

Chapter 5

Sharp and Uniform in Time Error Analysis in Time-Dependent Flows

Comparing with Chapter 4, we will construct stochastic structure-preserving schemes for a two-dimensional passive tracer model in separable incompressible flow. This is because in time-dependent case, velocity field defined by $\nabla^\perp H$ does not preserve the Hamiltonian. The structure in this chapter is similar to Chapter 4, but the proof and the numerical phenomenon in time-dependent flow are different from ones in time-independent cases. On one hand, we will focus on the distinctness. On the other hand, we will retain the main definition and derivation for courtesy of readers directly starting from this chapter.

Remark 5.1. *Generalization of Eq.2.23 can be obtained as follows. First we define, the (vector) corrector field $\chi(x)$ satisfies the cell problem,*

$$-D_0\Delta\chi - v(\tau, y) \cdot \nabla\chi = v(\tau, y), \quad (\tau, y) \in \mathbb{T} \times \mathbb{T}^d, \quad (5.1)$$

Then

$$D^E = D_0I - \langle v \otimes \chi \rangle_p, \quad (5.2)$$

and $\langle \cdot \rangle_p$ denotes temporal and spatial average over $\mathbb{T} \times \mathbb{T}^d$.

5.1 Stochastic structure-preserving schemes

5.1.1 Derivation of numerical schemes

Let $X = (x^1, x^2)^T$ denote the position of the particle, then the model can be written as

$$\begin{cases} dx^1 = v_1 dt + \sigma dW_{1,t}, & x^1(0) = x_0^1, \\ dx^2 = v_2 dt + \sigma dW_{2,t}, & x^2(0) = x_0^2, \end{cases} \quad (5.3)$$

where $dW_{i,t}$, $i = 1, 2$ are independent Brownian motions. We assume that $v = (v_1, v_2)^T$ is divergence free and mean-zero at any time t , i.e.,

$$\nabla \cdot v := \partial_{x^1} v_1 + \partial_{x^2} v_2 = 0 \quad \forall t, \quad (5.4)$$

and

$$\begin{cases} \int_{\mathbb{T}} v_1(t, x^1, x^2) dx^2 = 0 & \forall x^1, t, \\ \int_{\mathbb{T}} v_2(t, x^1, x^2) dx^1 = 0 & \forall x^2, t, \end{cases} \quad (5.5)$$

where $\mathbb{T} = [0, 1]$ is the one dimensional period space. We assume that the diagonal of the Jacobian of the velocity field $v = (v_1, v_2)^T$ are all zeros for all $t \in \mathbb{T}$. We also assume the spacial mean of v_1 and v_2 is zero for all $t \in \mathbb{T}$.

Similar to Section 4.1.1, we proposed a stochastic structure-preserving scheme based on a Lie-Trotter splitting idea to solve the SDE (5.3). Specifically, we split the problem (5.3) into a deterministic subproblem,

$$\begin{cases} dx^1 = v_1(t, x^2) dt, \\ dx^2 = v_2(t, x^1) dt, \end{cases} \quad (5.6)$$

which is solved by using a symplectic-preserving scheme (e.g., the symplectic Euler scheme for deterministic equations with frozen time), and a stochastic subproblem,

$$\begin{cases} dx^1 = \sigma dW_{1,t}, \\ dx^2 = \sigma dW_{2,t}, \end{cases} \quad (5.7)$$

which is solved by using the Euler-Maruyama scheme [42]. Notice that when σ is a constant in (5.7), the Euler-Maruyama scheme is exact.

Now we discuss how to discretize Eq.(5.3). From time $t = t_n$ to time $t = t_{n+1}$, where $t_{n+1} = t_n + \Delta t$, $t_0 = 0$, and Δt is the time step, we assume the numerical solution $X_n = (x_n^1, x_n^2)^T$ is given, which approximates the exact solution $X(n\Delta t)$ to the SDE (5.3). Then, we apply the Lie-Trotter splitting method to solve the SDE (5.3) and obtain,

$$\begin{cases} x_{n+1}^1 = x_n^1 + v_1(t_{n+\frac{1}{2}}, x_n^2)\Delta t + \sigma N_n^1, \\ x_{n+1}^2 = x_n^2 + v_2(t_{n+\frac{1}{2}}, x_n^1 + v_1(t_{n+\frac{1}{2}}, x_n^2)\Delta t)\Delta t + \sigma N_n^2, \end{cases} \quad (5.8)$$

where $t_{n+\frac{1}{2}} = t_n + \frac{\Delta t}{2}$, $N_n^1 = \sqrt{\Delta t}\xi_1$, $N_n^2 = \sqrt{\Delta t}\xi_2$, and $\xi_1, \xi_2 \sim \mathcal{N}(0, 1)$ are i.i.d. normal random variables. The numerical solution converges to the exact one as the time step Δt approaches zero.

5.1.2 The backward Kolmogorov equation and related results

We first define the backward Kolmogorov equation associated with the Eq.(5.3) as

$$u_t = \mathcal{L}u, \quad u(0, \tau, x) = \phi(\tau, x), \quad (5.9)$$

where the generator \mathcal{L} associated with the Markov process in Eq.(5.3) is given by

$$\mathcal{L} = \partial_\tau + v_1(\tau, x^2)\partial_{x^1} + v_2(\tau, x^1)\partial_{x^2} + \frac{1}{2}\sigma^2(\partial_{x^1}^2 + \partial_{x^2}^2). \quad (5.10)$$

Recall that the solution $u(t, \tau, x)$ to the Eq.(5.9) satisfies, $u(t, \tau, x) = \mathbb{E}(\phi(t + \tau, X_{t+\tau})|X_\tau = x)$ where X_t is the solution to Eq.(5.3) and ϕ is a smooth function in $\mathbb{R}^1 \times \mathbb{R}^2$. In other words, $u(t, \tau, x)$ is the flow generated by the original SDE (5.3).

Similarly, we can study the flow generated by the stochastic structure-preserving scheme (5.8). According to the splitting method used in the derivation of the scheme in Section 5.1.1, we respectively define $\mathcal{L}_1 = \partial_\tau$, $\mathcal{L}_2 = v_1\partial_{x^1}$,

$\mathcal{L}_3 = v_2 \partial_{x^2}$, and $\mathcal{L}_4 = \frac{\sigma^2}{2}(\partial_{x^1 x^1} + \partial_{x^2 x^2})$. Starting from $u(0, \cdot, \cdot)$, during one time step Δt , we compute

$$\begin{cases} \partial_t u^1 = \mathcal{L}_1 u^1, & u^1(0, \cdot, \cdot) = u(0, \cdot, \cdot), \\ \partial_t u^2 = \mathcal{L}_2 u^2, & u^2(0, \cdot, \cdot) = u^1(\frac{\Delta t}{2}, \cdot, \cdot), \\ \partial_t u^3 = \mathcal{L}_3 u^3, & u^3(0, \cdot, \cdot) = u^2(\Delta t, \cdot, \cdot), \\ \partial_t u^4 = \mathcal{L}_1 u^4, & u^4(0, \cdot, \cdot) = u^3(\Delta t, \cdot, \cdot), \\ \partial_t u^5 = \mathcal{L}_4 u^5, & u^5(0, \cdot, \cdot) = u^4(\frac{\Delta t}{2}, \cdot, \cdot). \end{cases} \quad (5.11)$$

Then, $u^5(\Delta t, \cdot, \cdot)$ will be the flow at time $t = \Delta t$ generated by our stochastic structure-preserving scheme (5.8) and it approximates the solution $u(\Delta t, \cdot, \cdot)$ to the Eq.(5.9) well when Δt is small. It is also worth mentioning that, $u^3(\Delta t, \cdot, \cdot)$ is the exact flow generated by the deterministic symplectic Euler scheme in solving Eq.(5.6). We repeat this process to compute the flow equations of our scheme at other time steps, which approximate the solution $u(n\Delta t, \cdot, \cdot)$, $n = 2, 3, \dots$ to the Eq.(5.9) at different time steps.

Remark 5.2. *Given the operators \mathcal{L}_i , $i = 1, 2, 3, 4$, there are many possible choices in setting the coefficients for each operator \mathcal{L}_i and designing the splitting method; see Section 2.5 of [27]. Eq.(5.11) is a simple choice that was used for the scheme in this chapter.*

Similar to time-independent cases in Chapter 4, to analyze the error between the flow operator in Eq.(5.9) and the composited operator in Eq.(5.11), we shall resort to the Baker-Campbell-Hausdorff (BCH) formula. We replace the matrices in Eq.(4.8) by differential operators and the BCH formula yields critical insights into the particular structure of the splitting error. Let $I_{\Delta t}$ denote the composited flow operator associated with Eq.(5.11), i.e.,

$$I_{\Delta t} u(0, \cdot, \cdot) := \exp(\Delta t \mathcal{L}_4) \exp(\frac{\Delta t}{2} \mathcal{L}_1) \exp(\Delta t \mathcal{L}_3) \exp(\Delta t \mathcal{L}_2) \exp(\frac{\Delta t}{2} \mathcal{L}_1) u(0, \cdot, \cdot). \quad (5.12)$$

Notice that after propagating time $t = \Delta t$, the exact solution to the Eq.(5.9) started at any τ can be represented as

$$u(\Delta t, \cdot, \cdot) = \exp(\Delta t \mathcal{L}) u(0, \cdot, \cdot) = \exp(\Delta t (\mathcal{L}_1 + \mathcal{L}_2 + \mathcal{L}_3 + \mathcal{L}_4)) u(0, \cdot, \cdot). \quad (5.13)$$

Therefore, we can apply the BCH formula to analyze the error between the original flow and the approximated flow. Moreover, we find that computing the k -th order modified equation associated with Eq.(5.3) in the backward error analysis (BEA)[46] is equivalent to computing the terms of BCH formula up to order $(\Delta t)^k$ in the Eq.(5.12). To show that the solution generated by Eq.(5.8) follows a perturbed Hamiltonian system (with divergence free velocity and additive noise) at any order p , we only need to consider the $(p+1)$ -nested Lie bracket consists of $\{\partial_\tau, v_1\partial_{x^1}, v_2\partial_{x^2}, \frac{\sigma^2}{2}(\partial_{x^1x^1} + \partial_{x^2x^2})\}$ and we can easily see that they will not generate non-divergence free field.

We remark that given any explicit splitting scheme for deterministic systems, by adding additive noise we shall obtain a similar form of flow propagation. And we shall see in later proof that, such operator formulation is very effective in analyzing the order of convergence and volume-preserving property.

5.2 Convergence analysis

We can view the Eq.5.11 as a modification of Eq.5.11. While, the velocity in τ direction is mean 1 and the diffusion is degenerated. So there will be huge difference in convergence analysis. This is also the case in comparing parabolic equation to elliptic equation.

5.2.1 Convergence to an invariant measure

To compute the effective diffusivity of a passive tracer model using a Lagrangian numerical scheme is closely related to study the limit of a solution sequence (a stochastic process) generated by the numerical scheme. Therefore, we can apply the results from ergodic theory to study the convergence behaviors of the solution. We first prove a lemma as follows.

Lemma 5.1. *Let $\tilde{Y} = \mathbb{R}^d/\mathbb{Z}^d$ denote the physical torus space and \mathbb{T} be the time periodic space. Let $I_{\tau,1+\tau}^*$ denote the transform of the density on \tilde{Y} during*

$[\tau, 1 + \tau]$ (time period is 1) using the numerical scheme (5.8). In addition, let $I_{\tau, 1+\tau}$ denote the adjoint operator (i.e., the flow operator) of $I_{\tau, 1+\tau}^*$ in the space of $\mathcal{B}(\tilde{Y})$, which is the set of bounded measurable functions on \tilde{Y} . Then, there exists one and only one invariant probability measure on (\tilde{Y}, Σ) , denoted by π_τ , satisfying,

$$\sup_{x \in \tilde{Y}} \left| \left((I_{\tau, 1+\tau})^n \phi \right)(x) - \int \phi(x') \pi_\tau(dx') \right| \leq C \|\phi\|_{L_\infty} e^{-\rho n}, \quad \forall \phi \in \mathcal{B}(\tilde{Y}), \quad (5.14)$$

where $\rho > 0$, $C > 0$ are independent of $\phi(\cdot)$. Moreover, the kernel space of $(I_d - I_{\tau, 1+\tau})$ is the constant functions in \tilde{Y} , where I_d is the identity operator.

Proof. We shall verify that the transition kernel associated with the numerical scheme (5.8) satisfies the assumptions required by Prop. 2.3. First notice that in the space \mathbb{R}^2 , the integration process associated with the numerical scheme (5.8) can be expressed as a Markov process with the transition kernel,

$$K_t(X_n, X_{n+1}) = \frac{1}{2\pi\sigma^2\Delta t} \exp \left(- \frac{\left(x_{n+1}^1 - x_n^1 - v_1 \left(t + \frac{\Delta t}{2}, x_n^2 \right) \Delta t \right)^2 + \left(x_{n+1}^2 - x_n^2 - v_2 \left(t + \frac{\Delta t}{2}, x_{n+1}^1 - x_n^1 - v_1 \left(t + \frac{\Delta t}{2}, x_n^2 \right) \Delta t \right) \Delta t \right)^2}{2\sigma^2\Delta t} \right), \quad (5.15)$$

where $X_n = (x_n^1, x_n^2)^T$ and $X_{n+1} = (x_{n+1}^1, x_{n+1}^2)^T$ are the numerical solutions at time $t = t_n$ and $t = t_{n+1}$, respectively.

Then, using the periodicity of v , we directly extend Eq.(5.15) to the torus space \tilde{Y} as

$$\tilde{\mathbf{K}}_\tau(X_n, X_{n+1}) = \sum_{i, j \in \mathbb{Z}} \frac{1}{2\pi\sigma^2\Delta t} \exp \left(- \frac{\left(x_{n+1}^1 + i - x_n^1 - v_1 \left(\tau + \frac{\Delta t}{2}, x_n^2 \right) \Delta t \right)^2 + \left(x_{n+1}^2 + j - x_n^2 - v_2 \left(\tau + \frac{\Delta t}{2}, x_{n+1}^1 - x_n^1 - v_1 \left(\tau + \frac{\Delta t}{2}, x_n^2 \right) \Delta t \right) \Delta t \right)^2}{2\sigma^2\Delta t} \right). \quad (5.16)$$

Let $\tilde{\mathbf{K}}_{\tau, \tau+k\Delta t}$ denote the kernel from τ to $\tau + k\Delta t$, which is the density of the transition kernel associated with applying our scheme starting from time τ for k steps. Then, we have

$$\tilde{\mathbf{K}}_{\tau, \tau+k\Delta t}(X_0, X_k) = \int_{(\tilde{Y})^{k-1}} \prod_{m=0}^{k-1} \tilde{\mathbf{K}}_{\tau+m\Delta t}(X_m, X_{m+1}) dX_1 dX_2 \cdots dX_{k-1}. \quad (5.17)$$

We choose $k = \frac{1}{\Delta t}$ and obtain $\tilde{\mathbf{K}}_{\tau, \tau+1}$. One can see that the kernel $\tilde{\mathbf{K}}_{\tau, \tau+1}$ is essentially bounded above zero since $\tilde{\mathbf{K}}_{\tau+m\Delta t}$ in (5.17) are all positive. Moreover, if $0 < \Delta t \ll 1$, $\tilde{\mathbf{K}}_{\tau, \tau+1}$ is a continuous function on the domain $\tilde{Y} \times \tilde{Y}$. Then by noticing that the domain $\tilde{Y} \times \tilde{Y}$ is compact, the kernel $\tilde{\mathbf{K}}_{\tau, \tau+1}$ is strictly positive. Namely, there exists $\delta_\tau > 0$ such that $\tilde{\mathbf{K}}_{\tau, \tau+1}(X_0, X_k) > \delta_\tau, \forall (X_0, X_k) \in \tilde{Y} \times \tilde{Y}$. If we apply Prop.2.3 to $I_{\tau, 1+\tau}$ (whose kernel is $\tilde{\mathbf{K}}_{\tau, \tau+1}$), we prove the statement in (5.14).

Finally, we know that the operator $I_{\tau, 1+\tau}$ is compact since it is an integral operator with a continuous kernel. By using the Fredholm alternative, we know that $\dim \ker(I_d - I_{\tau, 1+\tau}) = \dim \ker(I_d - I_{\tau, 1+\tau}^*) = 1$. Therefore, it is easy to verify that the constant functions are in the kernel of $I_d - I_{\tau, 1+\tau}$. \square

Equipped with the Lemma 5.1, we study the convergence rate of the space-time transition kernel associated with our numerical scheme (5.8).

Theorem 5.1. *Let $\Delta t = \frac{1}{N}$, N is a positive integer. We have the following properties hold:*

(a) *Given Δt , there exists $C > 0$ and $\rho > 0$, such that,*

$$\sup_{\tau, x} \left| (I_{\Delta t}^N)^n \phi(\tau, x) - \int \phi(\tau, x') \pi_\tau(dx') \right| \leq C \|\phi\|_{L^\infty} e^{-\rho n}, \quad \forall \phi \in \mathcal{B}(\mathbb{T} \times \tilde{Y}), \quad (5.18)$$

where C and ρ do not depend on ϕ and τ .

(b) *If $\int_{\tilde{Y}} \phi \pi_\tau = 0$, then we get*

$$\lim_{n \rightarrow \infty} \sum_{i=1}^n E\phi(\tau, X_{N\tau+i}) < \infty, \quad \forall \tau \in \mathbb{T}. \quad (5.19)$$

(c) *The kernel space of $(I_d - I_{\Delta t}^N)$ is $\{c(\tau) \mid c(\tau) \text{ is a periodic function in } \mathbb{T} \text{ with period } 1\}$.*

Proof. By definition of $I_{\Delta t}$ and $I_{\tau, 1+\tau}$ in Eq.(5.12) and Lemma 5.1, we have $(I_{\Delta t})^N \phi(\tau, \cdot) \equiv I_{\tau, 1+\tau} \phi(\tau, \cdot)$. To prove the property (a), we need to show that the lower bound of the kernel $\tilde{\mathbf{K}}_{\tau, \tau+1}$, which is defined in the proof of Lemma 5.1, does not depend on τ . For all $\tau \in \mathbb{T}$, $X_n = (x_n^1, x_n^2)^T \in \mathbb{T}^2$ and

$X_{n+1} = (x_{n+1}^1, x_{n+1}^2)^T \in \mathbb{T}^2$, we pick $i_0 = \lfloor -x_{n+1}^1 + x_n^1 + v_1(\tau + \frac{\Delta t}{2}, x_n^2)\Delta t \rfloor$ and $j_0 = \lfloor -x_{n+1}^2 + x_n^2 + v_2(\tau + \frac{\Delta t}{2}, x_{n+1}^1 - x_n^1 - v_1(\tau + \frac{\Delta t}{2}, x_n^2)\Delta t)\Delta t \rfloor$, where $\lfloor a \rfloor$ denotes the largest integer not greater than a . Applying to Eq.(5.16), we can see that

$$\begin{aligned} \tilde{\mathbf{K}}_\tau(X_n, X_{n+1}) &\geq \frac{1}{2\pi\sigma^2\Delta t} \cdot \\ &\exp\left(-\frac{\left(x_{n+1}^1+i_0-x_n^1-v_1(\tau+\frac{\Delta t}{2},x_n^2)\Delta t\right)^2+\left(x_{n+1}^2+j_0-x_n^2-v_2(\tau+\frac{\Delta t}{2},x_{n+1}^1-x_n^1-v_1(\tau+\frac{\Delta t}{2},x_n^2)\Delta t)\Delta t\right)^2}{2\sigma^2\Delta t}\right) \\ &\geq \frac{1}{2\pi\sigma^2\Delta t} \exp\left(-\frac{1}{\sigma^2\Delta t}\right) > 0. \end{aligned} \quad (5.20)$$

According to the definition of the kernel $\tilde{\mathbf{K}}_{\tau,\tau+1}$; see Eq.(5.17), we know the minimal value of $\tilde{\mathbf{K}}_{\tau,\tau+1}$ is above zero and is independent of τ . Now, we apply this observation to Lemma 5.1 and conclude the proof of the property (a). The property (b) is a simple conclusion of the exponential decay property proved in (a). For the property (c), we consider the equation $I_{\Delta t}^N w = w$. Then, for a given time τ , we have $I_{\tau,1+\tau} w(\tau, \cdot) = w(\tau, \cdot)$. Notice the fact that in Lemma 5.1 the invariant space of $I_{\tau,1+\tau}$ is constant in the spacial variable. Thus, we obtain $w = w(\tau)$. \square

5.2.2 A discrete-type cell problem

In the Eulerian framework, the periodic solution of the cell problem (5.1) and the corresponding formula for the effective diffusivity (5.2) play a key role in studying the behaviors of chaotic and stochastic flows. In the Lagrangian framework, we shall define a discrete analogue of cell problem that enables us to compute the effective diffusivity. We revisit the scheme (5.8),

$$\begin{cases} x_n^1 = x_{n-1}^1 + v_1(t_{n-\frac{1}{2}}, x_{n-1}^2)\Delta t + \sigma N_{n-1}^1, \\ x_n^2 = x_{n-1}^2 + v_2(t_{n-\frac{1}{2}}, x_{n-1}^1 + v_1(t_{n-\frac{1}{2}}, x_{n-1}^2)\Delta t)\Delta t + \sigma N_{n-1}^2, \end{cases} \quad (5.21)$$

where $N_{n-1}^1 = \sqrt{\Delta t}\xi_1$, $N_{n-1}^2 = \sqrt{\Delta t}\xi_2$, and $\xi_1, \xi_2 \sim \mathcal{N}(0, 1)$ are i.i.d. normal random variables. For convenience we have replaced $n+1$ by n .

First of all, we show that the solutions x_n^1 and x_n^2 obtained by the scheme (5.21) have bounded expectations if the initial values are bounded. Taking

expectation of the first equation of Eq.(5.21) on both sides, we obtain

$$Ex_n^1 = Ex_{n-1}^1 + \Delta t Ev_1(t_{n-\frac{1}{2}}, x_{n-1}^2) = Ex_0^1 + \Delta t \sum_{k=0}^{n-1} Ev_1(t_{k+\frac{1}{2}}, x_k^2). \quad (5.22)$$

Applying the result (b) of Theorem 5.1 and using the fact that v is a periodic function with zero mean, we know that,

$$\sup_{X_0 \in \tilde{Y}} |Ev_1(t_{k+\frac{1}{2}}, X_k)| \leq e^{-\rho k} C_N \sup_{m=1,2,\dots,N, x \in \mathbb{T}^d} \|v_1(t_{m+\frac{1}{2}}, x)\|_\infty. \quad (5.23)$$

By applying triangle inequalities in Eq.(5.22) and using the result in Eq.(5.23), we arrive at,

$$|Ex_n^1| \leq |Ex_0^1| + C_1 \|v_1\|_\infty, \quad (5.24)$$

where C_1 does not depend on n . Using the same approach, we know that expectation of the second component Ex_n^2 is also bounded.

Now, we are in the position to define the discrete-type cell problem. Starting at time τ with time step $\Delta t = \frac{1}{N}$, we denote the starting time index to be $N\tau$. Then, we define

$$\hat{v}_{1,N}(\tau, x) = \Delta t \sum_{i=0}^{\infty} E[v_1(t_{i+\frac{1}{2}} + \tau, X_{N\tau+i}) | X_{N\tau} = x], \quad (5.25)$$

where the summation is well defined due to the fact stated in Eq.(5.23). We will show that $\hat{v}_{1,N}(\tau, x)$ satisfies the following properties. Namely, $\hat{v}_{1,N}(\tau, x)$ is the solution of the discrete-type cell problem defined in Eq.(5.26).

Lemma 5.2. *According to our assumption on v , we know that v_1 is a periodic function with zero mean on \tilde{Y} , $\forall \tau$, i.e., $\int_{\tilde{Y}} v_1 = 0$. Therefore, $\hat{v}_{1,N}(\tau, x)$ is the unique solution in $\mathcal{B}_0(\mathbb{T} \times \tilde{Y})$ such that*

$$\hat{v}_{1,N}(\tau, x) = (I_{\Delta t} \hat{v}_{1,N})(\tau, x) + \Delta t v_1(\tau + \frac{\Delta t}{2}, x), \quad (5.26)$$

where $\Delta t = \frac{1}{N}$ and the operator $I_{\Delta t}$ is defined in (5.12). Moreover, $\hat{v}_{1,N}(\tau, x)$ is smooth.

Proof. Throughout the proof, we shall use the fact that if X, Y are random processes and Y is measurable under a filtration \mathcal{F} , then with appropriate integrability assumption, we have

$$E[XY] = E\left[E[XY|\mathcal{F}]\right] = E\left[E[X|\mathcal{F}]Y\right]. \quad (5.27)$$

Some simple calculations will give that

$$\begin{aligned}
 \hat{v}_{1,N}(\tau, x) - \Delta t v_1\left(\tau + \frac{\Delta t}{2}, x\right) &= \Delta t \sum_{i=1}^{\infty} E[v_1(t_{i+\frac{1}{2}} + \tau, X_{N\tau+i}) | X_{N\tau} = x] \\
 &= E\left[\Delta t \sum_{i=1}^{\infty} E[v_1(t_{i+\frac{1}{2}} + \tau, X_{N\tau+i}) | X_{N\tau+1}] | X_{N\tau} = x\right] \\
 &= E[\hat{v}_{1,N}(\tau + \Delta t, X_{N\tau+1}) | X_{N\tau} = x]. \tag{5.28}
 \end{aligned}$$

Recall the definition of the operator $I_{\Delta t}$ in (5.12), Eq.(5.28) implies that

$$\hat{v}_{1,N}(\tau, x) - \Delta t v_1\left(\tau + \frac{\Delta t}{2}, x\right) = (I_{\Delta t} \hat{v}_{1,N})(\tau, x). \tag{5.29}$$

Suppose we have that $I_{\Delta t} w = w$. Then, we get $(I_{\Delta t})^N w = w$. According to Theorem 5.1, we know that $w = 0$ if $\int_{\tilde{Y}} w dx = 0, \forall t$. So $\ker(I_{\Delta t} - I_d) = \{0\}$ and $\hat{v}_{1,N}$ is unique. Finally, by the definition of $\hat{v}_{1,N}$, we obtain that

$$\begin{aligned}
 \hat{v}_{1,N}(x, \tau) &= \Delta t \sum_{i=0}^{\infty} E[v_1(t_{i+\frac{1}{2}} + \tau, X_{N\tau+i}) | X_{N\tau} = x] \\
 &= \Delta t \sum_{i=0}^{\infty} \int_{\tilde{Y}} v_1(t_{i+\frac{1}{2}} + \tau, y) \tilde{\mathbf{K}}_{\tau, \tau+i\Delta t}(x, y) dy, \tag{5.30}
 \end{aligned}$$

which indicates that $\hat{v}_{1,N}$ has the same regularity as v_1 does. Notice the kernel $\tilde{\mathbf{K}}_{\tau, \tau+i\Delta t}(x, y)$ has a fast decay property, which guarantees the order of the differentiation and summation is interchangeable. \square

Remark 5.3. *When the flow is time-independent, we obtain*

$$E[\hat{v}_{1,N}(X_{n+1}) | X_n] - \hat{v}_{1,N}(X_n) = -\Delta t v_1(X_n), \quad a.s. \quad \forall n \in \mathbb{N}. \tag{5.31}$$

Therefore, the discrete-type cell problem defined in (5.26) is a generalization of the discrete-type cell problem for time-independent flow problems studied in Section 4.2.2, although technically it is more involved.

In the remaining part of this paper, we only need the result that $\hat{v}_{1,N}(x, \tau)$ is unique in an Hölder space $\mathbb{C}_0^{p_1, p_2, \alpha}(\mathbb{T} \times \tilde{Y}) \subsetneq \mathcal{B}(\mathbb{T} \times \tilde{Y})$. To be precise, given a smooth drift function v_1 , $\hat{v}_{1,N}(x, \tau)$ will be in $\mathbb{C}_0^{p_1, p_2, \alpha}(\tilde{Y})$, where $p_1 \geq 2, p_2 \geq 6, 0 < \alpha < 1$ and the subscript index 0 indicates that it is a subspace with zero-mean functions.

5.2.3 Convergence estimate of the discrete-type cell problem

In this section, we shall prove that the solution $\hat{v}_{1,N}(\tau, x)$ of the discrete-type cell problem (i.e., Eq.(5.26)) converges to the solution of a continuous cell problem in certain subspace. Here, we choose the space $\mathbb{C}_0^{2,6,\alpha}(\mathbb{T}^1 \times \tilde{Y})$ to carry out our analysis. However, there is no requirement that we have to choose this one. In fact, any space that has certain regularity (belongs to the domain of the operator \mathcal{L}) will work. Notice that the continuous cell problem (5.1) is defined for a vector function, where the first component satisfies

$$\mathcal{L}\chi_1 = -v_1. \quad (5.32)$$

For the two-dimensional problem, the operator \mathcal{L} is defined in Eq.(5.10). Given the fact that v_1 is a smooth function defined on $\mathbb{T}^1 \times \tilde{Y}$, which satisfies $\int_{\tilde{Y}} v_1(\tau, x) dx = 0, \forall \tau \in \mathbb{T}^1$. Then, Eq.(5.32) admits a unique solution χ_1 in $\mathbb{C}_0^{2,6,\alpha}(\mathbb{T}^1 \times \tilde{Y})$. This is a standard result of parabolic PDEs in Hölder space (see, e.g., the Theorem 8.7.3 in [34]). The following theorem states that under certain conditions the solution of the discrete-type cell problem converges to the solution of the continuous one.

Theorem 5.2. *Assume v_1 is a smooth function defined on $\mathbb{T}^1 \times \tilde{Y}$, satisfying $\int_{\tilde{Y}} v_1(\tau, x) dx = 0, \forall \tau \in \mathbb{T}^1$. Let \hat{v}_1 and χ_1 be the solutions of the discrete-type cell problem (5.26) and continuous cell problem (5.32), respectively. Then, we have the following convergence estimate holds*

$$\|\chi_1 - \hat{v}_1\| = O(\Delta t), \quad (5.33)$$

where $\|\cdot\|$ is a function norm associated with the space $\mathbb{C}_0^{2,6,\alpha}(\mathbb{T}^1 \times \tilde{Y})$.

Proof. Using Prop. 4.2, one can easily verify that \mathcal{L} is a bijection between two Banach spaces $\mathbb{C}_0^{2,6,\alpha}(\mathbb{T}^1 \times \tilde{Y})$ and $\mathbb{C}_0^{1,4,\alpha}(\mathbb{T}^1 \times \tilde{Y})$ and its inverse is bounded. Integrating Eq.(5.32) along time gives,

$$\exp(\Delta t \mathcal{L})\chi_1 - \chi_1 = -v_1 \Delta t + O((\Delta t)^2) \equiv -\Delta t \bar{v}_1, \quad (5.34)$$

where $\bar{v}_1 = v_1 + O(\Delta t)$. Combining Eq.(5.29) and Eq.(5.34), we obtain

$$\exp(\Delta t \mathcal{L})\chi_1 - I_{\Delta t}\hat{v}_1 - (\chi_1 - \hat{v}_1) = \Delta t(v_1 - \bar{v}_1). \quad (5.35)$$

Notice that Eq.(5.35) shows the connection between χ_1 and \hat{v}_1 . After some simple calculations, we get that

$$\mathcal{L}(\chi_1 - \hat{v}_1) = (\mathcal{L} - \tilde{L}_1)(\chi_1 - \hat{v}_1) + \tilde{L}_2\hat{v}_1 + (v_1 - \bar{v}_1), \quad (5.36)$$

where

$$\tilde{L}_1 = \frac{\exp(\Delta t \mathcal{L}) - I_d}{\Delta t}, \quad \text{and} \quad \tilde{L}_2 = \frac{I_{\Delta t} - \exp(\Delta t \mathcal{L})}{\Delta t}. \quad (5.37)$$

Moreover, we can verify that in the space of bounded linear operators from $\mathbb{C}_0^{2,6,\alpha}(\tilde{Y})$ to $\mathbb{C}_0^{1,4,\alpha}(\tilde{Y})$, there is a strong convergence in the operator norm $\|\cdot\|$,

$$\|\mathcal{L} - \tilde{L}_1\| = O(\Delta t) \quad \text{as } \Delta t \rightarrow 0. \quad (5.38)$$

For the operator \tilde{L}_2 , noticing that $\mathcal{L} = \mathcal{L}_1 + \mathcal{L}_2 + \mathcal{L}_3 + \mathcal{L}_4$ and operator $I_{\Delta t}$ is defined in (5.12), we can use the BCH formula and obtain

$$\begin{aligned} \tilde{L}_2 &= \frac{\exp\left(\frac{(\Delta t)^2}{2}([\mathcal{L}_4, \mathcal{L}_3] + [\mathcal{L}_4, \mathcal{L}_2] + [\mathcal{L}_4, \mathcal{L}_1] + [\mathcal{L}_3, \mathcal{L}_2] + [\mathcal{L}_2, \mathcal{L}_1] + [\mathcal{L}_3, \mathcal{L}_1]) + O(\Delta t)^3\right) - I_d}{\Delta t} \cdot \exp(\Delta t \mathcal{L}) \\ &\rightarrow \frac{\Delta t}{2}([\mathcal{L}_4, \mathcal{L}_3] + [\mathcal{L}_4, \mathcal{L}_2] + [\mathcal{L}_4, \mathcal{L}_1] + [\mathcal{L}_3, \mathcal{L}_2] + [\mathcal{L}_2, \mathcal{L}_1] + [\mathcal{L}_3, \mathcal{L}_1]) + O((\Delta t)^2). \end{aligned} \quad (5.39)$$

Denoting $\tilde{L}_3 \equiv \tilde{L}_1 + \tilde{L}_2 = \frac{I_{\Delta t} - I_d}{\Delta t}$, we have $\tilde{L}_3 \rightarrow \mathcal{L}$ in $\mathcal{B}(\mathbb{C}_0^{2,6,\alpha}(\mathbb{T}^1 \times \tilde{Y}), \mathbb{C}_0^{1,4,\alpha}(\mathbb{T}^1 \times \tilde{Y}))$ as Δt approaches zero. Then, applying the Prop. 4.2, we get,

$$\lim_{\Delta t \rightarrow 0} \hat{v}_1 = \lim_{\Delta t \rightarrow 0} \tilde{L}_3^{-1}(-v_1) = \mathcal{L}^{-1}(-v_1) = \chi_1. \quad (5.40)$$

In addition, combining the results of the Eq.(5.34), Eq.(5.38), Eq.(5.39) and (5.40) for the right hand side of Eq.(5.36), we know that when Δt is small enough, the assertion in (5.33) is proved. The constant in the $O(\Delta t)$ of (5.33) does not depend on the total computational time T , but may depend on the regularities of v_1, v_2 and the constant σ . \square

5.2.4 Convergence analysis for the effective diffusivity

This section contains the main results of our convergence analysis. We first prove that the second-order moment of the solution obtained by using our

numerical scheme has an (at most) linear growth rate. Secondly, we provide the convergence rate of our numerical method in computing the effective diffusivity.

Theorem 5.3. *Let $X_n = (x_n^1, x_n^2)^T$ denote the solution of the two-dimensional passive tracer model (5.3) obtained by using our numerical scheme (5.21) with time step Δt . If the Hamiltonian function $H(t, x^1, x^2)$ is separable, periodic and smooth (in order to guarantee the existence and uniqueness of the solution to the SDE (5.3)), then we can prove that the second-order moment of the solution X_n (which can be viewed as a discrete Markov process) is at most linear growth, i.e.,*

$$\max_n \left\{ E \frac{\|X_n\|^2}{n} \right\} \text{ is bounded.} \quad (5.41)$$

Proof. We first estimate the second-order moment of the first component of $X_n = (x_n^1, x_n^2)^T$, since the other one can be estimated in the same manner. Simple calculations show that

$$\begin{aligned} E[(x_n^1)^2 | (x_{n-1}^1, x_{n-1}^2)] &= E \left(x_{n-1}^1 + v_1(t_{n-\frac{1}{2}}, x_{n-1}^2) \Delta t + \sigma N_{i-1}^1 \right)^2 \\ &= E(x_{n-1}^1)^2 + \Delta t (\sigma^2 + 2E[x_{n-1}^1 v_1(t_{n-\frac{1}{2}}, x_{n-1}^2)]) \\ &\quad + (\Delta t)^2 E v_1^2(t_{n-\frac{1}{2}}, x_{n-1}^2). \end{aligned} \quad (5.42)$$

The term $E[x_{n-1}^1 v_1(t_{n-\frac{1}{2}}, x_{n-1}^2)]$ corresponds to the strength of the convection-enhanced diffusion. Our goal here is to prove that it is bounded over n , though it may depend on v_1 , v_2 and σ . We now directly compute the contribution of the term $E[x_{n-1}^1 v_1(t_{n-\frac{1}{2}}, x_{n-1}^2)]$ to the effective diffusivity with the help of Eq.(5.28),

$$\Delta t \sum_{i=0}^{n-1} E[x_i^1 v_1(t_{i+\frac{1}{2}}, x_i^2)] = \sum_{i=0}^{n-1} E[x_i^1 (\hat{v}_1(t_i, X_i) - E[\hat{v}_1(t_{i+1}, X_{i+1}) | X_i])]. \quad (5.43)$$

Let \mathcal{F}_i denote the filtration generated by the solution process until X_i . Notice

that $x_i^1 \in \mathcal{F}_i$. For the Eq.(5.43), we have

$$\begin{aligned}
 RHS &= \sum_{i=0}^{n-1} E[x_i^1(\hat{v}_1(t_i, X_i) - \hat{v}_1(t_{i+1}, X_{i+1}))], \\
 &= \sum_{i=1}^n E[\hat{v}_1(t_i, X_i)(x_i^1 - x_{i-1}^1)] + \hat{v}_1(t_0, X_0)x_0^1 - E[\hat{v}_1(t_n, X_n)x_n^1], \\
 &= \sum_{i=1}^n E[\hat{v}_1(t_i, X_i)(v_1(t_{i-\frac{1}{2}}, x_{i-1}^2)\Delta t + \sigma N_{i-1}^1)] + \hat{v}_1(t_0, X_0)x_0^1 - E[\hat{v}_1(t_n, X_n)x_n^1].
 \end{aligned} \tag{5.44}$$

Hence, we obtain the following result

$$\begin{aligned}
 \frac{1}{n}E[(x_n^1)^2|(x_0^1, x_0^2)] &= \frac{1}{n}(x_0^1)^2 + \Delta t\sigma^2 + 2\Delta t\frac{1}{n}\sum_{i=0}^{n-1} E[x_i^1v_1(t_{i+\frac{1}{2}}, x_i^2)] \\
 &\quad + (\Delta t)^2\frac{1}{n}\sum_{i=0}^{n-1} E v_1^2(t_{i+\frac{1}{2}}, x_i^2), \\
 &= \frac{1}{n}(x_0^1)^2 + \Delta t\sigma^2 + (\Delta t)^2\frac{1}{n}\sum_{i=0}^{n-1} E v_1^2(t_{i+\frac{1}{2}}, x_i^2) \\
 &\quad + \frac{2}{n}\sum_{i=1}^n E[\hat{v}_1(t_i, X_i)(v_1(t_{i-\frac{1}{2}}, x_{i-1}^2)\Delta t + \sigma N_{i-1}^1)] \\
 &\quad + \frac{2}{n}(\hat{v}_1(t_0, X_0)x_0^1 - E[\hat{v}_1(t_n, X_n)x_n^1]).
 \end{aligned} \tag{5.45}$$

By using the Cauchy-Schwarz inequality, we know the term

$$\begin{aligned}
 &\frac{2}{n}\sum_{i=1}^n E[\hat{v}_1(t_i, X_i)(v_1(t_{i-\frac{1}{2}}, x_{i-1}^2)\Delta t + \sigma N_{i-1}^1)], \\
 &\leq \frac{2}{n}\sum_{i=1}^n E[2(\hat{v}_1(t_i, X_i))^2 + ((v_1(t_{i-\frac{1}{2}}, x_{i-1}^2)\Delta t)^2 + (\sigma N_{i-1}^1)^2)], \\
 &= \frac{2}{n}\sum_{i=1}^n E[2(\hat{v}_1(t_i, X_i))^2 + (v_1(t_{i-\frac{1}{2}}, x_{i-1}^2))^2(\Delta t)^2 + \sigma^2\Delta t].
 \end{aligned} \tag{5.46}$$

Notice that if v_1 and \hat{v}_1 are bounded in sup norm, right-hand-side of Eq.(5.46) is bounded for any n . Other terms on the right-hand side of Eq.(5.45) are also bounded, which can be checked easily. Therefore, we can prove that $\frac{1}{n}E[(x_n^1)^2|(x_0^1, x_0^2)]$ is bounded. Repeat the same trick, we know that $\frac{1}{n}E[(x_n^2)^2|(x_0^1, x_0^2)]$ is also bounded. Thus, the assertion in Eq.(5.41) is proved. \square

In practice, we shall first choose a time step Δt and run our numerical scheme (5.8) to compute the effective diffusivity until the result converges

to a constant, which may depend on Δt . As such, we shall prove that the limit of the constant converges to the exact effective diffusivity of the original passive tracer model as Δt approaches zero. Namely, we shall prove that our numerical scheme is robust in computing the effective diffusivity. More details on the numerical results will be given in Section 5.3.

Theorem 5.4. *Let x_n^1 , $n = 0, 1, \dots$ be the first component of the numerical solution obtained by using the scheme (5.8) and Δt denote the time step. We have the convergence estimate of the effective diffusivity as*

$$\lim_{n \rightarrow \infty} \frac{E(x_n^1)^2}{n\Delta t} = \sigma^2 + 2 \int_{\mathbb{T}^2} \chi_1 v_1 + O(\Delta t), \quad (5.47)$$

where the constant in $O(\Delta t)$ may depend on the regularity of v_1 , v_2 and the constant σ , but does not depend on the computational time T .

Proof. We will prove the statement by direct computation. We divide both sides of the Eq.(5.45) by Δt and obtain

$$\begin{aligned} \frac{1}{n\Delta t} E[(x_n^1)^2 | (x_0^1, x_0^2)] &= \frac{1}{n\Delta t} (x_0^1)^2 + \sigma^2 + \frac{\Delta t}{n} \sum_{i=0}^{n-1} E v_1^2(t_{i+\frac{1}{2}}, x_i^2) \\ &\quad + \frac{2}{n\Delta t} \sum_{i=1}^n E[\hat{v}_1(t_i, X_i)(v_1(t_{i-\frac{1}{2}}, x_{i-1}^2)\Delta t + \sigma N_{i-1}^1)] \\ &\quad + \frac{2}{n\Delta t} (\hat{v}_1(t_0, X_0)x_0^1 - E[\hat{v}_1(t_n, X_n)x_n^1]). \end{aligned} \quad (5.48)$$

First, we notice that for a fixed Δt , the terms $\frac{1}{n\Delta t}(x_0^1)^2$ and $\frac{2}{n\Delta t}\hat{v}_1(t_0, X_0)x_0^1$ converge to zero as $n \rightarrow \infty$, where we have used the fact that $\hat{v}_1(t_0, X_0)$ is bounded. Also notice that the term $\frac{\Delta t}{n} \sum_{i=0}^{n-1} E v_1^2(t_{i+\frac{1}{2}}, x_i^2)$ is $O(\Delta t)$, due to the term v_1^2 is bounded. Then, for a fixed Δt , we have

$$\begin{aligned} \lim_{n \rightarrow \infty} \frac{2}{n\Delta t} |E[\hat{v}_1(X_n)x_n^1]| &\leq \lim_{n \rightarrow \infty} \frac{2}{\sqrt{n}\Delta t} \|\hat{v}_1\|_\infty E\left|\frac{x_n^1}{\sqrt{n}}\right| \\ &\leq \lim_{n \rightarrow \infty} \frac{1}{\sqrt{n}\Delta t} \|\hat{v}_1\|_\infty E\left[\frac{(x_n^1)^2}{n} + 1\right] = 0, \end{aligned} \quad (5.49)$$

where the term $E[\frac{(x_n^1)^2}{n}]$ is bounded due to the Theorem 5.3 and $\|\hat{v}_1\|_\infty \rightarrow \|\chi_1\|_\infty < \infty$ due to the Theorem 5.2.

Therefore, we only need to focus on the estimate of terms in the second line of Eq.(5.48), which correspond to the convection-enhanced diffusion effect.

Notice that $\hat{v}_1 \in \mathbb{C}^{2,6,\alpha}$, we compute the Ito-Taylor series approximation of $\hat{v}_1(t_i, X_i)$,

$$\begin{aligned} \hat{v}_1(t_i, X_i) &= \hat{v}_1(t_{i-1}, X_{i-1}) + \hat{v}_{1,x^1}(t_{i-1}, X_{i-1})(v_1(t_{i-\frac{1}{2}}, x_{i-1}^2)\Delta t + \sigma N_{i-1}^1) \\ &\quad + \hat{v}_{1,x^2}(t_{i-1}, X_{i-1})(v_2(t_{i-\frac{1}{2}}, x_{i-1}^1)\Delta t + \sigma N_{i-1}^2) \\ &\quad + \frac{1}{2}(\hat{v}_{1,x^1,x^1}(t_{i-1}, X_{i-1}) + \hat{v}_{1,x^2,x^2}(t_{i-1}, X_{i-1}))\sigma^2\Delta t + O((\Delta t)^2), \end{aligned} \quad (5.50)$$

where we have used the fact that $v_2(t_{i-\frac{1}{2}}, x_{i-1}^1 + v_1(t_{i-\frac{1}{2}}, x_{i-1}^2)\Delta t) = v_2(t_{i-\frac{1}{2}}, x_{i-1}^1) + O(\Delta t)$, when Δt is small and v_2 is smooth. Since $\hat{v}_1 \rightarrow \chi_1$ in $\mathbb{C}_0^{2,6,\alpha}$, the truncated term $O((\Delta t)^2)$ in Eq.(5.50) is uniformly bounded when Δt is small enough. Substituting the Taylor expansion of $\hat{v}_1(t_i, X_i)$ in Eq.(5.50) into the target term of our estimate (i.e., terms in the second line of Eq.(5.48)), we get

$$\begin{aligned} E[\hat{v}_1(t_i, X_i)(v_1(t_{i-\frac{1}{2}}, x_{i-1}^2)\Delta t + \sigma N_{i-1}^1)] &= E\left[\left(v_1(t_{i-\frac{1}{2}}, x_{i-1}^2)\Delta t + \sigma N_{i-1}^1\right) \cdot \right. \\ &\quad \left. \left(\hat{v}_1(t_{i-1}, X_{i-1}) + \hat{v}_{1,x^1}(t_{i-1}, X_{i-1})(v_1(t_{i-\frac{1}{2}}, x_{i-1}^2)\Delta t + \sigma N_{i-1}^1) \right. \right. \\ &\quad \left. \left. + \hat{v}_{1,x^2}(t_{i-1}, X_{i-1})(v_2(t_{i-\frac{1}{2}}, x_{i-1}^1)\Delta t + \sigma N_{i-1}^2) \right. \right. \\ &\quad \left. \left. + \frac{1}{2}(\hat{v}_{1,x^1,x^1}(t_{i-1}, X_{i-1}) + \hat{v}_{1,x^2,x^2}(t_{i-1}, X_{i-1}))\sigma^2\Delta t + O((\Delta t)^2)\right)\right]. \end{aligned} \quad (5.51)$$

Combining the terms with the same order of Δt , we obtain

$$\begin{aligned} &E[\hat{v}_1(t_i, X_i)(v_1(t_{i-\frac{1}{2}}, x_{i-1}^2)\Delta t + \sigma N_{i-1}^1)] \\ &= \Delta t E[\hat{v}_1(t_{i-1}, X_{i-1})v_1(t_{i-\frac{1}{2}}, x_{i-1}^2) + \sigma^2 \hat{v}_{1,x^1}(t_{i-1}, X_{i-1})] + O((\Delta t)^2), \end{aligned} \quad (5.52)$$

where we have used the facts that: (1) X_{i-1} is independent with N_{i-1}^1 and N_{i-1}^2 so the expectations of the corresponding terms vanish; (2) N_{i-1}^1 and N_{i-1}^2 are independent so $E(N_{i-1}^1 N_{i-1}^2) = 0$; and (3) $E(N_{i-1}^1)^2 = \Delta t$.

Finally, by using the Theorem 5.1 and noticing the invariant measure is the uniform measure, we obtain from Eq.(5.48) that

$$\lim_{n \rightarrow \infty} \frac{1}{n\Delta t} E[(x_n^1)^2 | (x_0^1, x_0^2)] = \sigma^2 + 2 \int (\hat{v}_1 v_1 + \sigma^2 \hat{v}_{1,x^1}) + O(\Delta t). \quad (5.53)$$

Thus, our statement in the Eq.(5.47) is proved using the facts that \hat{v}_1 converges to χ_1 (see Theorem 5.2) and $\int \hat{v}_{1,x^1} = 0$. \square

Remark 5.4. *If we divide two on both sides of the Eq.(5.47), we can find that our result recovers the definition of the effective diffusivity D_{11}^E defined in the Eq.(5.2). Recall that $D_0 = \sigma^2/2$. Theorem 5.4 reveals the connection of the definition of the effective diffusivity using the Eulerian framework and Lagrangian framework; see Eq.(5.2) and Eq.(2.29), which is fundamental in this context. For 3D time-dependent flows problems, the former has good theoretical values but the latter is computationally accessible.*

Remark 5.5. *For the second component of the numerical solution, i.e., x_n^2 , $n = 0, 1, \dots$, we can obtain the similar convergence result in computing the effective diffusivity. First we consider $\tilde{v}_2(t, x_1, x_2) := v_2(t, x^1 + v_1(t, x^2)\Delta t)$ and notice that $\tilde{v}_2 - v_2 = O(\Delta t)$ and $\int_{\mathbb{T}} \tilde{v}_2 dx^1 = 0$. The remaining part of the proof is essentially the same as the results obtained in Sections 5.2.2, 5.2.3 and 5.2.4, so we skip the details here.*

5.2.5 Generalizations to high-dimensional cases

To show the essential idea of our probabilistic approach in proving the convergence rate of the numerical schemes, we have carried out our convergence analysis based on a two-dimensional model problem (5.3). In fact, the extension of our approach to higher-dimensional problems is straightforward. Now we consider a high-dimensional problem as follow,

$$dX = v(t, X)dt + \Sigma dw(t), \quad (5.54)$$

where $X = (x^1, x^2, \dots, x^d)^T \in \mathbb{R}^d$ is the position of a particle, $v = (v_1, v_2, \dots, v_d)^T \in \mathbb{R}^d$ is the Eulerian velocity field at position X , Σ is a $d \times d$ constant non-singular matrix, and $dw(t)$ is a d -dimension Brownian motion vector. In particular, we assume the component v_i does not depend on x^i , $i = 1, \dots, d$. Thus, the incompressible condition for $v(t, X)$ (i.e. $\nabla_X \cdot v(t, X) = 0$) is easily guaranteed.

For a deterministic and divergence-free dynamic system, Feng et. al. proposed a volume-preserving method [20], which splits a d -dimensional problem into $d - 1$ subproblems with each of them being volume-preserving. We shall

modify Feng's method (first-order case) by including the randomness as the last subproblem to take into account the additive noise. Assume the numerical solution $X_0 = (x_0^1, \dots, x_0^d)^T$ is given, the numerical scheme gives

$$\begin{cases} x^{1*} = x_0^1 + \Delta t v_1(\frac{\Delta t}{2}, x_0^1, x_0^2, x_0^3, \dots, x_0^{d-1}, x_0^d), \\ x^{2*} = x_0^2 + \Delta t v_2(\frac{\Delta t}{2}, x^{1*}, x_0^2, x_0^3, \dots, x_0^{d-1}, x_0^d), \\ \dots, \\ x^{d*} = x_0^d + \Delta t v_d(\frac{\Delta t}{2}, x^{1*}, x^{2*}, x^{3*}, \dots, x^{(d-1)*}, x_0^d), \\ X_1 = X^* + \Sigma N^*, \end{cases} \quad (5.55)$$

where N^* is a d -dimensional independent random vector with each component of the form $\sqrt{\Delta t} \xi_i$, $\xi_i \sim \mathcal{N}(0, 1)$.

The techniques of the convergence analysis for the two-dimensional problem can be applied to high-dimensional problems without much difficulty. For the high-dimensional problem (5.54), the smoothness and strict positivity of the transition kernel in the discrete process can be guaranteed if one assumes that the covariance matrix Σ is non-singular and the scheme (5.55) is explicit.

According to our assumption for the velocity field, the scheme (5.55) is volume-preserving for each step. Thus, the solution to the first-order modified equation is divergence-free and the invariant measure on the torus (defined by $\mathbb{R}^d/\mathbb{Z}^d$, when the period is 1) remains uniform for all t . Finally, the convergence of the cell problem can be studied by using the BCH formula (4.8) with $d + 2$ differential operators. Recall that in the Eq.(5.12) we have four differential operators when we study the two-dimensional problem. Therefore, our numerical methods are robust in computing effective diffusivity for high-dimensional problems, which will be demonstrated through time-dependent chaotic flow problems in three-dimensional space in the Section 5.3.

5.3 Numerical results

In this section, we will present numerical examples to verify the convergence analysis of the proposed method in computing effective diffusivity for time-dependent chaotic flows. In addition, we will investigate the convection-enhanced diffusion phenomenon in 3D time-dependent flow, i.e., the time-dependent ABC flow and the time-dependent Kolmogorov flow. Without loss of generality, we compute the quantity $\frac{E(x^1(T))^2}{2T}$, which is used to approximate D_{11}^E in the effective diffusivity matrix (5.2).

5.3.1 Verification of the convergence rate

We first consider a two-dimensional passive tracer model. Let $(x^1, x^2)^T \in \mathbb{R}^2$ denote the position of a particle. Its motion is described by the following SDE,

$$\begin{cases} dx^1 = \sin(4x^2 + 1 + \sin(2\pi t)) \exp(\cos(4x^2 + 1 + \sin(2\pi t))) dt + \sigma W_{1,t}, \\ dx^2 = \cos(2x^1 + \sin(2\pi t)) \exp(\sin(2x^1 + \sin(2\pi t))) dt + \sigma W_{2,t}, \end{cases} \quad (5.56)$$

where $\sigma = \sqrt{2 \times 0.1}$, $W_{i,t}$, $i = 1, 2$ are independent Brownian motions, and the initial data $(x_0^1, x_0^2)^T$ follows uniform distributions in $[-0.5, 0.5]^2$. One can easily verify the velocity field in (5.56) is time-dependent and divergence free.

In our numerical experiments, we use Monte Carlo samples to discretize the Brownian motions $W_{1,t}$ and $W_{2,t}$. The sample number is denoted by N_{mc} . We choose $\Delta t_{ref} = \frac{1}{2^{12}}$ and $N_{mc} = 3,200,000$ to solve the SDE (5.56) to compute the reference solution, i.e., the ‘‘exact’’ effective diffusivity, where the final computational time is $T = 3000$ so that the calculated effective diffusivity converges to a constant. In fact, we find that the passive tracer model will enter a mixing stage if the computational time is bigger than $T = 1000$. It takes about 17 hours to compute the reference solution on a 80-core server (HPC2015 System at HKU). The reference solution for the effective diffusivity is $D_{11}^E = 0.219$.

In Fig.5.1(a), we plot the convergence results of the effective diffusivity using our method (i.e., $\frac{E(x^1(T))^2}{2T}$) with respect to different time-step Δt at $T = 3000$. In addition, we show a fitted straight line with the slope 1.04, i.e., the convergence rate is about $(\Delta t)^{1.04}$. This numerical result verifies the convergence analysis in Theorem 5.4.

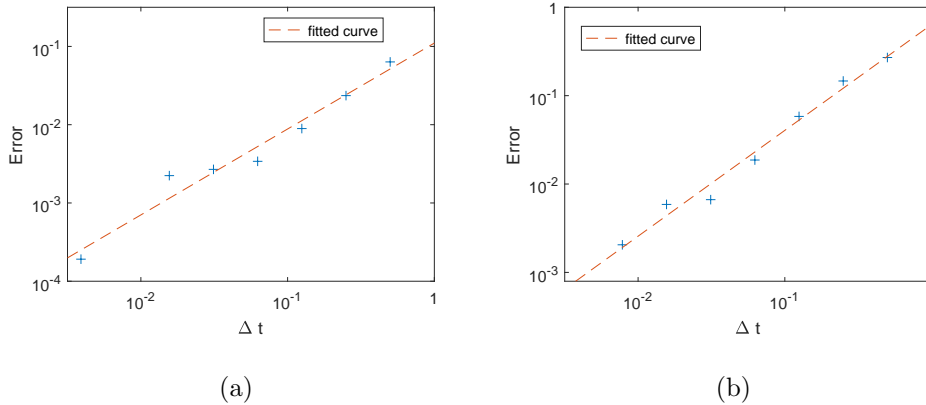


Figure 5.1: Error of D_{11}^E for two time-dependent flows with different time-steps. (a) 2D time-dependent chaotic flow, fitted slope ≈ 1.04 ; (b) 3D time-dependent Kolmogorov flow, fitted slope ≈ 1.22 .

To further study the accuracy and robustness of our method for long-time integration, we consider a 3D time-dependent Kolmogorov flow problem. Let $(x^1, x^2, x^3)^T \in \mathbb{R}^3$ denote the position of a particle. The motion of a particle moving in the 3D time-dependent Kolmogorov flow is described by the following SDE,

$$\begin{cases} dx^1 = \sin(x^3 + \epsilon \sin(2\pi t))dt + \sigma dW_{1,t}, \\ dx^2 = \sin(x^1 + \epsilon \sin(2\pi t))dt + \sigma dW_{2,t}, \\ dx^3 = \sin(x^2 + \epsilon \sin(2\pi t))dt + \sigma dW_{3,t}. \end{cases} \quad (5.57)$$

where $W_{1,t}$, $W_{2,t}$ and $W_{3,t}$ are independent Brownian motions. When $\epsilon = 0$, the velocity field in (5.57) corresponds to the Kolmogorov flow [23]. The Kolmogorov flow possesses very chaotic behaviors [10], which brings challenges for our method.

In our numerical experiment, we choose $\epsilon = 10^{-1}$ and $\sigma = \sqrt{2 \times 10^{-3}}$ in the Eq.(5.57). We choose $\Delta t_{ref} = \frac{1}{2048}$ and $N_{mc} = 480,000$ to compute the

reference solution for the SDE (5.57), i.e., the “exact” effective diffusivity. In our numerical tests, we find that the passive tracer model will enter a mixing stage if the computational time is bigger than $T = 2000$. To show the accuracy and robustness of our numerical scheme, we set $T = 10^5$ here. It takes about 59 hours to compute the reference solution on the server and the reference solution for the effective diffusivity is $D_{11}^E = 0.693$.

In Fig.5.1(b), we plot the convergence results of the effective diffusivity using our method with respect to different time-step Δt . In addition, we show a fitted straight line with the slope 1.22, i.e., the convergence rate is about $(\Delta t)^{1.22}$. This numerical result again agrees with our error analysis.

5.3.2 Investigation of the convection-enhanced diffusion phenomenon

As we have already demonstrated in Section 5.3.1, our method is very accurate and robust for long-time integration. Here, we will study the dependence of the effective diffusivity D_{11}^E on different parameters in the time-dependent flows. First of all, we solve Eq.(5.57) and carry out the test for the 3D time-dependent Kolmogorov flow.

In Fig.5.2, we show the time evolution of $\frac{E(x^1(t))^2}{2t}$ for different D_0 's (here $D_0 = \sigma^2/2$) and for four different ϵ 's, where the result in Fig.5.2(d) corresponding to the time-independent Kolmogorov flow (see 4.6(a)). Notice that in Eq.(5.57) the parameter ϵ controls the strength of the time dependence. For each D_0 and ϵ , we use $N_{mc} = 240,000$ particles to solve the SDE (5.57). We find that for each given D_0 , the time evolution of $\frac{E(x^1(t))^2}{2t}$ converges as ϵ approaches zero. This can be rigorously justified through analysis. In addition, we observe a certain amount of enhanced diffusion when D_0 decreases. However, the dependency of D_{11}^E on D_0 is quite different from the pattern of the time-dependent ABC flow, which is known as the maximal enhancement and will be discussed later; see Fig.5.5.

To study the dependence of D_{11}^E on D_0 and ϵ , we choose different ϵ 's and D_0 's and compute the corresponding effective diffusivity D_{11}^E . In this experiment, we use $\Delta t = 2^{-7}$ and $N_{mc} = 240,000$ particles to compute. The final computational time is $T = 10^5$ so that the particles are fully mixed. We show the numerical results in Fig.5.3.

We find that for each given D_0 as ϵ decreases the corresponding effective diffusivity D_{11}^E converges to the effective diffusivity D_{11}^E associated with $\epsilon = 0$. This means the time dependency of ϵ improves the chaotic property of Kolmogorov flow though, it does not change the pattern of convection-enhanced diffusion in the Kolmogorov flow. When $\epsilon \leq 1$ the fitted slope within $D_0 \in [10^{-5}, 10^{-3}]$ is -0.2 , which indicates that $D_{11}^E \sim \mathcal{O}(1/D_0^{0.2})$. We call this behavior as a sub-maximal enhancement, which may be explained by the fact that the Kolmogorov flow is more chaotic than the ABC flow [23]. The chaotic trajectories in Kolmogorov flow enhance diffusion much less than channel-like structures such as the ballistic orbits of ABC flows [39, 55].

Next, we use our stochastic structure-preserving scheme to solve time-dependent ABC flow problems. Let $(x^1, x^2, x^3)^T \in \mathbb{R}^3$ denote the position of a particle in the 3D Cartesian coordinate system. The motion of a particle moving in the 3D time-dependent ABC flow is described by the following SDE,

$$\begin{cases} dx^1 = A \sin(x^3 + \epsilon \sin(2\pi t))dt + C \cos(x^2 + \epsilon \sin(2\pi t))dt + \sigma dW_{1,t}, \\ dx^2 = B \sin(x^1 + \epsilon \sin(2\pi t))dt + A \cos(x^3 + \epsilon \sin(2\pi t))dt + \sigma dW_{2,t}, \\ dx^3 = C \sin(x^2 + \epsilon \sin(2\pi t))dt + B \cos(x^1 + \epsilon \sin(2\pi t))dt + \sigma dW_{3,t}, \end{cases} \quad (5.58)$$

where $W_{1,t}$, $W_{2,t}$ and $W_{3,t}$ are independent Brownian motions. For $\epsilon = 0$ and $\sigma = 0$, the velocity field in (5.58) corresponds to the standard ABC flow [13]. The ABC flow is a three-dimensional incompressible velocity field which is an exact solution to the Euler's equation. It is notable as a simple example of a fluid flow that can have chaotic trajectories. In our numerical experiments, we set $A = B = C = 1$.

In Fig.5.4, we show the time evolution of the $\frac{E(x^1(t))^2}{2t}$ for different D_0 's

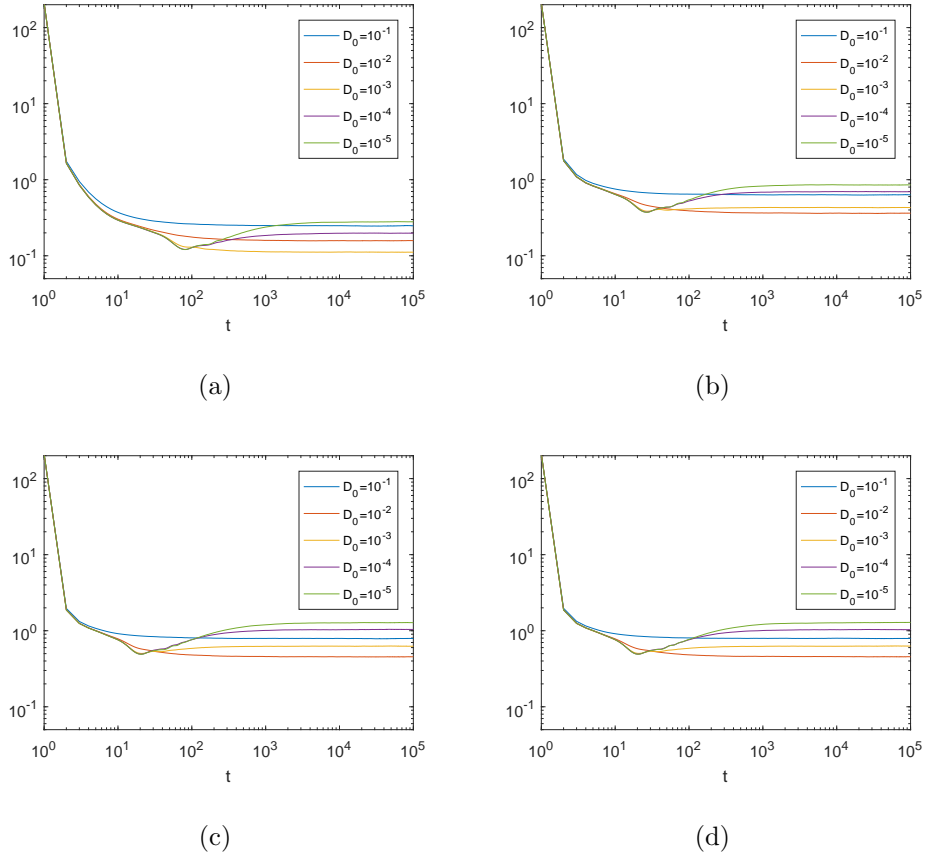


Figure 5.2: Time evolution of the $\frac{E(x^1(t))^2}{2t}$ for different D_0 's and ϵ 's. (a) $\epsilon = 10$, (b) $\epsilon = 1$, (c) $\epsilon = 0.1$, (d) $\epsilon = 0$.

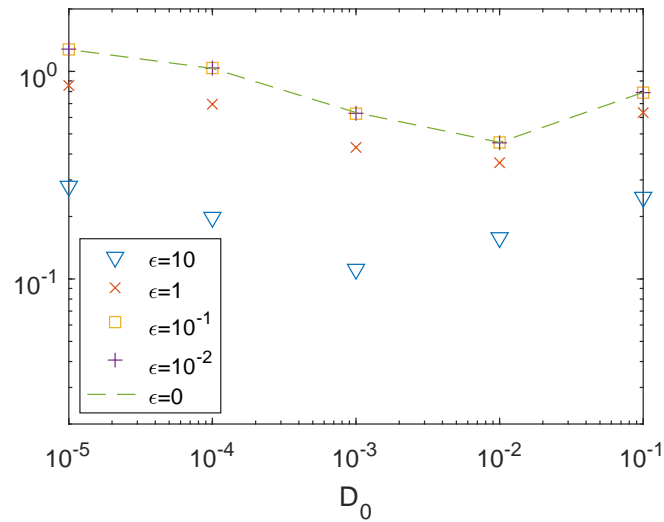


Figure 5.3: Convection-enhanced diffusion with a sub-maximal enhancement in the time-dependent Kolmogorov flow.

(here $D_0 = \sigma^2/2$) and for four different ϵ 's, where the result in Fig.5.4(d) corresponding to the time-independent ABC flow (see Fig.4.3(a)). Again the parameter ϵ controls the strength of the time dependence. For each D_0 and ϵ , we use $N_{mc} = 240,000$ particles to solve the SDE (5.58). We find that for each given D_0 , the time evolution of the $\frac{E(x^1(t))^2}{2t}$ converges when ϵ converges to zero. However, we observe two different patterns compared with the results shown in Fig.5.2. First, when we decrease D_0 , it takes a longer time for the system to enter a mixing stage. Second, we observe a large amount of enhanced diffusion when D_0 decreases.

To further investigate the dependence of D_{11}^E on D_0 and ϵ , we choose different ϵ 's and D_0 's and compute the corresponding effective diffusivity D_{11}^E . In this experiment, we use $\Delta t = 2^{-7}$ and $N_{mc} = 240,000$ particles to compute. The final computational time is $T = 10^5$ so that the particles are fully mixed.

In Fig.5.5, we show the numerical results. We find that for each given D_0 , as ϵ decreases the corresponding effective diffusivity D_{11}^E converges to the effective diffusivity D_{11}^E associated with $\epsilon = 0$. Thus, the time-dependent ABC flow has a similar convection-enhanced diffusion behavior as the time-independent ABC flow. The fitted slope within $D_0 \in [10^{-5}, 10^{-1}]$ is about -1.0 , which indicates that $D_{11}^E \sim \mathcal{O}(1/D_0)$. This result indicates that the D_{11}^E of the time-dependent ABC flow achieves the upper-bound of Eq.(2.28), i.e. the maximal enhancement. This maximal enhancement phenomenon may be attributed to the ballistic orbits of the ABC flow, where the time-independent case was discussed in [39, 55].

Moreover, our result for $D_0 \in [10^{-3}, 10^{-1}]$ and $\epsilon = 0$ recovers the same phenomenon as the Fig.2 in [5], which was obtained by using the Eulerian framework, i.e., solving a cell problem. In Fig.5.5, our method can be easily used to compute the effective diffusivity when $D_0 \in [10^{-5}, 10^{-4}]$. It will be, however, extremely expensive for the Eulerian framework since one needs to solve a convection-dominated PDE (5.1) in 3D space, whose Péclet number is proportion to $1/D_0$.

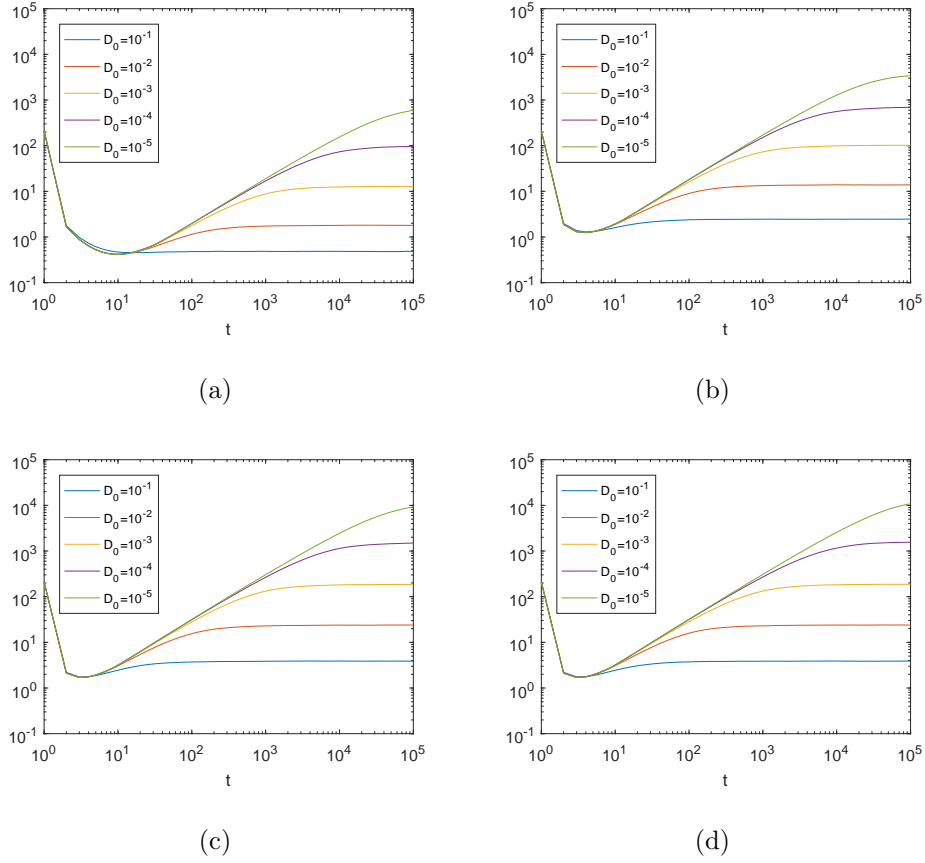


Figure 5.4: Time evolution of the $\frac{E(x^1(t))^2}{2t}$ for different D_0 and ϵ . (a) $\epsilon = 10$, (b) $\epsilon = 1$, (c) $\epsilon = 0.1$, (d) $\epsilon = 0$.

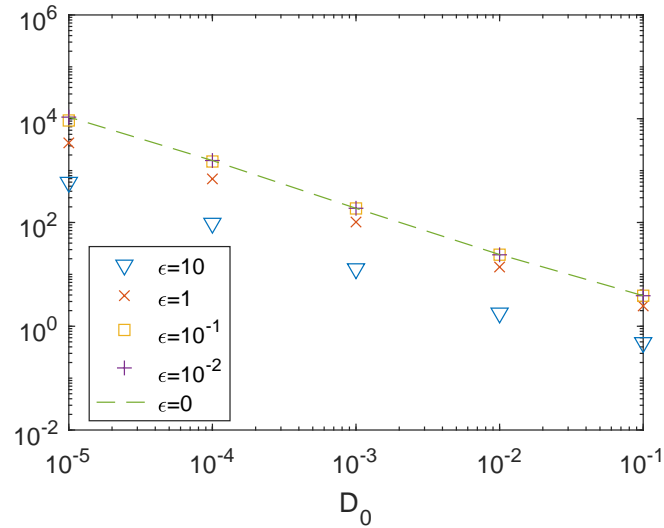


Figure 5.5: Convection-enhanced diffusion with a maximal enhancement in the time-dependent ABC flow.

Finally, we investigate the dependence of D_{11}^E on the frequency of the time-dependent ABC flow. Specifically, we solve the following SDE,

$$\begin{cases} dx^1 = A \sin(x^3 + \sin(\Omega t))dt + C \cos(x^2 + \sin(\Omega t))dt + \sigma dW_{1,t}, \\ dx^2 = B \sin(x^1 + \sin(\Omega t))dt + A \cos(x^3 + \sin(\Omega t))dt + \sigma dW_{2,t}, \\ dx^3 = C \sin(x^2 + \sin(\Omega t))dt + B \cos(x^1 + \sin(\Omega t))dt + \sigma dW_{3,t}, \end{cases} \quad (5.59)$$

where $A = B = C = 1$ and Ω is the frequency. Here we first choose $\Delta t = 2^{-7}$, $N_{mc} = 240,000$ and $T = 10^5$. Then, we choose different Ω and compute the corresponding effective diffusivity D_{11}^E .

In Fig.5.6, we show the numerical results. We find that when Ω is near 0.1 the diffusion enhancement is weak. When Ω is away from 0.1, say $\Omega < 0.05$ or $\Omega > 0.2$, we observe the maximal enhancement phenomenon. A similar sensitive dependence on the frequency of time-dependent ABC flows was reported in [7], where the Lyapunov exponent of the deterministic time-dependent ABC flow problem (i.e., $\sigma = 0$ in Eq. (5.59)) was studied as the indicator of the extent of chaos; see Fig.2 and Fig.3 of [7].

When $\Omega = 0$, the flow of (5.59) is the same as that for $\epsilon = 0$ case in (5.58), which will give the maximal enhancement phenomenon. When Ω is positive, the flow becomes time-dependent and the regions of chaos expand until the extent of chaos (i.e. the Lyapunov exponent) appears to reach a maximum, which is corresponding to $\Omega = 0.1$. It seems that the diffusion enhancement is significantly weakened in this range of Ω . When Ω continues to grow, the islands of the integrability regrow and the chaotic regions have shrunk significantly. We again observe the maximal enhancement phenomenon in this range of Ω . Our numerical results suggest that the level of chaos and the strength of diffusion enhancement seem to compete with each other. More intensive theoretic and numerical studies will be reported in our future work.

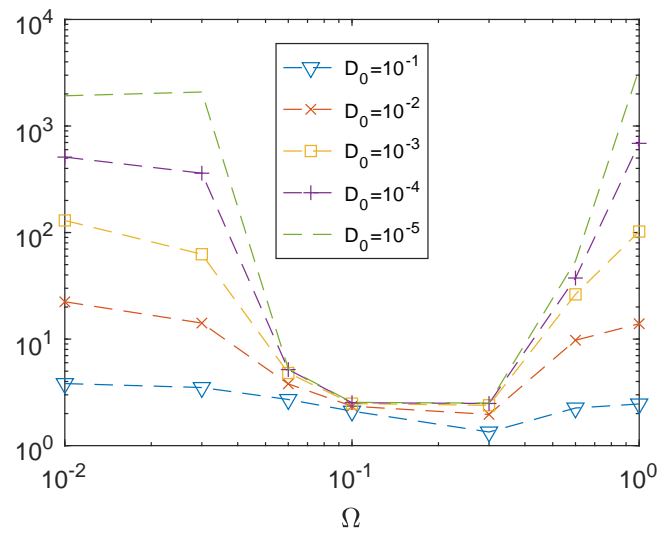


Figure 5.6: Dependence of D_{11}^E on the frequency of the time-dependent ABC flow.

Chapter 6

Sharp and Uniform in Time Error Analysis in Random Flows

6.1 Preliminaries

To make this chapter self-contained, we give a brief review of existing results on convection-enhanced diffusion in random flows and the effective diffusivity. Since these are standard results, we adopt the notations that were used in [17, 19].

6.1.1 Some formulations and results for diffusion in random flows

Let $(\mathcal{X}, \mathcal{H}, P_0)$ be a probability space. Let $\tau_x, x \in \mathbb{R}^d$ be an almost surely continuous, jointly measurable group of measure preserving transformation on \mathcal{X} with the following properties:

(T1) $\tau_0 = Id_{\mathcal{X}}$ and $\tau_{x+y} = \tau_x \tau_y, \forall x, y \in \mathbb{R}^d$.

(T2) The mapping $(\chi, x) \mapsto \tau_x \chi$ is jointly measurable.

(T3) $P_0(\tau_x(A)) = P_0(A)$, for $x \in \mathbb{R}^d, A \in \mathcal{H}$.

(T4) $\lim_{x \rightarrow 0} P_0(\chi : |f \circ \tau_x(\chi) - f(\chi)| \geq \eta) = 0, \forall f \in L^2(\mathcal{X})$ and $\forall \eta > 0$.

(T5) If $P_0(A \Delta \tau_x(A)) = 0, \forall x \in \mathbb{R}^d$, then A is a trivial event, i.e., $P_0(A)$ is either 0 or 1.

One can verify that τ_x induces a strongly continuous group of unitary mapping U^x on $L^2(\mathcal{X})$, which satisfies

$$U^x f(\chi) = f(\tau_x(\chi)), f \in L^2(\mathcal{X}), x \in \mathbb{R}^d. \quad (6.1)$$

In addition, it is easily to find that the group U^x has d independent, skew-adjoint generators $D_k : \mathcal{D}_k \rightarrow L^2(\mathcal{X})$ corresponding to directions $\mathbf{e}_k, k = 1, \dots, d$.

We introduce some function spaces that are useful in the analysis. Let $C_b^m(\mathcal{X})$ be the space of functions f in the intersection of the domains of D_k^n with $\|D_k^n f\|_{L^\infty(\mathcal{X})} < +\infty, k = 1, \dots, d, n = 1, \dots, m$. It is well known that $C_b^\infty(\mathcal{X}) = \bigcap_{m \geq 1} C_b^m(\mathcal{X})$ is dense in $L^p(\mathcal{X}), 1 \leq p < +\infty$; see [12]. Let $L_0^2(\mathcal{X}) = \{f \in L^2(\mathcal{X}) | E_0 f = 0\}$, where E_0 is the expectation associated with the probability measure P_0 .

Let Ω be the space of \mathcal{X} -valued continuous function $C([0, \infty); \mathcal{X})$ and let ℓ be its Borel σ -algebra. Let $P^t, t \geq 0$, be a strongly continuous Markov semigroup on $L^2(\mathcal{X})$, which satisfies the following properties.

(P1) $P^t \mathbf{1} = \mathbf{1}$ and $P^t f \geq 0$, if $f \geq 0$.

(P2) $\int P^t f dP_0 = \int f dP_0$, for all $f \in L^2(\mathcal{X}), t \geq 0$.

(P3) $E_\chi[f(\theta_{t+h}(\omega)) | \ell_{\leq t}] = P^h F(\omega(t))$, where $F(\chi) := E_\chi f$, for any $f \in L^1(\Omega), t, h \geq 0, \chi \in \mathcal{X}$.

In the property P3, $E_\chi[\cdot]$ is the expectation associated with the probability measures $P_\chi, \ell_{\leq t}$ are the σ -algebras generated by events measurable up to time t , and $\theta_t(\omega)(\cdot) := \omega(\cdot + t), t \geq 0$ is the standard shift operator on the path space (Ω, ℓ) .

Moreover, we can define a Markovian measure P on the path space (Ω, ℓ) through

$$P(A) = \int P_x(A) P_0(d\chi), \quad A \in \ell \quad (6.2)$$

and define E to be the corresponding expectation operator with respect to the measure P . As a direct consequence of (T3) and (P2), we know that P is stationary.

Proposition 6.1. *P is invariant under the action of θ_t and τ_x for any $(t, x) \in \mathbb{R}^+ \times \mathbb{R}^d$.*

Let $L : \mathcal{D}(L) \rightarrow L^2(\mathcal{X})$ be the generator of the semigroup P^t . To establish the central limit theorem for the Markov process associated with P^t , we assume the generator L satisfies the following time relaxation property, also known as the spectral gap condition,

$$-(Lf, f)_{L^2(\mathcal{X})} \geq c_1 \|f\|_{L^2(\mathcal{X})}^2, \quad \text{where } c_1 > 0. \quad (6.3)$$

The time relaxation property (6.3) is equivalent to the exponential decay property

$$\|P^t f\|_{L^2(\mathcal{X})} \leq \exp(-c_1 t) \|f\|_{L^2(\mathcal{X})}, \quad f \in L_0^2(\mathcal{X}). \quad (6.4)$$

In addition, time relaxation property (6.3) is equivalent to ρ -mixing of the process $X(t)$, $t \geq 0$. Specifically, let

$$\rho(h) = \sup\{Cor(Y_1, Y_2) : Y_1 \text{ is } \ell_{\geq t+h} \text{ measurable, } Y_2 \text{ is } \ell_{\leq t} \text{ measurable}\}$$

, where $Cor(Y_1, Y_2)$ is the correlation function. Then, (6.3) or (6.4) implies that $\lim_{h \rightarrow \infty} \rho(h) = 0$; see [14, 48]. The time relaxation property (6.3) (or the exponential decay property (6.4)) plays an important role in proving the existence of the effective diffusivity. We will numerically investigate this property in Section 6.4.

6.1.2 The continuous-type corrector problem and effective diffusivity

Equipped with the necessary properties and notations, we are ready to study the effective diffusivity of the random flows associated with the passive tracer model (2.1). First we assume that the random flow $v = (b_1, \dots, b_d) \in (L^2(\mathcal{X}))^d$ is jointly continuous in (t, x) , locally Lipschitz in x , with finite second moments, and is divergence free. We are interested in the statistical properties of the solution $X(t)$, which only requires convergence in law. Therefore, our assumptions on the velocity field v are reasonable.

For each fixed realization ω of the environment, we consider the stochastic process generated by the following SDE,

$$\begin{cases} dX_t^\omega = v(t, X_t^\omega, \omega)dt + \sigma dW_t, \\ X_0^\omega = 0, \end{cases} \quad (6.5)$$

where $X_t^\omega \in \mathbb{R}^d$ is the position of the particle and the superscript in X_t^ω means that it depends on the realization of the environment ω . Here, the random flow means $v(t, x, \omega) = v(\tau_x \omega(t))$. Viewed from a particle at any instant of time t , we can define an environment process $\eta : [0, \infty) \times \Omega \rightarrow \mathcal{X}$ as

$$\begin{cases} \eta(t) = \tau_{X_t^\omega} \omega(t), \\ \eta(0) = \omega(0). \end{cases} \quad (6.6)$$

In addition, environment process generates a semigroup of transformation

$$S^t f(x) = E_x f(\eta(t)), \quad t \geq 0, \quad \forall f \in L^\infty(\mathcal{X}), \quad (6.7)$$

where $\eta(t)$ is defined by (6.6). And S^t satisfies the following properties,

Proposition 6.2. [(P1)]

1. $S^t, t \geq 0$ is a strongly continuous, Markov semigroup of contraction on $L^2(\mathcal{X})$.
2. $S^t, t \geq 0$ is measure-preserving, that is,

$$\int S^t f dP_0 = \int f dP_0, \quad t \geq 0, \quad f \in L^2(\mathcal{X}). \quad (6.8)$$

Let $D_1 = \mathcal{D}(L) \cap C_b^2(\mathcal{X})$ and \mathcal{L} denote the generator of the semigroup S^t , $t \geq 0$, i.e.,

$$\mathcal{L}f = Lf + \frac{\sigma^2}{2}\Delta f + v \cdot \nabla f, \quad (6.9)$$

where L is the generator of the semigroup P^t . One can easily verify the following properties.

Proposition 6.3. [(P1)]

1. D_1 is dense in $L^2(\mathcal{X})$ and is invariant under the semigroup P^t , $t \geq 0$, i.e., $P^t(D_1) \subseteq D_1$ for all $t \geq 0$.
2. Assume that the random flow v is bounded. Then, D_1 is invariant under the semigroup S^t , $t \geq 0$, i.e., $S^t(D_1) \subseteq D_1$ for all $t \geq 0$.

Lemma 6.1. From the spectral gap condition (6.3), we obtain that for any $f \in L_0^2(\mathcal{X})$

$$\|S^t f\|_{L^2(\mathcal{X})} \leq \exp(-c_1 t) \|f\|_{L^2(\mathcal{X})}, \quad \text{where } c_1 > 0. \quad (6.10)$$

Proof. We first assume v is bounded and $f \in D_1 \subseteq \mathcal{D}(\mathcal{L})$. Using the spectral gap condition and v is divergence free, we have

$$(-\mathcal{L}f, f)_{L_0^2(\mathcal{X})} \geq (-Lf, f)_{L_0^2(\mathcal{X})} \geq c_1 \|f\|_{L_0^2(\mathcal{X})}^2 \quad (6.11)$$

for all $f \in D_1 \cap L_0^2(\mathcal{X})$. By Proposition 6.3, $S^t f \in D_1$, $t \geq 0$ for any $f \in D_1$. Consequently,

$$\frac{d}{dt} \|S^t f\|_{L^2(\mathcal{X})}^2 = 2(\mathcal{L}S^t f, S^t f)_{L^2(\mathcal{X})} \leq -2c_1 \|S^t f\|_{L^2(\mathcal{X})}^2, \quad (6.12)$$

thus

$$\|S^t f\|_{L^2(\mathcal{X})}^2 \leq \exp(-c_1 t) \|f\|_{L^2(\mathcal{X})}^2 \quad \forall t \geq 0 \quad (6.13)$$

and $f \in D_1 \cap L_0^2(\mathcal{X})$. Then, the statement in (6.10) is extended to $L_0^2(\mathcal{X})$ by using an approximation argument. Finally, the boundedness of the random flow v is removed by using another approximation argument. \square

Given the semigroup of transformation S^t in (6.7) and its associated properties; see Proposition 6.2, we can define

$$\psi = \int_0^\infty S^t v dt \quad (6.14)$$

which satisfies the following continuous-type corrector problem

$$\mathcal{L}\psi = -v \tag{6.15}$$

where \mathcal{L} is the generator of S^t defined in (6.9). By solving the corrector problem (6.15), we are able to define the effective diffusivity. This can be summarized into the following result.

Proposition 6.4. *Let $X(t)$ be the solution to (2.1) and $X_\epsilon(t) \equiv \epsilon X(t/\epsilon^2)$. For any unit vector $\mathbf{v} \in \mathbb{R}^d$, let $\psi_{\mathbf{v}} = \boldsymbol{\psi} \cdot \mathbf{v}$ denote the projection of the vector solution $\boldsymbol{\psi}$ along the direction \mathbf{v} , where $\boldsymbol{\psi}$ is the solution to corrector problem (6.15). Then, the law of the process $X_\epsilon(t) \cdot \mathbf{v}$ converges weakly in $C[0, +\infty)$ to a Brownian motion with diffusion coefficient given by*

$$\mathbf{v}^T D^E \mathbf{v} = \frac{\sigma^2}{2} + (-\mathcal{L}\psi_{\mathbf{v}}, \psi_{\mathbf{v}})_{L^2(\mathcal{X})}, \tag{6.16}$$

where D^E is the effective diffusivity associated with the passive tracer model (2.1).

The proof of Prop. 6.4 relies on an approximation of the additive functional of an ergodic Markov process by a martingale and applying the central limit theorem to continuous-time Markov process, which is very useful in studying the long-time behavior of random dynamics; see Lemma 1 of [19] or Theorem of [8]. We shall prove in Theorem 6.7 that the numerical solutions obtained by our Lagrangian numerical scheme recover the definition of the effective diffusivity in (6.16).

6.2 Stochastic structure-preserving schemes and related properties

6.2.1 Derivation of numerical schemes

In this part, we construct numerical schemes for the passive tracer model (6.5), which is based on an operator splitting method [51]. For each fixed

realization ω of the environment, we first split the original problem (6.5) into two sub-problems.

$$dX_t^\omega = v(t, X_t^\omega, \omega)dt, \quad (6.17)$$

$$dX_t^\omega = \sigma dW_t. \quad (6.18)$$

Let X_n^ω denote the numerical solution of X_t^ω at time $t = t_n$, $n = 0, 1, 2, \dots$. From time $t = t_n$ to time $t = t_{n+1}$, where $t_{n+1} = t_n + \Delta t$, $t_0 = 0$, assuming the solution X_n^ω is given, we now discuss how to discretize the above two sub-problems (6.17)-(6.18), separately.

In the sub-problem (6.17), the velocity $v(t, x, \omega)$ is almost surely divergence-free and has certain regularity in the physical space. Thus, we apply a volume-preserving scheme to discretize (6.17). Let $\Phi_{\Delta t}$ denote the numerical integrator associated with the volume-preserving scheme during Δt time and let $\mathbf{D}\Phi_{\Delta t}$ denote the corresponding Jacobian matrix. The volume-preserving property requests $\det(\mathbf{D}\Phi_{\Delta t}) = 1$. We obtain the numerical integrator for the sub-problem (6.17) as follows,

$$X_{n+1}^\omega = \Phi_{\Delta t}^{\omega(n\Delta t)}(X_n^\omega), \quad (6.19)$$

where the superscript in $\Phi_{\Delta t}^{\omega(n\Delta t)}$ means that the numerical integrator implicitly depends on the realization of v at different computational times. Suppose v has bounded first derivatives with respect to x for almost all ω , it is easy to verify that the volume-preserving integrator $\Phi_{\Delta t}^{\omega(n\Delta t)}$ also has bounded first derivatives for Δt small enough. Thus, $\Phi_{\Delta t}^{\omega(n\Delta t)}$ is well defined.

In addition, we assume that the numerical scheme only relies on the information of X and v at the beginning of each computational time, in order to make sure the solution process generated by our method is a Markov process. For instance, to compute X_{n+1}^ω the numerical scheme only relies on the information of X and v at $t = t_n$.

We illustrate this idea by constructing a volume-preserving scheme for a two-dimensional problem. Let $X_n^\omega = (X_{n,1}^\omega, X_{n,2}^\omega)^T$ denote the numerical solution at time $t = t_n$ and the velocity $v(t, x, \omega) = (b_1(t, x, \omega), b_2(t, x, \omega))^T$. Then,

we apply a midpoint scheme to discretize (6.17) and obtain

$$(X_{n+1,1}^\omega, X_{n+1,2}^\omega)^T = (X_{n,1}^\omega, X_{n,2}^\omega)^T + \Delta t v\left(t_n, \left(\frac{X_{n,1}^\omega + X_{n+1,1}^\omega}{2}, \frac{X_{n,2}^\omega + X_{n+1,2}^\omega}{2}\right)^T, \omega\right). \quad (6.20)$$

By solving Eq.(6.20) to get $(X_{n+1,1}^\omega, X_{n+1,2}^\omega)^T$, we implicitly define a numerical integrator $\Phi_{\Delta t}^{\omega(n\Delta t)}$; see Eq.(6.19). Since $v(t, x, \omega)$ is almost surely divergence-free, we can easily verify that the scheme (6.20) is volume-preserving, i.e, $\det(\mathbf{D}\Phi_{\Delta t}^{\omega(n\Delta t)}) = 1$. Moreover, simple Taylor-expansion analysis shows that the local truncation error of the scheme (6.20) is $O(\Delta t)^2$.

For a d -dimensional sub-problem (6.17), we split the velocity field $v(t, x, \omega)$ into a summation of $d - 1$ velocity fields, where each of them will generate a two-dimensional problem and thus we can design the volume-preserving scheme accordingly. By applying a splitting method [38], we can construct volume-preserving schemes for the original d -dimensional sub-problem (6.17). More details can be found in [20, 27].

Given the numerical integrator $\Phi_{\Delta t}^{\omega(n\Delta t)}$, we define the mapping

$$V_{\Delta t}^{\omega(n\Delta t)}(x) = \Phi_{\Delta t}^{\omega(n\Delta t)}(x) - x. \quad (6.21)$$

One can easily verify that $V_{\Delta t}^{\omega(n\Delta t)}(X_n^\omega)$ is an approximation of the increment for the exact solution of the sub-problem (6.17) as follows,

$$X_{(n+1)\Delta t}^\omega - X_{n\Delta t}^\omega = \int_{n\Delta t}^{(n+1)\Delta t} v(t, X_t^\omega, \omega) dt. \quad (6.22)$$

The sub-problem (6.18) can be approximated easily using the Euler-Maruyama scheme [32].

Finally, we apply the Lie-Trotter splitting method and get the stochastic structure-preserving scheme as follows,

$$X_{n+1}^\omega = X_n^\omega + V_{\Delta t}^{\omega(n\Delta t)}(X_n^\omega) + \sigma N_n, \quad (6.23)$$

where $N_n = (N_1, \dots, N_d)^T$ is a d -dimensional i.i.d. mean-free Gaussian random vector with $EN_n \otimes N_n = \Delta t I_d$. Here I_d is an identity matrix.

The volume-preserving schemes for the sub-problem (6.17) are implicit in general. Compared with explicit schemes, however, they allow us to choose a relatively larger time step to compute. In practice, we find that a few steps of Newton iterations are good enough to maintain accurate results. Therefore, the computational cost is controllable. To design adaptive time-stepping method for the passive tracer model (6.5) is an interesting issue, which will be studied in our future work.

In general, the second-order Strang splitting [51] is more frequently used in developing numerical schemes. In fact, the only difference between the Strang splitting method and the Lie-Trotter splitting method is that the first and last steps are half of the time step Δt . For the SDEs, however, the dominant source of error comes from the random subproblem (6.18). Thus, it is not necessary to implement the Strang splitting scheme here.

6.2.2 Some properties of the numerical schemes

In this subsection, we shall prove some properties of the proposed stochastic structure-preserving scheme. Especially, we shall show that some important properties of the random flows are maintained after numerical discretization. Before proceeding to the analysis, we first introduce some notations and assumptions. To emphasize the properties in spatial-domain, for any $f \in L^1(\mathcal{X})$, we use $f^\chi(x)$ to represent $f(\tau_x\chi)$. Moreover, we denote $v(t, x, \omega) = v(\tau_x\omega(t))$, where $\tau_x\omega(t) \in \mathcal{X}$.

Assumption 6.1. *Suppose the velocity field has certain regularity in the physical space, i.e., $v \in (C_b^m(\mathcal{X}))^d$ for some $m \geq 2$.*

Assumption 6.2. *$V_{\Delta t}^\chi(x)$ defined in (6.21) is a stationary process with respect to x , i.e., we can write $V_{\Delta t}^\chi(x) = V_{\Delta t}(\tau_x\chi)$.*

Assumption 6.3. *If Δt is small enough, we have $V_{\Delta t} \in (C_b^m(\mathcal{X}))^d$ provides that $v \in (C_b^m(\mathcal{X}))^d$. In addition, $\|V_{\Delta t}\|_{C_b^m(\mathcal{X})} = K\|v\|_{C_b^m(\mathcal{X})}\Delta t$, where K is a constant that does not depend on Δt .*

As an analogy to the continuous-time case (6.6), we define the environment process as viewed from the numerical solution X_n^ω at different time steps

$$\begin{cases} \eta_n = \tau_{X_n^\omega} \omega(n\Delta t), \\ \eta_0 = \omega(0). \end{cases} \quad (6.24)$$

The above environment process induces a probability measure Q_χ on the space of trajectories $(\tilde{\Omega}, \ell)$, where $\tilde{\Omega} = C([0, \infty) \cap \Delta t\mathbb{Z}; \mathcal{X})$. We denote the corresponding expectation operator as E_χ . Under this process, we can write $V_{\Delta t}(\eta_n) = V_{\Delta t}^{\omega(n\Delta t)}(X_n^\omega)$. In addition, we define

$$S_n f(\chi) = E_\chi f(\eta_n). \quad (6.25)$$

We shall prove that S_n is a discrete-time Markov semi-group of contraction on $L^2(\mathcal{X})$ and is measure-preserving with respect to P_0 defined in Section 6.1.1.

Theorem 6.1. *P_0 is an invariant probability measure of η_n , i.e., P_0 is an invariant measure of the Markov semigroup $\{S_n\}$.*

Proof. Let $p_\chi^1(x, y)$ denote the transition probability density of the solution process, which is defined by applying the numerical scheme (6.23) for one time step. For simplicity of notation, let x be the current solution and y be the solution obtained by applying the scheme (6.23) with time step Δt . Notice that N_n in (6.23) is a mean-free Gaussian random vector. We have

$$p_\chi^1(x, y) = \frac{1}{(2\pi\sigma^2\Delta t)^{d/2}} \exp\left(-\frac{\|y - x - B_{\Delta t}^\chi(x)\|^2}{2\sigma^2\Delta t}\right) \quad (6.26)$$

$$= \frac{1}{(2\pi\sigma^2\Delta t)^{d/2}} \exp\left(-\frac{\|y - \Phi_{\Delta t}^\chi(x)\|^2}{2\sigma^2\Delta t}\right). \quad (6.27)$$

Let us define $p_0(x, y) = \frac{1}{(2\pi\sigma^2\Delta t)^{d/2}} \exp\left(-\frac{\|y-x\|^2}{2\sigma^2\Delta t}\right)$. Then, we can verify that

$$\begin{aligned} \int p_\chi^1(x, y) dx &= \int p_0(x + B_{\Delta t}^\chi(x), y) dx, \\ &= \int p_0(z, y) \det(\mathbf{D}\Phi_{\Delta t}^\chi)^{-1} dz = \int p_0(z, y) dz = 1, \quad a.e. \chi, \end{aligned} \quad (6.28)$$

where we have used the fact that the numerical scheme (6.19) for sub-problem (6.17) is volume-preserving, i.e., $\det(\mathbf{D}\Phi_{\Delta t}^\chi) = 1$. Thus, for all $f \in L^2(\mathcal{X})$, we

have

$$\begin{aligned}
 \int_{\mathcal{X}} S_1 f(\chi) P_0(d\chi) &= \int_{\mathcal{X}} E_{\chi} f(\eta_1) P_0(d\chi) = \int_{\mathcal{X}} P_0(d\chi) \int_{\mathbb{R}^d} p_{\chi}^1(0, y) E_{\chi} f(\tau_y \omega(\Delta t)) dy, \\
 &= \int_{\mathcal{X}} E_{\chi} f(\omega(\Delta t)) P_0(d\chi) \int_{\mathbb{R}^d} p_{\tau_{-y}\chi}^1(0, y) dy, \\
 &= \int_{\mathcal{X}} E_{\chi} f(\omega(\Delta t)) P_0(d\chi) \int_{\mathbb{R}^d} p_{\chi}^1(-y, 0) dy, \\
 &= \int_{\mathcal{X}} E_{\chi} f(\omega(\Delta t)) P_0(d\chi), \tag{6.29}
 \end{aligned}$$

where we have used the facts that

$$p_{\tau_x\chi}^1(y, z) = p_{\chi}^1(y + x, z + x) \tag{6.30}$$

, and

$$\int_{\mathbb{R}^d} p_{\chi}^1(-y, 0) dy = 1. \tag{6.31}$$

Thus, we obtain from (6.29) that $ES_1 f = EP^{\Delta t} f = Ef$, where $P^{\Delta t}$ is measure-preserving by property (P2) in Section 6.1.1. Similar argument shows that $ES_n f = ES_{n-1} f$ for all n . We prove that S_n is measure-preserving. \square

Remark 6.1. *Theorem 6.1 plays an important role in the remaining part of our convergence analysis. Throughout the proof, one can see that using a volume-preserving numerical scheme for solving sub-problem (6.17) is essential.*

Remark 6.2. *In the proof of Theorem 6.1, the probability measures $p_{\chi}^1(x, y)$ and $p_0(x, y)$ are associated with the Brownian motion in the passive tracer model. While $P_0(d\chi)$ is the probability measure associate with the randomness in the velocity field and initial data. In the remaining part of this chapter, we shall keep the same notations.*

The following lemma will be very useful in our analysis.

Lemma 6.2. *For any $y \in \mathbb{R}^d$ and $f \in L^2(\mathcal{X})$, we have that*

$$Ef(\tau_y \eta_n) = Ef(\eta_{n-1}) = Ef. \tag{6.32}$$

Moreover,

$$Ef(\eta_{n+1}) = Ef\left(\tau_{X_n^{\omega} + V_{\Delta t}(\eta_n)} \omega((n+1)\Delta t)\right) = Ef. \tag{6.33}$$

Proof. We prove the above equations through direct calculations. For the equation (6.32), we have

$$\begin{aligned}
 Ef(\tau_y \eta_n) &= EE_{\eta_{n-1}} f(\tau_y \tilde{\eta}_1) = \int_{\mathcal{X}} P_0(d\chi) \int_{\mathbb{R}^d} p_{\eta_{n-1}}^1(0, z) E_{\eta_{n-1}} f(\tau_{y+z} \omega(\Delta t)) dz, \\
 &= \int_{\mathcal{X}} E_{\eta_{n-1}} f(\omega(\Delta t)) P_0(d\chi) \int_{\mathbb{R}^d} p_{\tau_{-y-z} \eta_{n-1}}^1(0, z) dz, \\
 &= \int_{\mathcal{X}} E_{\eta_{n-1}} f(\omega(\Delta t)) P_0(d\chi) \int_{\mathbb{R}^d} p_{\eta_{n-1}}^1(-y-z, -y) dz, \\
 &= \int_{\mathcal{X}} E_{\eta_{n-1}} f(\omega(\Delta t)) P_0(d\chi) = \int_{\mathcal{X}} f(\eta_{n-1}) P_0(d\chi), \tag{6.34}
 \end{aligned}$$

where $\tilde{\eta}_1$ is defined according to (6.24) but with initial condition $\tilde{\eta}_0 = \eta_{n-1}$. Thus, the first equation in (6.32) is proved. The second equation in (6.32) is obvious according to the definition (6.25) and S_n is measure-preserving.

To prove the equation (6.33), let $Y_n^\omega = X_n^\omega + V_{\Delta t}(\eta_n) = X_{n+1}^\omega - \sigma N_n$. Then, we have

$$\begin{aligned}
 Ef(\eta_{n+1}) &= EE_{\eta_n} f(\tau_{Y_n^\omega + \sigma N_n} \omega(\Delta t)) = \int_{\mathcal{X}} P_0(d\chi) \int_{\mathbb{R}^d} p_0(0, z) E_{\eta_n} f(\tau_z \tau_{Y_n^\omega} \omega(\Delta t)) dz, \\
 &= \int_{\mathcal{X}} E_{\eta_n} f(\tau_{Y_n^\omega} \omega(\Delta t)) P_0(d\chi) \int_{\mathbb{R}^d} p_0(0, z) dz, \\
 &= Ef\left(\tau_{X_n^\omega + V_{\Delta t}(\eta_n)} \omega((n+1)\Delta t)\right). \tag{6.35}
 \end{aligned}$$

Notice that in the proof we use the property that τ is a measure-preserving transformation. \square

Equipped with these preparations, we can state the main results. The first result is that the operator S_n defined in (6.25) is a contractive map on $L^2(\mathcal{X})$.

Theorem 6.2. S_n has the property that

$$\|S_n f\|_{L^2(\mathcal{X})} \leq \exp(-c_1 n \Delta t) \|f\|_{L^2(\mathcal{X})}, \tag{6.36}$$

for all $f \in L_0^2(\mathcal{X})$.

Proof. We first consider the case when $n = 1$. The key observation is that

$$\begin{aligned}
 & \int_{\mathcal{X}} S_1 f(\chi) \cdot S_1 f(\chi) P_0(d\chi) = \int_{\mathcal{X}} E_{\chi} f(\eta_1) \cdot E_{\chi} f(\eta_1) P_0(d\chi), \\
 &= \int_{\mathcal{X}} P_0(d\chi) \int_{\mathbb{R}^d} p_{\chi}^1(0, y) E_{\chi} f(\tau_y \omega(\Delta t)) dy \cdot \int_{\mathbb{R}^d} p_{\chi}^1(0, y) E_{\chi} f(\tau_y \omega(\Delta t)) dy, \\
 &\leq \int_{\mathcal{X}} P_0(d\chi) \int_{\mathbb{R}^d} p_{\chi}^1(0, y) E_{\chi} f(\tau_y \omega(\Delta t)) \cdot E_{\chi} f(\tau_y \omega(\Delta t)) dy, \\
 &= \int_{\mathcal{X}} E_{\chi} f(\omega(\Delta t)) \cdot E_{\chi} f(\omega(\Delta t)) P_0(d\chi) \int_{\mathbb{R}^d} p_{\chi}^1(-y, 0) dy, \\
 &= \int_{\mathcal{X}} P^{\Delta t} f(\chi) \cdot P^{\Delta t} f(\chi) P_0(d\chi), \tag{6.37}
 \end{aligned}$$

where $P^{\Delta t}$ is a strongly continuous Markov semigroup on $L^2(\mathcal{X})$. In the third line of (6.37), we use the fact that $p_{\chi}^1(0, y)$ is a probability density function so we can easily get the result by using the Cauchy-Schwarz inequality. Therefore, we obtain

$$\|S_1 f\|_{L^2(\mathcal{X})} \leq \|P^{\Delta t} f\|_{L^2(\mathcal{X})} \leq \exp(-c_1 \Delta t) \|f\|_{L^2(\mathcal{X})}, \tag{6.38}$$

where the exponential decay property (6.4) is used. The assertion in (6.36) can be obtained if we repeat to use the above property n times. \square

Next, we define $\bar{V}_{\Delta t} = EV_{\Delta t}$ and $\tilde{V}_{\Delta t} = V_{\Delta t} - \bar{V}_{\Delta t}$. We aim to get some estimates for the mean values $\bar{V}_{\Delta t}$ and EX_n^{ω} , which are important in our convergence analysis for the effective diffusivity later.

Theorem 6.3. *If we choose a volume-preserving numerical scheme (6.19) to compute the sub-problem (6.17), where the local truncation error is $O(\Delta t)^2$, then $\bar{V}_{\Delta t}$ is of order $O(\Delta t)^2$. In addition, $EX_n^{\omega} - n\bar{V}_{\Delta t}$ is bounded.*

Proof. By using a volume-preserving numerical scheme (with a local truncation error $O(\Delta t)^2$) to compute (6.17), we have

$$EV_{\Delta t} = E \int_0^{\Delta t} v(t, X_t^{\omega}, \omega) dt + O(\Delta t)^2 = E \int_0^{\Delta t} v(\eta_t^0) dt + O(\Delta t)^2, \tag{6.39}$$

where η_t^0 is the environment process defined in (6.6) with $\sigma = 0$. Notice that when we define $V_{\Delta t}$, we only consider the sub-problem (6.17). Recall the fact

that S^t is measure-preserving, so we get

$$E \int_0^{\Delta t} v(\eta_t^0) dt = \int_0^{\Delta t} \int_{\mathcal{X}} E_{\chi} v(\eta_t^0) dP_0(\chi) dt = \int_0^{\Delta t} ES^t v dt = \int_0^{\Delta t} Ebdt = 0, \quad (6.40)$$

where we have used the definition of S^t in (6.7) and v is mean-zero. Therefore, $EV_{\Delta t}$ is of the order $(\Delta t)^2$. Moreover, from the numerical scheme (6.23) we have

$$\begin{aligned} EX_n^{\omega} &= EX_{n-1}^{\omega} + EB_{\Delta t}^{\omega(n\Delta t)}(X_n^{\omega}) \\ &= EX_0^{\omega} + \sum_{i=0}^{n-1} ES_i V_{\Delta t} = EX_0^{\omega} + \sum_{i=0}^{n-1} ES_i \tilde{V}_{\Delta t} + n\bar{V}_{\Delta t}. \end{aligned} \quad (6.41)$$

According to (6.36) in Theorem 6.2, we can easily verify that $\sum_{i=0}^{n-1} S_i \tilde{V}_{\Delta t}$ is bounded in $L^2(\mathcal{X})$, which implies $|\sum_{i=0}^{n-1} ES_i \tilde{V}_{\Delta t}| < \infty$. Thus, we prove that $EX_n^{\omega} - n\bar{V}_{\Delta t}$ is bounded. \square

6.2.3 A discrete-type corrector problem

The corrector problem (6.15) plays an important role in defining the effective diffusivity for the random flow. To study the property of the numerical solutions, we will define a discrete-type corrector problem and study the property of its solution.

Theorem 6.4. *Let us define $\boldsymbol{\psi}_{\Delta t} = \sum_{i=0}^{\infty} S_i \tilde{V}_{\Delta t}$. Then, $\boldsymbol{\psi}_{\Delta t}$ is the unique solution of the discrete-type corrector problem in $(L_0^2(\mathcal{X}))^d$ defined as follows*

$$(S_1 - I)\boldsymbol{\psi}_{\Delta t} = -\tilde{V}_{\Delta t}. \quad (6.42)$$

Proof. The formulation of $\boldsymbol{\psi}_{\Delta t}$ solves the discrete-type corrector problem (6.42) can be easily verified through simple calculations, i.e.,

$$(S_1 - I)\boldsymbol{\psi}_{\Delta t} = \sum_{i=1}^{\infty} S_i \tilde{V}_{\Delta t} - \sum_{i=0}^{\infty} S_i \tilde{V}_{\Delta t} = -\tilde{V}_{\Delta t}. \quad (6.43)$$

The property $E\boldsymbol{\psi}_{\Delta t} = 0$ is a straightforward result from the formulation of $\boldsymbol{\psi}_{\Delta t}$. The uniqueness of the solution comes from Theorem 6.2. Suppose the

equation (6.42) has two different solutions $\boldsymbol{\psi}_1, \boldsymbol{\psi}_2 \in L_0^2(\mathcal{X})$, we have that $(S_1 - I)(\boldsymbol{\psi}_1 - \boldsymbol{\psi}_2) = 0$, then

$$\|\boldsymbol{\psi}_1 - \boldsymbol{\psi}_2\|_{L^2(\mathcal{X})} = \|S_1(\boldsymbol{\psi}_1 - \boldsymbol{\psi}_2)\|_{L^2(\mathcal{X})} \leq \exp(-c_1 \Delta t) \|\boldsymbol{\psi}_1 - \boldsymbol{\psi}_2\|_{L^2(\mathcal{X})},$$

which implies that $\boldsymbol{\psi}_1 - \boldsymbol{\psi}_2 = 0$. Thus, the uniqueness of solution for Eq.(6.42) is proved. \square

Remark 6.3. *The formulation of the discrete-type corrector problem (6.42) is equivalent to the equation*

$$E[\boldsymbol{\psi}_{\Delta t}^{\omega((i)\Delta t)}(X_i^\omega) | X_{i-1}^\omega] - \boldsymbol{\psi}_{\Delta t}^{\omega((i-1)\Delta t)}(X_{i-1}^\omega) = -\tilde{V}_{\Delta t}^{\omega((i-1)\Delta t)}(X_{i-1}^\omega). \quad (6.44)$$

This can be seen by replacing χ with η_{n-1} in the definition of S_1 ; see Eq.(6.25).

Finally, we study the regularity of the solution of the discrete-type corrector problem (6.42). The following result is based on the regularity assumption on the velocity field v . Since we are interested in statistical properties of the solution $X(t)$, which only requires convergence in law, we can choose smooth realizations of the velocity field v .

Theorem 6.5. *Suppose $v \in (C_b^m(\mathcal{X}))^d$, then $\boldsymbol{\psi}_{\Delta t}$ is in $(H^m(\mathcal{X}))^d$.*

Proof. First we prove that, under the assumption $v \in (C_b^m(\mathcal{X}))^d$ for $m \geq 1$, we have that for any $f \in L^2(\mathcal{X})$, $S_1 f \in H^1(\mathcal{X})$. Since

$$\begin{aligned} S_1 f(\tau_x \chi) &= \int_{\mathbb{R}^d} p_{\tau_x \chi}^1(0, y) P^{\Delta t} f(\tau_{x+y} \chi) dy = \int_{\mathbb{R}^d} p_\chi^1(x, x+y) P^{\Delta t} f(\tau_{x+y} \chi) dy, \\ &= \int_{\mathbb{R}^d} p_\chi^1(x, y) P^{\Delta t} f(\tau_y \chi) dy, \end{aligned} \quad (6.45)$$

where $p_\chi^1(x, y)$ is the transition probability density defined in (6.27). Notice that

$$\mathbf{D}_x p_\chi^1(x, y) = 2(I + \mathbf{D}V_{\Delta t}^\chi(x))(y - x - B_{\Delta t}^\chi(x)) p_\chi^1(x, y), \quad (6.46)$$

and $V_{\Delta t} \in (C_b^m(\mathcal{X}))^d$, we can obtain that $\int_{\mathbb{R}^d} (y - x - B_{\Delta t}^\chi(x))^2 p_\chi^1(x, y) dx$ is uniformly bounded for almost all χ . This concludes that

$$\int_{\mathbb{R}^d} \mathbf{D}_x p_\chi^1(x, y) P^{\Delta t} f(\tau_y \chi) dy \in L^2(\mathcal{X}). \quad (6.47)$$

The statement (6.47) implies that $\mathbf{D}S_1 f \in L^2(\mathcal{X})$ by the dominant convergence theorem. Thus $S_1 f \in H^1(\mathcal{X})$. According to the definition of the discrete-type corrector problem (6.42), $\boldsymbol{\psi}_{\Delta t}$ satisfies

$$\boldsymbol{\psi}_{\Delta t} = S_1 \boldsymbol{\psi}_{\Delta t} + \tilde{V}_{\Delta t}. \quad (6.48)$$

Therefore, we obtain that $\boldsymbol{\psi}_{\Delta t} \in (H^1(\mathcal{X}))^d$. Moreover, noticing that

$$\begin{aligned} \mathbf{D}S_1 f(\chi) &= \int_{\mathbb{R}^d} \mathbf{D}_x p_\chi^1(0, y) P^{\Delta t} f(\tau_y \chi) dy, \\ &= \int_{\mathbb{R}^d} 2(I + \mathbf{D}V_{\Delta t}^\chi(0))(y - 0 - B_{\Delta t}^\chi(0)) p_\chi^1(x, y) P^{\Delta t} f(\tau_y \chi) dy, \\ &= 2(I + \mathbf{D}V_{\Delta t}^\chi(0)) \int_{\mathbb{R}^d} -\mathbf{D}_y p_\chi^1(0, y) P^{\Delta t} f(\tau_y \chi) dy, \\ &= 2(I + \mathbf{D}V_{\Delta t}^\chi(0)) \int_{\mathbb{R}^d} p_\chi^1(0, y) \mathbf{D}_y P^{\Delta t} f(\tau_y \chi) dy, \\ &= 2(I + \mathbf{D}V_{\Delta t}^\chi(0)) S_1 \mathbf{D}f(\chi). \end{aligned} \quad (6.49)$$

We arrive that

$$\mathbf{D}\boldsymbol{\psi}_{\Delta t} = 2(I + \mathbf{D}V_{\Delta t}) S_1 \mathbf{D}\boldsymbol{\psi}_{\Delta t} + \mathbf{D}\tilde{V}_{\Delta t}. \quad (6.50)$$

Similar argument shows that $\mathbf{D}\boldsymbol{\psi}_{\Delta t} \in (H^1(\mathcal{X}))^{d \times d}$. Doing this argument recursively, we prove that $\boldsymbol{\psi}_{\Delta t}$ is in $(H^m(\mathcal{X}))^d$. \square

6.3 Convergence analysis

In this section, we shall prove the convergence rate of our stochastic structure-preserving scheme in computing effective diffusivity. The convergence analysis is based on a probabilistic approach, which allows us to get rid of the exponential growth factor in the error estimate.

6.3.1 Convergence of the discrete-type corrector problem to the continuous one

We first show that, if Δt is small enough, $S^{\Delta t}$ will converge to S_1 . Moreover, the following statement holds.

Lemma 6.3. *If f is a globally Lipschitz function with respect to x , then we have*

$$\|S_n f - S^{n\Delta t} f\|_{L^2(\mathcal{X})} \leq c_2 L(\Delta t)^2, \quad (6.51)$$

where L is the Lipschitz constant for f and c_2 depends only on the computational time $T = n\Delta t$.

Proof. According to the definitions of the semigroups in (6.7) and (6.25), we have that $(S_n - S^{n\Delta t})f(\chi) = E_\chi(f(\eta_n) - f(\eta(n\Delta t)))$, which implies

$$(S_n - S^{n\Delta t})f(\chi) \leq L E_\chi |X_n^\omega - X_{n\Delta t}^\omega|. \quad (6.52)$$

A basic comparison with Euler-Maruyama method [32] shows that $E_\chi |X_n^\omega - X_{n\Delta t}^\omega| < c_2(\Delta t)^2$ for all χ with the regularity assumption for v ; see Asm. 6.1. \square

Then, we show that under certain conditions the discrete-type corrector problem converges to the continuous one, which facilitates the convergence analysis of our numerical method in computing the effective diffusivity for random flows.

Theorem 6.6. *The solution $\psi_{\Delta t}$ converges to the solution ψ of the continuous-type corrector problem defined in (6.14) in $L^2(\mathcal{X})$, as $\Delta t \rightarrow 0$.*

Proof. Using the exponential decay properties of S^t and S_n , we first choose T and obtain the following two inequalities

$$\left\| \int_{T-\Delta t}^{\infty} S^t v dt \right\|_{L^2(\mathcal{X})} \leq \frac{1}{c_1} \exp(-c_1 T), \quad (6.53)$$

$$\left\| \sum_{n=[T/\Delta t]-1}^{\infty} S_n \tilde{V}_{\Delta t} \right\|_{L^2(\mathcal{X})} \leq \frac{1}{c_1} \exp(-c_1 T), \quad (6.54)$$

where $c_1 > 0$ is defined in (6.10). Then, for any $\epsilon > 0$, we choose T big enough such that $\frac{1}{c_1} \exp(-c_1 T) < \epsilon$. Next, we estimate the error between $\sum_{n=0}^{N-1} S_n \tilde{V}_{\Delta t}$ and $\int_0^{N\Delta t} S^t v dt$ for $N \leq T/\Delta t$. We know that

$$\left\| \int_0^{N\Delta t} S^t v dt - \sum_{n=0}^{N-1} S^{n\Delta t} v \Delta t \right\|_{L^2(\mathcal{X})} \leq C_1 \Delta t \quad (6.55)$$

due to the strongly continuity of S^t (see Prop. 6.2) and

$$\begin{aligned} \left\| \sum_{n=0}^{N-1} S_n \tilde{V}_{\Delta t} - \sum_{n=0}^{N-1} S^{n\Delta t} v \Delta t \right\|_{L^2(\mathcal{X})} &\leq \left\| \sum_{n=0}^{N-1} S_n \tilde{V}_{\Delta t} - \sum_{n=0}^{N-1} S_n v \Delta t \right\|_{L^2(\mathcal{X})} \\ &\quad + \left\| \sum_{n=0}^{N-1} S_n v \Delta t - \sum_{n=0}^{N-1} S^{n\Delta t} v \Delta t \right\|_{L^2(\mathcal{X})}. \end{aligned} \quad (6.56)$$

Since local truncation error of the numerical scheme (6.19) is at least second order, we have $\|\tilde{V}_{\Delta t} - v \Delta t\|_{L^2(\mathcal{X})} \leq O(\Delta t)^2$. The Lemma 6.3 implies $\|(S_n - S^{n\Delta t})v \Delta t\|_{L^2(\mathcal{X})} \leq O(\Delta t)^2$ for all $n \leq N$. This gives the estimate

$$\left\| \sum_{n=0}^{N-1} S_n \tilde{V}_{\Delta t} - \sum_{n=0}^{N-1} S^{n\Delta t} v \Delta t \right\|_{L^2(\mathcal{X})} \leq c_2 N (\Delta t)^2 \leq c_2 T \Delta t. \quad (6.57)$$

Finally, we take $\Delta t \leq \epsilon / (c_2 T)$ and obtain

$$\left\| \int_0^\infty S^t v dt - \sum_{n=0}^\infty S_n \tilde{V}_{\Delta t} \right\|_{L^2(\mathcal{X})} \leq 3\epsilon. \quad (6.58)$$

We prove the assertion of the Theorem. \square

Remark 6.4. *The constant c_2 in Lemma 6.3 is actually exponentially depends on T , i.e., $c_2 = \exp(c_3 T)$ with $c_3 > 0$. To balance each value of ϵ , we have $\frac{1}{c_1} \exp(-c_1 T) = \exp(c_3 T) T \Delta t$, which requires $T \approx -1 / (c_1 + c_3) \log \Delta t$ and $\epsilon \approx \frac{1}{c_1} \Delta t^{\frac{c_1}{c_1 + c_3}}$.*

6.3.2 Convergence of the numerical method in computing effective diffusivity

Now we are in a position to show the main results in random flows. We prove that the effective diffusivity obtained by our numerical method converges to the exact one defined in (6.16).

Theorem 6.7. *Let X_n^ω , $n = 0, 1, \dots$ be the numerical solution of the stochastic structure-preserving scheme (6.23) and Δt be the time step. Let $\bar{X}_n^\omega = X_n^\omega - n\bar{V}_{\Delta t}$. We have the convergence estimate of the numerical method in computing effective diffusivity as*

$$\frac{E \bar{X}_n^\omega \otimes \bar{X}_n^\omega}{n \Delta t} = \sigma^2 I_d + 2\mathbf{S} \int_{\mathcal{X}} \psi \otimes v dP_0 + \rho(\Delta t) + O\left(\frac{1}{\sqrt{n} \Delta t}\right), \quad (6.59)$$

where $\rho(\Delta t) = O(\Delta t^{\frac{c_1}{c_1+c_3}})$ is a function satisfying $\lim_{\Delta t \rightarrow 0} \rho(\Delta t) = 0$ and independent of the computational time T . The \mathbf{S} represents the symmetrization operator on a matrix, i.e., $\mathbf{SA} = \frac{\mathbf{A} + \mathbf{A}^T}{2}$.

Proof. First of all, from direct computations we can obtain that

$$\begin{aligned}
 & E\bar{X}_n^\omega \otimes \bar{X}_n^\omega \\
 &= E(\bar{X}_{n-1}^\omega + \tilde{V}_{\Delta t}^{\omega((n-1)\Delta t)}(X_{n-1}^\omega) + \sigma N_{n-1}) \otimes (\bar{X}_{n-1}^\omega + \tilde{V}_{\Delta t}^{\omega((n-1)\Delta t)}(X_{n-1}^\omega) + \sigma N_{n-1}), \\
 &= E\bar{X}_{n-1}^\omega \otimes \bar{X}_{n-1}^\omega + \sigma^2 I_d \Delta t + 2\mathbf{SE}\bar{X}_{n-1}^\omega \otimes \tilde{V}_{\Delta t}^{\omega((n-1)\Delta t)}(X_{n-1}^\omega) \\
 &\quad + E\tilde{V}_{\Delta t}^{\omega((n-1)\Delta t)}(\bar{X}_{n-1}^\omega) \otimes \tilde{V}_{\Delta t}^{\omega((n-1)\Delta t)}(X_{n-1}^\omega), \\
 &= E\bar{X}_0^\omega \otimes \bar{X}_0^\omega + \sigma^2 I_d n \Delta t + 2 \sum_{i=1}^n \mathbf{SE}\bar{X}_{i-1}^\omega \otimes \tilde{V}_{\Delta t}^{\omega((i-1)\Delta t)}(\bar{X}_{i-1}^\omega) \\
 &\quad + \sum_{i=1}^n E\tilde{V}_{\Delta t}^{\omega((i-1)\Delta t)}(X_{i-1}^\omega) \otimes \tilde{V}_{\Delta t}^{\omega((i-1)\Delta t)}(X_{i-1}^\omega), \tag{6.60}
 \end{aligned}$$

where we have used the conditions N_{n-1} is independent with \bar{X}_{n-1}^ω and $EN_n \otimes N_n = \Delta t I_d$.

The first two terms on the right hand side of Eq.(6.60) are easy to handle since $\frac{E\bar{X}_0^\omega \otimes \bar{X}_0^\omega}{n\Delta t} = O(\frac{1}{n\Delta t})$ and $\frac{\sigma^2 I_d n \Delta t}{n\Delta t} = \sigma^2 I_d$. For the forth term of the right hand side of Eq.(6.60), using the property that S_i is measure-preserving; see Theorem 6.1 and Assumption 6.3 , we can get

$$\begin{aligned}
 & \frac{1}{n} \sum_{i=1}^n E\tilde{V}_{\Delta t}^{\omega((i-1)\Delta t)}(X_{i-1}^\omega) \otimes \tilde{V}_{\Delta t}^{\omega((i-1)\Delta t)}(X_{i-1}^\omega) \\
 &= \frac{1}{n} \sum_{i=1}^n ES_{i-1}(\tilde{V}_{\Delta t} \otimes \tilde{V}_{\Delta t}) = \frac{1}{n} n E\tilde{V}_{\Delta t} \otimes \tilde{V}_{\Delta t} = O(\Delta t)^2. \tag{6.61}
 \end{aligned}$$

We shall focus on the third term on the right hand side of (6.60), which corresponds to the strengthen of the convection-enhanced diffusion and is the most difficult term. Substituting the formulation of the discrete-type corrector

problem (6.44) into it, we obtain that

$$\begin{aligned}
& \sum_{i=1}^n E \bar{X}_{i-1}^\omega \otimes \tilde{V}_{\Delta t}^{\omega((i-1)\Delta t)}(X_{i-1}^\omega) \\
&= - \sum_{i=1}^n E \bar{X}_{i-1}^\omega \otimes (E[\psi_{\Delta t}^{\omega(i\Delta t)}(X_i^\omega) | X_{i-1}^\omega] - \psi_{\Delta t}^{\omega((i-1)\Delta t)}(X_{i-1}^\omega)), \\
&= - \sum_{i=1}^n E \bar{X}_{i-1}^\omega \otimes (\psi_{\Delta t}^{\omega(i\Delta t)}(X_i^\omega) - \psi_{\Delta t}^{\omega((i-1)\Delta t)}(X_{i-1}^\omega)), \\
&= - \sum_{i=1}^n E(\bar{X}_{i-1}^\omega - \bar{X}_i^\omega) \otimes \psi_{\Delta t}^{\omega(i\Delta t)}(X_i^\omega) + E \bar{X}_0^\omega \otimes \psi_{\Delta t}^{\omega(0)}(X_0^\omega) - E \bar{X}_n^\omega \otimes \psi_{\Delta t}^{\omega(n\Delta t)}(X_n^\omega), \\
&= \sum_{i=1}^n E(\tilde{V}_{\Delta t}^{\omega((i-1)\Delta t)}(X_{i-1}^\omega) + \sigma N_{i-1}) \otimes \psi_{\Delta t}^{\omega(i\Delta t)}(X_i^\omega) \\
&\quad + E \bar{X}_0^\omega \otimes \psi_{\Delta t}^{\omega(0)}(X_0^\omega) - E \bar{X}_n^\omega \otimes \psi_{\Delta t}^{\omega(n\Delta t)}(X_n^\omega). \tag{6.62}
\end{aligned}$$

Let us first estimate the summation term on the right hand side of (6.62). For each index i , we have

$$\begin{aligned}
& E(\tilde{V}_{\Delta t}^{\omega((i-1)\Delta t)}(X_{i-1}^\omega) + \sigma N_{i-1}) \otimes \psi_{\Delta t}^{\omega(i\Delta t)}(X_i^\omega), \\
&= E \tilde{V}_{\Delta t}^{\omega((i-1)\Delta t)}(X_{i-1}^\omega) \otimes \psi_{\Delta t}^{\omega(i\Delta t)}(X_i^\omega) + E \sigma N_{i-1} \otimes \psi_{\Delta t}^{\omega(i\Delta t)}(X_i^\omega). \tag{6.63}
\end{aligned}$$

Through simple calculations, we will show that the second term of the right hand side of (6.63) is zero. Specifically, we have

$$\begin{aligned}
& E \sigma N_{i-1} \otimes \psi_{\Delta t}^{\omega(i\Delta t)}(X_i^\omega) \\
&= E \sigma N_{i-1} \otimes \psi_{\Delta t}^{\omega(i\Delta t)}(X_{i-1}^\omega + V_{\Delta t}^{\omega((i-1)\Delta t)}(X_{i-1}^\omega) + \sigma N_{i-1}), \\
&= \int_{\mathcal{X}} \int_{\mathbb{R}^d} p_0(0, y) \sigma y \otimes \psi_{\Delta t}(\tau_{\sigma y} \tau_{X_{i-1}^\omega + V_{\Delta t}(\eta_{i-1})} \omega(i\Delta t)) dy P_0(d\chi), \\
&= \int_{\mathbb{R}^d} p_0(0, y) \sigma y \otimes \int_{\mathcal{X}} \psi_{\Delta t}(\tau_{\sigma y} \tau_{X_{i-1}^\omega + V_{\Delta t}(\eta_{i-1})} \omega(i\Delta t)) P_0(d\chi) dy, \\
&= \int_{\mathbb{R}^d} p_0(0, y) \sigma y \otimes E \psi dy = 0. \tag{6.64}
\end{aligned}$$

Here, the expectation is taken over all the randomness in the system. Thus, in the third row of (6.64), y is a realization of N_{i-1} and $p_0(0, y) dy$ is the measure associated with the Brownian motion, while $P_0(d\chi)$ is the measure associate with the randomness in the velocity field and initial data. The Fubini's theorem is used in the fourth row of (6.64) to switch the order of integration. The fifth row of (6.64) is derived from Lemma 6.2; see Eq.(6.33). Moreover, $E \psi = 0$

since the solution of the discrete-type corrector problem is mean-zero; see Theorem 6.4.

Then, we compute the first term of the right hand side of (6.63) as follows,

$$\begin{aligned}
 & E\tilde{V}_{\Delta t}^{\omega((i-1)\Delta t)}(X_{i-1}^\omega) \otimes \boldsymbol{\psi}_{\Delta t}^{\omega(i\Delta t)}(X_i^\omega) = E\tilde{V}_{\Delta t}(\eta_{i-1}) \otimes \boldsymbol{\psi}_{\Delta t}(\eta_i) \\
 & = EE(\tilde{V}_{\Delta t}(\eta_{i-1}) \otimes \boldsymbol{\psi}_{\Delta t}(\eta_i) | \eta_{i-1}) = E\tilde{V}_{\Delta t}(\eta_{i-1}) \otimes E(\boldsymbol{\psi}_{\Delta t}(\eta_i) | \eta_{i-1}) \\
 & = E\tilde{V}_{\Delta t}(\eta_{i-1}) \otimes S_1 \boldsymbol{\psi}_{\Delta t}(\eta_{i-1}) = E\tilde{V}_{\Delta t}(\eta_{i-1}) \otimes (\boldsymbol{\psi}_{\Delta t}(\eta_{i-1}) - \tilde{V}_{\Delta t}(\eta_{i-1})) \\
 & = E\tilde{V}_{\Delta t}(\eta_{i-1}) \otimes \boldsymbol{\psi}_{\Delta t}(\eta_{i-1}) - E\tilde{V}_{\Delta t}(\eta_{i-1}) \otimes \tilde{V}_{\Delta t}(\eta_{i-1}) \\
 & = ES_{i-1}(\tilde{V}_{\Delta t} \otimes \boldsymbol{\psi}_{\Delta t}) - ES_{i-1}(\tilde{V}_{\Delta t} \otimes \tilde{V}_{\Delta t}). \tag{6.65}
 \end{aligned}$$

Using the property that each S_{i-1} is measure-preserving; see Theorem 6.1, we have

$$\frac{1}{n} \sum_{i=1}^n E\tilde{V}_{\Delta t}^{\omega((i-1)\Delta t)}(X_{i-1}^\omega) \otimes \boldsymbol{\psi}_{\Delta t}^{\omega(i\Delta t)}(X_i^\omega) = E\tilde{V}_{\Delta t} \otimes \boldsymbol{\psi}_{\Delta t} - E\tilde{V}_{\Delta t} \otimes \tilde{V}_{\Delta t}. \tag{6.66}$$

The term $E\tilde{V}_{\Delta t} \otimes \boldsymbol{\psi}_{\Delta t}$ in (6.66) is corresponding to the strengthen of the convection-enhanced diffusion. The term $E\tilde{V}_{\Delta t} \otimes \tilde{V}_{\Delta t}$ in (6.66) is of the order $O(\Delta t)^2$ due to (6.3). This completes the estimate of the first term in Eq.(6.62).

Now, we estimate the second term and third term in Eq.(6.62). The second term $E\bar{X}_0^\omega \otimes \boldsymbol{\psi}_{\Delta t}^{\omega(0)}(X_0^\omega)$ is trivial since it does not depend on n and is bounded. For the third term, we want to prove that

$$\frac{1}{n\Delta t} \|E\bar{X}_n^\omega \otimes \boldsymbol{\psi}_{\Delta t}^{\omega(n\Delta t)}(X_n^\omega)\| \leq O\left(\frac{1}{\sqrt{n}\Delta t}\right), \tag{6.67}$$

where $\|\cdot\|$ is a matrix norm. By using the Holder's inequality, we know that each entry of $E\bar{X}_n^\omega \otimes \boldsymbol{\psi}_{\Delta t}^{\omega(n\Delta t)}(X_n^\omega)$ satisfies

$$|E(\bar{X}_n^\omega)_i (\boldsymbol{\psi}_{\Delta t}^{\omega(n\Delta t)}(X_n^\omega))_j| \leq (E[(\bar{X}_n^\omega)_i]^2)^{1/2} (E[(\boldsymbol{\psi}_{\Delta t}^{\omega(n\Delta t)}(X_n^\omega))_j]^2)^{1/2}, \quad 1 \leq i, j \leq d. \tag{6.68}$$

Again, using the property that S_n is measure-preserving; see Theorem 6.1, we have

$$E[(\boldsymbol{\psi}_{\Delta t}^{\omega(n\Delta t)}(X_n^\omega))_j]^2 = E(\boldsymbol{\psi}_{\Delta t,j}(\eta_n))^2 = ES_n(\boldsymbol{\psi}_{\Delta t,j})^2 = E(\boldsymbol{\psi}_{\Delta t,j})^2, \tag{6.69}$$

which is bounded since $\boldsymbol{\psi}_{\Delta t} \in (L_0^2(\mathcal{X}))^d$ according to Theorem 6.4. Thus, if

we can prove $\frac{1}{n}E[(\bar{X}_n^\omega)_i]^2$ is bounded, then

$$\begin{aligned} \frac{1}{n\Delta t} |E(\bar{X}_n^\omega)_i(\psi_{\Delta t}^{\omega(n\Delta t)}(X_n^\omega))_j| &\leq \frac{1}{\sqrt{n\Delta t}} \left(\frac{1}{n}E[(\bar{X}_n^\omega)_i]^2\right)^{1/2} \left(E[(\psi_{\Delta t}^{\omega(n\Delta t)}(X_n^\omega))_j]^2\right)^{1/2} \\ &= O\left(\frac{1}{\sqrt{n\Delta t}}\right). \end{aligned} \quad (6.70)$$

In order to prove that $\frac{1}{n}E[(\bar{X}_n^\omega)_i]^2$ is bounded, we apply the AM-GM inequality on the diagonal entries of $E\bar{X}_n^\omega \otimes \psi_{\Delta t}^{\omega(n\Delta t)}(X_n^\omega)$ and obtain,

$$|E(\bar{X}_n^\omega)_i(\psi_{\Delta t}^{\omega(n\Delta t)}(X_n^\omega))_i| \leq \epsilon E[(\bar{X}_n^\omega)_i]^2 + (4\epsilon)^{-1} E[(\psi_{\Delta t}^{\omega(n\Delta t)}(X_n^\omega))_i]^2, \quad 1 \leq i \leq d, \quad (6.71)$$

where $\epsilon > 0$.

We substitute the result (6.71) into (6.62), and then substitute the estimated results of (6.62) (including Eqns.(6.64)(6.66)) into the original equation 6.60. Here we only consider the equations for the diagonal elements. Combining all the estimate results for terms on the right hand side of 6.60, we obtain an estimate for $E[(\bar{X}_n^\omega)_i]^2$ as follows,

$$E[(\bar{X}_n^\omega)_i]^2 \leq (\mathbf{R}_n)_i + \epsilon E[(\bar{X}_n^\omega)_i]^2, \quad (6.72)$$

where $(\mathbf{R}_n)_i$ denotes all the remaining terms with $(\mathbf{R}_n)_i = O(n)$. Thus, we choose $0 < \epsilon < 1$ (e.g. $\epsilon = 1/3$), move $\epsilon E[(\bar{X}_n^\omega)_i]^2$ to the left hand side of (6.72), and obtain that $\frac{1}{n}E\|\bar{X}_n^\omega\|^2$ is bounded by the ergodicity of \bar{X}_n^ω . Hence, we prove the claim in (6.67).

Finally, we combine the estimate results in Eqns.(6.60)(6.61)(6.62)(6.66)(6.70) and obtain that

$$\frac{E\bar{X}_n^\omega \otimes \bar{X}_n^\omega}{n\Delta t} = \sigma^2 I_d + 2\mathbf{S}E\psi_{\Delta t} \otimes \tilde{V}_{\Delta t}/\Delta t + O(\Delta t) + O\left(\frac{1}{\sqrt{n\Delta t}}\right). \quad (6.73)$$

According to Theorem 6.6 and Remark 6.4, we have the estimate

$$\|2\mathbf{S}E\psi_{\Delta t} \otimes \tilde{V}_{\Delta t}/\Delta t - 2\mathbf{S}E\psi \otimes v\|_{L^2(\mathcal{X})} = O(\Delta t^{\frac{c_1}{c_1+c_3}}) := \rho(\Delta t), \quad (6.74)$$

where $\lim_{\Delta t \rightarrow 0} \rho(\Delta t) = 0$. Thus, the statement in (6.59) is proved. \square

Remark 6.5. *Theorem 6.7 shows that when the time step is given and fixed, we have*

$$\lim_{n \rightarrow \infty} \frac{E\bar{X}_n^\omega \otimes \bar{X}_n^\omega}{n\Delta t} = \sigma^2 I_d + 2\mathbf{S} \int_{\mathcal{X}} \psi \otimes v dP_0 + \rho(\Delta t), \quad (6.75)$$

which reveals the connection of the definition of the effective diffusivity by solving discrete-type and continuous-type corrector problems. Our result appears to be the first one in the literature to build this connection.

Notice that in the Theorem 6.7, we assume $\bar{X}_n^\omega = X_n^\omega - n\bar{V}_{\Delta t}$ are given, where we use Monte carlo method to compute $\bar{V}_{\Delta t}$. In some cases, if we cannot calculate the drift constant $\bar{V}_{\Delta t}$ exactly, we can directly estimate the term $EX_n^\omega \otimes X_n^\omega$, which is summarized in the following corollary.

Corollary 6.1. *Let X_n^ω , $n = 0, 1, \dots$ be the numerical solution of the stochastic structure-preserving scheme (6.23) and Δt be the time step that is fixed. Suppose $n(\Delta t)^3$ and $\frac{1}{\sqrt{n\Delta t}}$ are small enough, we have*

$$\frac{EX_n^\omega \otimes X_n^\omega}{n\Delta t} = \sigma^2 I_d + 2\mathbf{S} \int_{\mathcal{X}} \psi \otimes v dP_0 + \rho(\Delta t) + O\left(\frac{1}{\sqrt{n\Delta t}}\right) + O(n(\Delta t)^3), \quad (6.76)$$

where $\rho(\Delta t) = O(\Delta t^{\frac{c_1}{c_1+c_3}})$ is a function satisfying $\lim_{\Delta t \rightarrow 0} \rho(\Delta t) = 0$ and independent of the computational time T , and the \mathbf{S} represents the symmetrization operator.

Proof. Using the observation that

$$\frac{EX_n^\omega \otimes X_n^\omega}{n\Delta t} = \frac{E\bar{X}_n^\omega \otimes \bar{X}_n^\omega}{n\Delta t} + \frac{2\mathbf{S}E\bar{X}_n^\omega \otimes \bar{V}_{\Delta t}}{\Delta t} + \frac{n^2\bar{V}_{\Delta t} \otimes \bar{V}_{\Delta t}}{n\Delta t} \quad (6.77)$$

and Theorem 6.3, we can straightforwardly get the proof. \square

Remark 6.6. *In our convergence analysis, we interpret the solution process generated by our numerical scheme as a Markov process. By exploring the ergodicity of the solution process (i.e., Markov process), we give a sharp error estimate of the proposed numerical scheme in computing effective diffusivity.*

6.4 Numerical results

The aim of this section is two-fold. First, we will verify the convergence results obtained in Section 6.3.2. Second, we will use the proposed method

to compute effective diffusivity in random flows, where incompressible random flows in two- and three-dimensional space will be studied. Without loss of generality, we compute the quantity $\frac{E[(X_{n,1}^\omega)^2]}{2n\Delta t}$, which is used to approximate D_{11}^E in the effective diffusivity matrix D^E . Notice that $X_{n,1}^\omega$ is the first component of the solution vector X_n^ω . One can obtain D_{11}^E by choosing $\mathbf{v} = (1, 0)^T$ in the equation (6.16) of the Prop. 6.4.

6.4.1 Numerical methods for generating random flows

To start with, we discuss how to generate random flows that will be used in our numerical experiments. Assume the vector field $v(t, x, \omega)$ has a spectral measure

$$\exp(-r(\mathbf{k})|t|)\Gamma(\mathbf{k})(\mathbf{I} - \frac{\mathbf{k} \otimes \mathbf{k}}{|\mathbf{k}|^2}), \quad (6.78)$$

where $\mathbf{k} = (k_1, k_2)^T$ or $\mathbf{k} = (k_1, k_2, k_3)^T$, $r(\mathbf{k}) > c_0$ for some positive constant c_0 , and $\Gamma(\mathbf{k})$ is integrable and decays fast for large \mathbf{k} . Under such settings, the velocity field $v(t, x, \omega)$ satisfies the ρ mixing condition and is stationary and divergence free [48, 14]. In order to mimic the energy spectrum of real flows, we assume $\Gamma(\mathbf{k}) \propto 1/|\mathbf{k}|^{2\alpha+d-2}$ with ultraviolet cutoff $|\mathbf{k}| \leq K < \infty$ and $r(\mathbf{k}) \propto |\mathbf{k}|^{2\beta}$. The spectral gap condition 6.3 requires $\beta \leq 0$ and the integrability of $\Gamma(\mathbf{k})$ requires $\alpha < 1$. Here for simplicity, we choose $\beta = 0$.

Given the spectral measure (6.78), we use the randomization method [33, 37] to generate realizations of the velocity field. Specifically, we approximate it as

$$v(t, x) = \frac{1}{\sqrt{M}} \sum_{m=1}^M [\mathbf{u}_m \cos(\mathbf{k}_m \cdot x) + \mathbf{v}_m \sin(\mathbf{k}_m \cdot x)]. \quad (6.79)$$

Notice that we have suppressed the dependence of the velocity on ω for notation simplicity here. In fact, the parameters \mathbf{k}_m , \mathbf{u}_m and \mathbf{v}_m contain randomness. The spectrum points \mathbf{k}_m were chosen independently according to the spectral measure $\Gamma(\mathbf{k})$. Due to the isotropicity, we first generate a point uniformly distributed on the unit sphere or unit circle, which represents the direction of

the \mathbf{k}_m . Then we generate the length r of \mathbf{k}_m , which satisfies a density function $\rho(r) \propto 1/r^{2\alpha-1}, 0 < r \leq K$.

For the random flows in two-dimensional space, we have

$$\mathbf{u}_m = N_m(t) \frac{\mathbf{k}_m^\perp}{|\mathbf{k}_m^\perp|}, \quad \mathbf{v}_m = \eta_m(t) \frac{\mathbf{k}_m^\perp}{|\mathbf{k}_m^\perp|}, \quad \mathbf{k}_m = (k_m^1, k_m^2), \quad m = 1, \dots, M, \quad (6.80)$$

where $\mathbf{k}_m^\perp = (-k_m^2, k_m^1)$, $N_m(t)$ and $\eta_m(t)$ are independent 1D Ornstein-Uhlenbeck (OU) processes with covariance function

$$\text{Cov}(N_m(t_1), N_m(t_2)) = \text{Cov}(\eta_m(t_1), \eta_m(t_2)) = \exp(-\theta|t_1 - t_2|).$$

Here $\theta > 0$ is a parameter to control the roughness of the OU process. To obtain the OU path for $N_m(t)$, we generate a series of $\{N_m(n\Delta t)\}$ satisfies

$$N_m(n\Delta t) = e^{-\theta\Delta t} N_m((n-1)\Delta t) + \sqrt{1 - e^{-2\theta\Delta t}} \zeta_n, \quad n = 1, 2, 3, \dots \quad (6.81)$$

where $N_m(0)$, ζ_n , $n = 1, 2, 3, \dots$ are i.i.d. $N(0, 1)$ distributed random variables. One can easily verify that $\text{Cov}(N_m(i\Delta t), N_m(j\Delta t)) = \exp(-\theta|i - j|\Delta t)$. The OU path for $\eta_m(t)$ can be generated by using the same approach.

For the random flows in three-dimensional space, we have

$$\mathbf{u}_m = N_m(t) \times \frac{\mathbf{k}_m}{|\mathbf{k}_m|}, \quad \mathbf{v}_m = \boldsymbol{\eta}_m(t) \times \frac{\mathbf{k}_m}{|\mathbf{k}_m|}, \quad \mathbf{k}_m = (k_m^1, k_m^2, k_m^3), \quad (6.82)$$

where the samples $N_m(t)$ and $\boldsymbol{\eta}_m(t)$ are independent 3D random vectors, whose components are independent stationary OU process having the covariance function $\text{Cov}(N_m(t_1), N_m(t_2)) = \text{Cov}(\boldsymbol{\eta}_m(t_1), \boldsymbol{\eta}_m(t_2)) = \exp(-\theta|t_1 - t_2|)I_3$. Each component of $N_m(t)$ and $\boldsymbol{\eta}_m(t)$ can be generated by using the method (6.81). One can easily verify that in both the 2D and 3D cases the velocity fields generated by (6.79) satisfy the divergence free condition.

6.4.2 Verification of the convergence analysis

In this subsection, we study the convergence rate of our method in computing incompressible random flow in 2D and 3D space.

For the random flow in 2D space, we solve the SDE (2.1), where the velocity field is chosen as (6.79) with the setting (6.80). The velocity field were simulated with $M = 1000$. The parameters in the spectral measure $\Gamma(\mathbf{k})$ are $K = 10$ and $\alpha = 0.75$. The time-mixing constant $\theta = 10$ in the covariance function. The molecular diffusivity $\sigma = 0.1$. We use Monte Carlo method to generate dependent samples for the Brownian motion W_t and velocity field $v(t, x)$. The sample number is denoted by N_{mc} .

We choose time step $\Delta t_{ref} = 0.001$ and $N_{mc} = 100,000$ to solve the SDE (2.1) and compute the reference solution, i.e., the “exact” effective diffusivity, where the final computational time is $T = 22$ so that the calculated effective diffusivity converges to a constant. It takes about 24 hours to compute the reference solution on a 64-core server (Gridpoint System at HKU). The reference solution for the effective diffusivity is $D_{11}^E = 0.1736$.

For the random flow in 3D space, we solve the SDE (2.1), where the velocity field is chosen as (6.79) with the setting (6.82). The velocity field were simulated with $M = 100$. The parameters in the spectral measure $\Gamma(\mathbf{k})$ are $K = 10$ and $\alpha = 0.75$. The time-mixing constant $\theta = 10$ in the covariance function. The molecular diffusivity $\sigma = 0.1$. Again, we use Monte Carlo method to generate dependent samples for the Brownian motion W_t and velocity field $v(t, x)$.

We choose $\Delta t_{ref} = 0.001$ and $N_{mc} = 180,000$ to solve the SDE (2.1) and compute the reference solution, i.e., the “exact” effective diffusivity, where the final computational time is $T = 25$ so that the calculated effective diffusivity converges to a constant. It takes about 21 hours to compute the reference solution on a 64-core server (Gridpoint System at HKU). The reference solution for the effective diffusivity is $D_{11}^E = 0.1137$. We remark that in our numerical experiment, we choose $M = 1000$ for 2D random flow and $M = 100$ for 3D random flow so that the velocity field numerically satisfies the ergodicity assumption.

In Fig.6.1(a), we plot the convergence results of the effective diffusivity

for the 2D random flow using our method (i.e., $\frac{E[(X_{n,1}^\omega)^2]}{2n\Delta t}$) with respect to different time-step Δt at $T = 22$, where the number of the Monte Carlo samples $N_{mc} = 50,000$. In addition, we show a fitted straight line with the slope 1.17, i.e., the convergence rate is about $\mathcal{O}(\Delta t)^{1.17}$. Similarly, we show the convergence results of $\frac{E[(X_{n,1}^\omega)^2]}{2n\Delta t}$ for the 3D random flow in Fig.6.1(b) with respect to different time-step Δt at $T = 25$, where the number of the Monte Carlo samples $N_{mc} = 50,000$. We also show a fitted straight line with the slope 0.98, i.e., the convergence rate is about $\mathcal{O}(\Delta t)^{0.98}$. These numerical results agree with our error analysis.

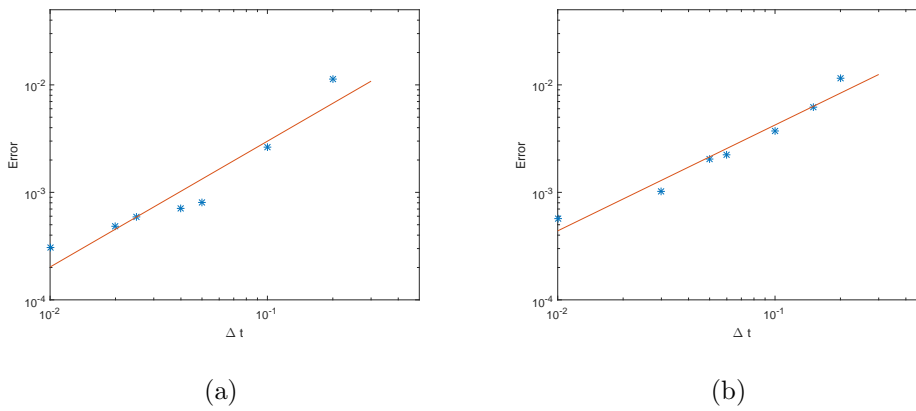


Figure 6.1: Error of D_{11}^E for random flows with different time-steps. Left: 2D, fitted slope ≈ 1.17 ; right 3D, fitted slope ≈ 0.98 .

6.4.3 Verification of the exponential decay property.

The time relaxation property (6.3), which is equivalent to the exponential decay property (6.4), plays an important role in the existence of the effective diffusivity; see Prop. 6.4. In Theorem 6.2, we prove that the numerical solutions inherit the exponential decay property. Based on this key fact, we can define the discrete-type corrector problem and prove the convergence analysis of our method. In this subsection, we will verify that the velocity field propagated by the random flow (6.79) has the exponential decay property, where both the 2D and 3D cases will be tested.

In the experiment for 3D random flow, we choose the time step size $\Delta t =$

0.05. The velocity field will be approximated by $M = 100$ terms in (6.79) with the setting (6.82). The parameters in the spectral measure $\Gamma(\mathbf{k})$ are $K = 10$ and $\alpha = 0.75$. The molecular diffusivity $\sigma = 0.1$. We randomly generate 200 samples $\{\mathbf{k}_m^i, N_m^i(0), \boldsymbol{\eta}_m^i(0), m = 1, \dots, M\}$, $i = 1, \dots, 200$, which will be used to generate initial states for the velocity field (6.79), i.e.,

$$v^i(0, x) = \frac{1}{\sqrt{M}} \sum_{m=1}^M \left[N_m^i(0) \times \frac{\mathbf{k}_m^i}{|\mathbf{k}_m^i|} \cos(\mathbf{k}_m^i \cdot x) + \boldsymbol{\eta}_m^i(0) \times \frac{\mathbf{k}_m^i}{|\mathbf{k}_m^i|} \sin(\mathbf{k}_m^i \cdot x) \right],$$

$$i = 1, \dots, 200.$$
(6.83)

Then, for each initial state $v^i(0, x)$, we generate 5000 different samples of the OU paths $N_m^{i,p}(n\Delta t)$ and $\boldsymbol{\eta}_m^{i,p}(n\Delta t)$ and Brownian motion paths $\mathbf{w}^{i,p}(n\Delta t)$, $1 \leq p \leq 5000$. Given the sample data, we calculate the corresponding solution paths $\{X_n^{i,p}\}_{0 \leq n < \infty}$ and then calculate the value

$$v^{i,p}(n\Delta t, X_n^{i,p}) = \frac{1}{\sqrt{M}} \sum_{m=1}^M \left[N_m^{i,p}(n\Delta t) \times \frac{\mathbf{k}_m^i}{|\mathbf{k}_m^i|} \cos(\mathbf{k}_m^i \cdot X_n^{i,p}) \right. \\ \left. + \boldsymbol{\eta}_m^{i,p}(n\Delta t) \times \frac{\mathbf{k}_m^i}{|\mathbf{k}_m^i|} \sin(\mathbf{k}_m^i \cdot X_n^{i,p}) \right],$$

$$i = 1, \dots, 200, \quad 1 \leq p \leq 5000.$$
(6.84)

Finally, we compute $\bar{v}_n^i = \frac{1}{5000} \sum_{p=1}^{5000} v^{i,p}(n\Delta t, X_n^{i,p})$ and the sample variance of \bar{v}_n^i with respect to i . The experiment for 2D random flow is almost the same except the setting of the velocity field (6.82) is replaced by (6.80) and we choose $M = 1000$.

In Fig. 6.2(a) and Fig. 6.2(b), we plot the calculated sample variance of the first component of \bar{v}_n^i for the 2D random flow and 3D random flow, respectively. We observe exponential decay of the sample variance with respect to time. Moreover, we find that larger θ leads to a faster decay in the sample variance, since larger θ results in a fast decorrelation in the random flow. Our numerical results show that the exponential decay property (see Theorem 6.2) holds for the random flows we studied here.

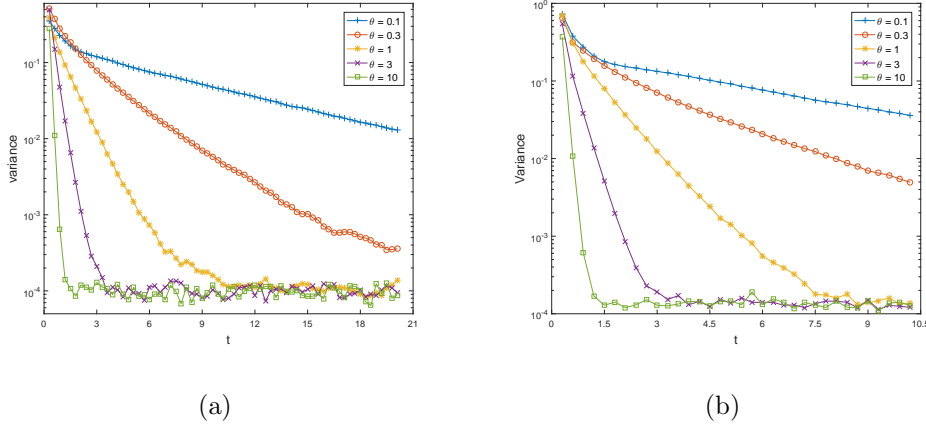


Figure 6.2: Decay behaviors of the sample variance in 2D and 3D random flows. Left: 2D; right 3D.

6.4.4 Investigation of the convection-enhanced diffusion phenomenon

In the first experiment, we study the relation between the numerical effective diffusivity $\frac{E[(X_{n,1}^\omega)^2]}{2n\Delta t}$ and the parameter θ , which controls the de-correlation rate in the temporal dimension of the random flow. In this experiment, the setting of the velocity field and the implementation of our method is the same as we used in Section 6.4.3. We only choose different parameter θ to compute the numerical effective diffusivity.

In Fig.6.3(a), we plot the numerical effective diffusivity of 2D random flow obtained at different computational times, where the flow is generated with different θ . The result for 3D random flow is shown in Fig.6.3(b). We find that different θ affects the mixing time of the system. When we increase the θ , the system will quickly enter a mixing stage.

In the second experiment, we choose different molecular diffusivity σ to compute the corresponding numerical effective diffusivity, which allows us to study the existence of residual diffusivity for this random flow. The residual diffusivity, a special yet remarkable convection-enhanced diffusion phenomenon, refers to the non-zero and finite effective diffusivity in the limit of zero molec-

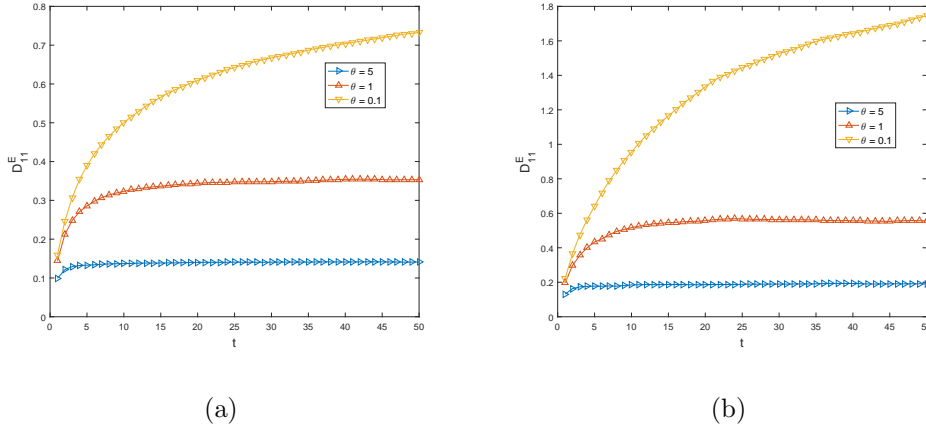


Figure 6.3: The relation between numerical effective diffusivity and θ . Left: 2D; right 3D.

ular diffusivity as a result of a fully chaotic mixing of the streamlines.

In the experiment for 2D random flow, we choose the time step $\Delta t = 0.05$, the velocity field were simulated with $M = 1000$, the time-mixing constant $\theta = 0.1$ and the parameters in the spectral measure $\Gamma(\mathbf{k})$ are $K = 10$ and $\alpha = 0.75$. For the 3D random flow, we choose $M = 100$ and keep other parameters the same.

Let $\kappa = \sigma^2/2$. In Fig.6.4(a), we show the relation between numerical effective diffusivity of 2D random flow obtained at different computational times, where the result is generated with different σ . The result for 3D random flow is shown in Fig. 6.4(b). We find that as κ approaches zero, the quantity $\frac{E[(\bar{X}_{n,1}^\omega)^2]}{2n\Delta t}$ converges to a non-zero (positive) constant, which indicates the existence of residual diffusivity in the random flows here.

In Fig.6.5(a) and Fig.6.5(b), we plot the convergence behaviors of $D_{11}^E(\kappa)$ approaching $D_{11}^E(0)$ for the 2D and 3D random flows, respectively, when the systems enter a mixing stage. The convergence behaviors when κ approaches zero are slightly different though, both figures show that residual diffusivity exists in the random flows we studied here.

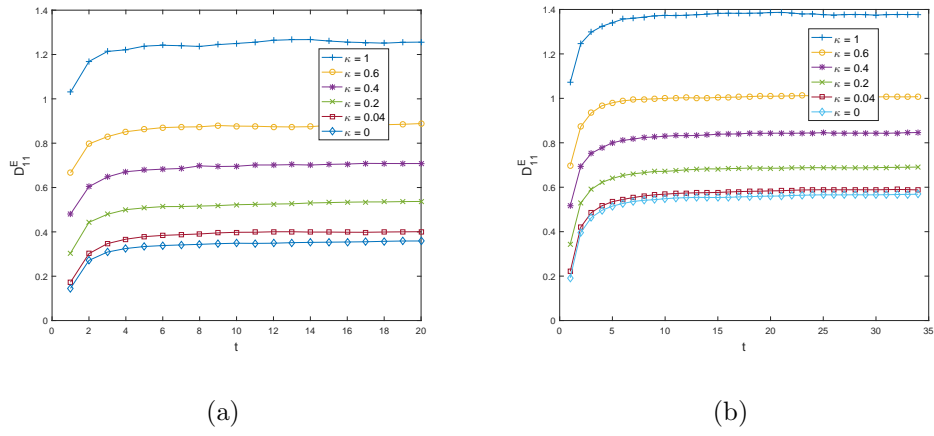


Figure 6.4: The relation between numerical effective diffusivity and molecular diffusivity σ . Left: 2D; right 3D.

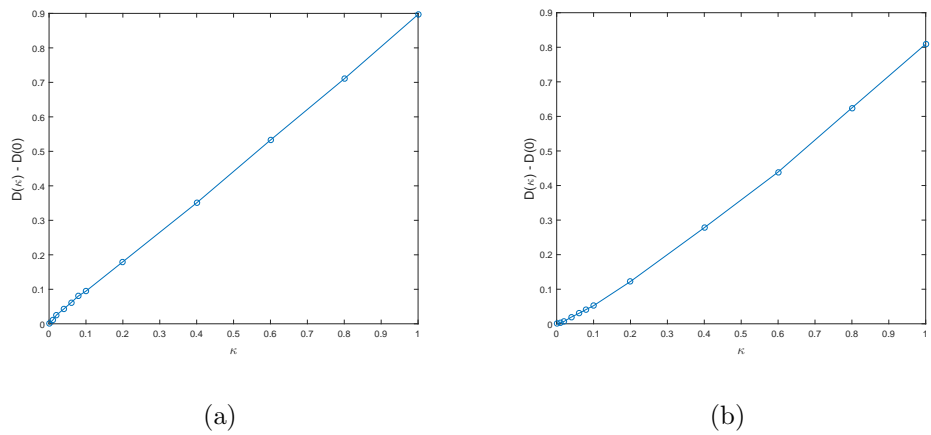


Figure 6.5: Convergence behaviors of $D_{11}^E(\kappa)$ approaching $D_{11}^E(0)$. Left: 2D; right 3D

Chapter 7

Concluding Discussions

In this thesis, we explored the Lagrangian numerical schemes in computing effective diffusivities for chaotic and random flows. The schemes relied on the Lagrangian formulation of the effective diffusivities in the parabolic homogenization. To facilitate the possible long time integration in Lagrangian approach, the schemes were proposed to be structure preserving.

To be specific, we decomposed the dynamical systems into two sub-systems and applied the idea of operator splitting. The first sub-system is volume-preserving transform defined by the velocity fields, so we applied a volume-preserving scheme. The second sub-system is driven by Brownian motion. Since we have assumed there is no spatial dependence for the Brownian motion, Euler Maruyama scheme gives the exact solution. Combining together, the schemes preserve the invariant measure for the system on torus. Base on this, and the ergodicity of the scheme, we proved the error of our Lagrangian schemes converges asymptotically, then uniformly in time.

In numerical examples, we verified the convergence rate of our scheme in all types of flows within the scope of the thesis. The novelty of the thesis in numerical parts is to observe the scaling of diffusion enhancement in vanishing monocular diffusion regime for chaotic and random flows, especially in 3D. Currently we categorized the scaling to four types: vanishing, residual,

sub-maximal and maximal. We conclude the phenomena in different flows as follows.

Taylor Green flow in 2D As an unsteady flow in 2D, the diffusion enhancement is proven to attain $\mathcal{O}(\sqrt{D_0})$ scaling. Our Lagrangian schemes also captured such vanishing scaling.

Random flows Two types of random flows were investigated. The first one is by involving stochastic processes as coefficients in deterministic streamlines and the second is directly generated by given energy spectra. In both cases, we observed a residual diffusion phenomenon. The residual diffusivities in such cases may be the chaotic characteristics of the random advection.

ABC flow As the possible result of existence of ballistic orbits, chaos in ABC flows are weakest among the flows in this thesis. We found maximal enhancement phenomena in ABC flows. Also as a non-mixing flow, the mixing time lasts as long as $\mathcal{O}(\frac{1}{D_0})$.

Kolmogorov flow Comparing to ABC flows, Kolmogorov flows are more chaotic, even possibly weakly mixing. We identified the enhancement as sub-maximal and the mixing time is significantly shorter than one in ABC flows.

Time dependent flows We also investigated several time dependent flows which resembles Taylor Green, ABC and Kolmogorov flows correspondingly. For different setting of parameters, the scaling ranges in residual, sub-maximal and maximal. The effects of parameters are usually non-uniform. On the other hand, in general, the time dependency breaks the closed (or ballistic) orbits in convection, so the flow always becomes more chaotic.

As a final conclusion, schemes, proposed in this thesis, developed a novel and numerical attainable way to quantify chaos in the flows.

7.1 Future direction

There are several possible or on-going directions that might deserve further investigation.

Calculation of KPP front speed The KPP problem was raised by Kolmogorov, Petrovskii, and Piskunov in 1937. It is a homogenization problem in reaction-convection-diffusion equation. It is shown in [49] that KPP front speed is bounded by effective diffusivities up to constants in 2D periodic flows. As schemes proposed in this thesis perform well in calculating effective diffusivities, we are seeking schemes that best fit in calculating front speed numerically. Moreover, the critical speed can be calculated by principal eigenvalues of a series of Fokker-Planck operators defined by the flow [54]. In [22] a semigroup analysis shows that the numerical schemes for SDE may preserve the principle eigenvalues of the Fokker-Planck operators. Our study in this aspect may bring very promising result both in theory and in physics.

Investigation of mixing properties Our numerical experiment shows there are two factors that influence the mixing time. First is the molecular diffusivities D_0 , it decorrelates (mix) the particles exponentially fast. So the mixing time is bounded by $\mathcal{O}(\frac{1}{D_0})$. However, when D_0 turns to 0, the second factor dominates. It is the mixing properties of the flow. Currently during our calculation of effective diffusivities, we can also infer the mixing time of the dynamics. Fig.6.4 shows there is strong mixing in our proposed random flows. Fig.4.6(a) implies Kolmogorov flow might be weakly mixing. Fig.4.3(a) shows different case in ABC flows that as a type of chaotic flow it is non-mixing.

Our study may include two steps. The first is the relation mixing phenomenon in our discrete calculation and one in continuous dynamics. [21] shows that there are gaps between these two in general. While we may find the equivalence in cases we concerns. The second is to decide a robust statistic to quantify the mixing time.

Unification in categorizing chaos To the best knowledge of the authors, none of definitions of chaos are in agreement with [50]. The scaling metric proposed has shown strong correlation in numerical experiments with several other chaotic properties of flows, including, mixing time, Lyapunov exponent, etc. And the proposed schemes in calculating the scaling are shown to be robust. Our goal from this orientation can be twofold. First is to propose robust schemes to investigate diffusion enhancement in all types of flows. Second, we may investigate the relation between different properties bridging by the enhancement.

Appendix: Notations and Abbreviations

I. The following notations are used in the thesis.

\mathbb{Z} : the set of integers.

\mathbb{R}^d : d -dimensional real Euclidean space.

\mathbb{T}^d : d -dimensional torus space, a quotient space defined by $\mathbb{T}^d = \mathbb{R}^d / \mathbb{Z}^d$.

$\|v\|$: the Euclidean norm of vector v .

$\|v\|_p$: the p -norm of vector v .

$|x|$: the absolute value of a scalar, equivalent to $\|x\|$.

∇ : gradient operator in spacial direction (x).

Δ : Laplacian operator in spacial direction (x).

$v \cdot w$: inner product, given two \mathbb{R}^d vector, $v = (v_1, v_2, \dots, v_d)$, $w = (w_1, w_2, \dots, w_d)$,

$$v \cdot w = \sum_{i=1}^d v_i w_i.$$

$v \otimes w$: Kronecker product, given two vector, $v = (v_1, v_2, \dots, v_m)$, $w = (w_1, w_2, \dots, w_n)$,

$$v \otimes w = \begin{bmatrix} v_1 w_1 & \cdots & v_1 w_n \\ \vdots & \ddots & \vdots \\ v_m w_1 & \cdots & v_m w_n \end{bmatrix}.$$

x^T : the transpose of the vector (or matrix) x .

I_d : constant identity matrix in $\mathbb{R}^{d \times d}$.

$a \propto b$: a is proportional to b .

$A(\alpha) = \mathcal{O}(|\alpha|^p)$, $A(\alpha) \preceq |\alpha|^p$: $\|A(\alpha)\|/|\alpha|^p \leq C$ as $\alpha \rightarrow 0$, where C is a non-negative bounded constant.

$O(|\alpha|^p)$: only appears in equation, means the term is bounded by $C|\alpha|^p$ as $\alpha \rightarrow 0$, where C is a non-negative bounded constant.

$A \cup B$: the union of A and B .

$A \cap B$: the intersection of A and B .

\emptyset : the empty set.

$\mathcal{C}^{p,\alpha}(Y)$: the Hölder space whose p -th order derivatives are α -Hölder continuous.

$\mathcal{C}^{p,\alpha}(Y)$: the homogeneous Hölder space whose p -th order derivatives are α -Hölder continuous and spacial mean is zero.

$[A, B]$: commutator of A and B , $[A, B] = AB - BA$.

$(\Omega, \mathcal{F}_t, P)$: probability space.

$E[X|\mathcal{F}]$: conditional expectation of X given \mathcal{F} .

$P(A|B)$: the probability of A given B .

D_0 : the coefficient of Laplacian in generators, related to monocular diffusion coefficient σ by $D_0 = \frac{\sigma^2}{2}$.

D^E : effective diffusivities matrix

II. The following abbreviations are used in the thesis.

ABC: Arnold-Beltrami-Childress

BCH: Baker-Campbell-Hausdorff

BEA: Backward Error Analysis

EM: Euler-Maruyama

KPP: Kolmogorov-Petrovskii-Piskunov

ODE: ordinary differential equation.

PDE: partial differential equation.

SDE: stochastic differential equation.

Bibliography

- [1] B. Afkham and J. Hesthaven. Structure preserving model reduction of parametric hamiltonian systems. *SIAM Journal on Scientific Computing*, 39(6):A2616–A2644, 2017.
- [2] G. Ben Arous and H. Owhadi. Multiscale homogenization with bounded ratios and anomalous slow diffusion. *Communications on Pure and Applied Mathematics*, 56(1):80–113, 2003.
- [3] A. Bensoussan, J. L. Lions, and G. Papanicolaou. *Asymptotic analysis for periodic structures*. AMS Chelsea publishing, Providence, Rhode Island, 1978.
- [4] A. Bensoussan, J. L. Lions, and G. Papanicolaou. *Asymptotic analysis for periodic structures*, volume 374. American Mathematical Soc., 2011.
- [5] L. Biferale, A. Crisanti, M. Vergassola, and A. Vulpiani. Eddy diffusivities in scalar transport. *Phys. Fluids*, 7:2725–2734, 1995.
- [6] N. Bou-Rabee and H. Owhadi. Long-run accuracy of variational integrators in the stochastic context. *SIAM J. Numer. Anal*, 48:278–297, 2010.
- [7] NH Brummell, F Cattaneo, and SM Tobias. Linear and nonlinear dynamo properties of time-dependent abc flows. *Fluid Dynamics Research*, 28(4):237, 2001.
- [8] R. Carmona and L. Xu. Homogenization for time-dependent two-dimensional incompressible Gaussian flows. *The Annals of Applied Probability*, 7(1):265–279, 1997.

- [9] J. Cartwright, U. Feudel, G. Karolyi, A. Moura, and O. Tamas Tel. *Dynamics of Finite-Size Particles in Chaotic Fluid Flows, Chapter in Book Nonlinear Dynamics and Chaos: Advances and Perspectives*, page 51–87. Springer, 2010.
- [10] Stephen Childress and Andrew D Gilbert. *Stretch, twist, fold: the fast dynamo*, volume 37. Springer Science & Business Media, 1995.
- [11] Arnaud Debussche and Erwan Faou. Weak backward error analysis for sdes. *SIAM Journal on Numerical Analysis*, 50(3):1735–1752, 2012.
- [12] PE Dedik and MA Subin. Random pseudodifferential operators and the stabilization of solutions of parabolic equations with random coefficients. *Sbornik: Mathematics*, 41:33–52, 1982.
- [13] T. Dombre, U. Frisch, J. Greene, M. Hénon, A. Mehr, and A. Soward. Chaotic streamlines in the ABC flows. *Journal of Fluid Mechanics*, 167:353–391, 1986.
- [14] Paul Doukhan. *Mixing: properties and examples*, volume 85. Springer Science & Business Media, 2012.
- [15] L. C. Evans. *Partial Differential Equations*, volume 2. American Mathematical Society, 2010.
- [16] A. Fannjiang and G. Papanicolaou. Convection-enhanced diffusion for periodic flows. *SIAM J Appl. Math.*, 54:333–408, 1994.
- [17] A. Fannjiang and G. Papanicolaou. Diffusion in turbulence. *Probability Theory and Related Fields*, 105(3):279–334, 1996.
- [18] A. Fannjiang and G. Papanicolaou. Convection-enhanced diffusion for random flows. *J. Stat. Phys.*, 88:1033–1076, 1997.
- [19] Albert Fannjiang and Tomasz Komorowski. Turbulent diffusion in markovian flows. *Annals of Applied Probability*, pages 591–610, 1999.
- [20] K. Feng and Z. Shang. Volume-preserving algorithms for source-free dynamical systems. *Numerische Mathematik*, 71(4):451–463, 1995.

- [21] Yuanyuan Feng and Gautam Iyer. Dissipation enhancement by mixing. *Nonlinearity*, 32(5):1810, 2019.
- [22] Grégoire Ferré and Gabriel Stoltz. Error estimates on ergodic properties of discretized feynman–kac semigroups. *Numerische Mathematik*, 143(2):261–313, 2019.
- [23] D. Galloway and M. Proctor. Numerical calculations of fast dynamos in smooth velocity fields with realistic diffusion. *Nature*, 356(6371):691, 1992.
- [24] J. Garnier. Homogenization in a periodic and time-dependent potential. *SIAM Journal on Applied Mathematics*, 57(1):95–111, 1997.
- [25] Alexander V Getling. *Rayleigh-Bénard convection: structures and dynamics*, volume 11. World Scientific, 1998.
- [26] R. Gilmore. Baker-Campbell-Hausdorff formulas. *Journal of Mathematical Physics*, 15(12):2090–2092, 1974.
- [27] E. Hairer, C. Lubich, and G Wanner. *Geometric numerical integration: structure-preserving algorithms for ordinary differential equations*. Springer Science and Business Media, 2006.
- [28] J. Hong, H. Liu, and G. Sun. The multi-symplecticity of partitioned runge-kutta methods for hamiltonian pdes. *Mathematics of computation*, 75(253):167–181, 2006.
- [29] V. V. Jikov, S. Kozlov, and O. A. Oleinik. *Homogenization of Differential Operators and Integral Functionals*. Springer, Berlin, 1994.
- [30] Ioannis Karatzas and Steven E Shreve. *Brownian Motion and Stochastic Calculus*. Springer, 1998.
- [31] Tosio Kato. *Perturbation theory for linear operators*, volume 132. Springer Science & Business Media, 2013.
- [32] P. E. Kloeden and E. Platen. *Numerical solution of Stochastic Differential Equations*. Springer-Verlag Berlin, Heidelberg, 1992.

- [33] Robert H Kraichnan. Diffusion by a random velocity field. *The physics of fluids*, 13(1):22–31, 1970.
- [34] N. V. Krylov. *Lectures on elliptic and parabolic equations in Hölder spaces*, volume 12 of *Graduate studies in mathematics*. American Mathematical Soc., 1996.
- [35] C. Landim, S. Olla, and H. T. Yau. Convection–diffusion equation with space–time ergodic random flow. *Probability theory and related fields*, 112(2):203–220, 1998.
- [36] J. Lyu, J. Xin, and Y. Yu. Computing residual diffusivity by adaptive basis learning via spectral method. *Numerical Mathematics: Theory, Methods and Applications*, 10(2):351–372, 2017.
- [37] A. J. Majda and P. R. Kramer. Simplified models for turbulent diffusion: theory, numerical modelling, and physical phenomena. *Phys. Rep.*, 314:237–574, 1999.
- [38] R. I. McLachlan and G. R. Quispel. Splitting methods. *Acta Numerica*, 11:341–434, 2001.
- [39] T. McMillen, J. Xin, Y. F. Yu, and A. Zlatos. Ballistic orbits and front speed enhancement for abc flows. *SIAM Journal on Applied Dynamical Systems*, 15(3):1753–1782, 2016.
- [40] I. Mezić, J. F. Brady, and S. Wiggins. Maximal effective diffusivity for time-periodic incompressible fluid flows. *SIAM Journal on Applied Mathematics*, 56(1):40–56, 1996.
- [41] G. Milstein, Y. Repin, and M. Tretyakov. Symplectic integration of Hamiltonian systems with additive noise. *SIAM J. Numer. Anal.*, 39:2066–2088, 2002.
- [42] B. Oksendal. *Stochastic Differential Equations: an introduction with applications*. Springer Science and Business Media, 2013.

- [43] G. Pavliotis and A. Stuart. *Multiscale methods: averaging and homogenization*. Springer Science and Business Media, 2008.
- [44] G. Pavliotis, A. Stuart, and K. Zygalakis. Calculating effective diffusivities in the limit of vanishing molecular diffusion. *J. Comput. Phys.*, 228:1030–1055, 2009.
- [45] GA Pavliotis. Asymptotic analysis of the green–kubo formula. *IMA journal of applied mathematics*, 75(6):951–967, 2010.
- [46] S. Reich. Backward error analysis for numerical integrators. *SIAM J. Numer. Anal.*, 36:1549–1570, 1999.
- [47] H. Risken. *The fokker-planck equation*, volume 18 of Springer Series in synergetics, 1989.
- [48] Murray Rosenblatt. *Markov Processes, Structure and Asymptotic Behavior: Structure and Asymptotic Behavior*, volume 184. Springer Science & Business Media, 2012.
- [49] Lenya Ryzhik, Andrej Zlatoš, et al. Kpp pulsating front speed-up by flows. *Communications in Mathematical Sciences*, 5(3):575–593, 2007.
- [50] Evelyn Sander and James A Yorke. The many facets of chaos. *International Journal of Bifurcation and Chaos*, 25(04):1530011, 2015.
- [51] G. Strang. On the construction and comparison of difference schemes. *SIAM J. Numer. Anal.*, 5:506–517, 1968.
- [52] G. E. Uhlenbeck and L. S. Ornstein. On the theory of the Brownian motion. *Physical review*, 36(5):823, 1930.
- [53] Zhongjian Wang. Convergence analysis of strong approximation to stochastic differential equation. *Bachelor Thesis, advisor: Espen Robstad Jakobsen and Chunxiong Zheng*, 2016.
- [54] J. Xin. Front propagation in heterogeneous media. *SIAM review*, 42:161–230, 2000.

- [55] J. Xin, Y. Yu, and A. Zlatos. Periodic orbits of the abc flow with $A = B = C = 1$. *SIAM Journal on Mathematical Analysis*, 48(6):4087–4093, 2016.

- [56] K.C. Zygalakis. On the existence and the applications of modified equations for stochastic differential equations. *SIAM Journal on Scientific Computing*, 33(1):102–130, 2011.